REMARKS

Claims 1-31 were originally pending in the Application. Claims 20-28 and 30 are withdrawn as non-elected subject matter. Applicants preserve the right to pursue the withdrawn subject matter by way of divisional application(s) if Applicants choose to do so.

The allowance of Claims 18-19 is sincerely appreciated. Claims 5 and 7-9 are objected to.

Claims 2 and 10 were rejected under 35 U.S.C. § 112, second paragraph, on indefiniteness reasoning. The infractions that the Examiner pointed out are corrected in this Amendment.

Claims 1-4, 10, 12-17, 29 and 31 were rejected under 35 U.S.C. § 102 (a) or 102(b) based on various published compounds. Applicants have now added a proviso to claim 1 to remove these compounds form the claim. Applicants believe that this Amendment adequately addresses the Examiner's concerns, and respectfully request the withdrawal of the 102(a) and 102(b) rejections.

Claims 1-4, 6, 10-17, 29 and 31 were rejected under 35 U.S.C. § 103 (a) as being unpatentable over Oku, U.S. 5,574,042. The Examiner points out that the reference compound has a methyl in the 2-position, whereas the present compounds do not. However, the Examiner states: "At the time of the invention, one of ordinary skill in the art would have been motivated to replace the methyl with the alternative hydrogen to arrive at the instant invention with the reasonable expectation of obtaining an additional bradykinin antagonist compound ... ". Applicants respectfully disagree with the Examiner's contention for the following reasons:

The instantly claimed compounds are structurally dissimilar from the reference's teaching and their structures or synthesis are not taught by the reference. Additionally, pharmaceutical art is notoriously unpredictable. Any changes in the structure of a molecule may so drastically and significantly change the biological activity that the prediction of the utilities becomes impossible. This

fact is well known in the art. Applicants are enclosing five articles to illustrate this point:

1st illustration (EXHIBIT A): Applicants would like to bring to the attention of the Examiner the attached copy of C. Breitenlechner *et al*, *Structure*, 11, 1595-

5   1607 (December 2003), with relevant passages highlighted. The article compares two kinase inhibitors (H-1152P and HA-1077) whose structures shown on page 1596 differ only as methyl versus non-methyl compounds. As the article clearly shows, the methyl compound H-1152P shows a 200-fold increase in inhibitory activity and also a 40- to 100-fold increase in selectivity, when compared to the

10   non-methyl analog, HA-1077.

2nd illustration (EXHIBIT B): Yet another evidence to the same effect is provided by R. Capdeville *et al*, *Nature Reviews*, 1, 493-502 (July 2002). The authors, all from Novartis Pharmaceuticals (the makers of the commercial anti-cancer compound Glivec®) discuss (on page 494, left column, marked part) the

15   activity of a methyl-substituted compound (structure **c** in Fig. 1) with its non-methyl analog (structure **b** in Fig. 1). The authors state: "At this point, a key observation from analysis of structure-activity relationships was that a substitution at position 6 of the diaminophenyl ring **abolished PKC inhibitory activity completely**. Indeed, although the introduction of a simple 'flag-methyl' led to loss of activity

20   against PKC, the activity against protein tyrosine kinases was retained or even enhanced... " (bolding added). Thus, as the authors note, the substitution of a methyl for a H abolished the PKC inhibitory activity completely. Applicants submit that owing to such unpredictable nature of biological activity, neither the instant compounds nor their utilities can be predicted from the cited art, and, therefore,

25   the instant claims cannot be considered to be obvious over the art cited.

3rd illustration (EXHIBIT C): Applicants would like to bring to the attention of the Examiner the attached copy of J. Hunt *et al*, *J. Med. Chem.*, 47, 4054- 4059 (2004), with relevant data on page 4056 highlighted. This article compares the effect of changing H to methyl, among others, in the structure of pyrrolotriazines

30   on their kinase inhibitory activity. Thus, for example, compounds 13 and 16 in Table 1 in EXHIBIT C differ only as H versus methyl. As the article clearly shows,

the activity *drops* from 0.51 nM for the H-containing compound to 29.4 nM for the methyl compound, which is a huge and significant drop.

4th illustration (EXHIBIT D): Yet another evidence to the same effect is provided by G. Rewcastle *et al, J. Med. Chem.*, <u>41</u>, 742-751 (1998). Here too, the
5   effect of changing H to Me can be seen in the highlighted compounds 6b and 9b in Table 1 on page 744. When X is changed from H to Me, the kinase inhibitory activity (IC_{50}) goes *up* from 9 nM to 0.45 nM (the reverse to what EXHIBIT C shows), demonstrating the unpredictability of structural changes on biological activity.

10   5th illustration (EXHIBIT E): Yet another evidence to the same effect is provided by Y-T Chang *et al, Chemistry & Biology*, <u>6(6)</u>, 361-375 (June 1999). Here too, the effect of changing H to Me to ethyl to isopropyl to n-butyl to cyclopentyl can be seen in the highlighted compounds 1, 24, 12, 3, 2 and 21 respectively in Figure 9 on page 366. When R is changed from H to Me to ethyl to
15   isopropyl to n-butyl to cyclopentyl, the CDK2/cyclic A activity ratio changes all over the place from about 7 (see the bar chart) to about 3.8, to about 0.5, to about 1, to about 2.4, to about 0.8 respectively, demonstrating the unpredictability of structural changes on biological activity.

Therefore, Applicants want to emphasize the lack of predictability or
20   correlation between even minor structural changes (even homologs) and biological activity in a molecule. Such a change in activity can at times lead to lack of utility too in certain compounds as evidenced above. Therefore, Applicants strongly and respectfully disagree with the Examiner's contention that when two compounds differ by having a methyl group in place of hydrogen, i.e., differing as
25   homologs, such structurally homologous compounds would be expected to possess similar utilities. Withdrawal of the 103(a) rejection is, therefore, respectfully requested.

There being no other rejections pending, Applicants believe that the claims, as amended, are in allowable condition and such an action is earnestly solicited. If the Examiner has any questions, the Examiner is invited to contact the undersigned.

5

December 23, 2004
Schering-Plough Corporation
2000 Galloping Hill Road
Patent Department, K-6-1,1990
Kenilworth, NJ 07033
Tel: (908) 298-5068
Fax: (908) 298-5388

Respectfully submitted,

Dr. Palaiyur S. Kalyanaraman
Attorney for Applicants
Reg. No. 34,634

Protein Kinase A in Complex with Rho-Kinase Inhibitors Y-27632, Fasudil, and H-1152P: Structural Basis of Selectivity

Christine Breitenlechner,[1] Michael Gaßel,[2]
Hiroyoshi Hidaka,[4] Volker Kinzel,[2]
Robert Huber,[1] Richard A. Engh,[1,3,*]
and Dirk Bossemeyer[2,*]
[1]Abteilung Strukturforschung
Max-Planck-Institut fuer Biochemie
82152 Martinsried
[2]Department for Pathochemistry
German Cancer Research Center
69120 Heidelberg
[3]Department of Medicinal Chemistry
Roche Diagnostics GmbH
82372 Penzberg
Germany
[4]D-Western Therapeutics Institute
Yagota Building 2C
100-32 Yagotohonmachi
Showa-ku, Nagoya 466 0825
Japan

Summary

Protein kinases require strict inactivation to prevent spurious cellular signaling; overactivity can cause cancer or other diseases and necessitates selective inhibition for therapy. Rho-kinase is involved in such processes as tumor invasion, cell adhesion, smooth muscle contraction, and formation of focal adhesion fibers, as revealed using inhibitor Y-27632. Another Rho-kinase inhibitor, HA-1077 or Fasudil, is currently used in the treatment of cerebral vasospasm; the related nanomolar inhibitor H-1152P improves on its selectivity and potency. We have determined the crystal structures of HA-1077, H-1152P, and Y-27632 in complexes with protein kinase A (PKA) as a surrogate kinase to analyze Rho-kinase inhibitor binding properties. Features conserved between PKA and Rho-kinase are involved in the key binding interactions, while a combination of residues at the ATP binding pocket that are unique to Rho-kinase may explain the inhibitors' Rho-kinase selectivity. Further, a second H-1152P binding site potentially points toward PKA regulatory domain interaction modulators.

Introduction

Protein kinases are phosphorylation enzymes that control cellular signaling events and accordingly may cause a wide range of diseases when defective. Since they are typically active only when signaling, most of the diseases associated with protein kinase deregulation (including the majority of all cancers) arise from excess activity due to mutation, overexpression, or disabled cellular inhibition. Other protein kinases contribute to disease in the course of their normal function in cellular

*Correspondence: d.bossemeyer@dkfz.de (D.B.), engh@biochem.
mpg.de (R.A.E.)

processes such as cell survival or cell migration. The prevalence of kinases to cause or augment disease underscores the need for therapeutic protein kinase inhibitors, with the caveat that they must be highly selective for their disregulated targets to avoid inhibition of other ubiquitous but essential protein kinases. Several protein kinase inhibitors have been approved for human treatment or are in advanced clinical trials. The first was fasudil (HA-1077 or AT877), which was approved in 1995 for the treatment of cerebral vasospasm, a painful and potentially deadly result of subarachnoid hemorrhage. Fasudil has significant vasodilatatory activity (Ono-Saito et al., 1999) and is now undergoing clinical trials for the treatment of angina pectoris (Shimokawa et al., 2001). Fasudil's activity has been attributed to inhibition of Rho-kinase (Matsui et al., 1996) and its role in signaling for myosin light chain phosphorylation and arterial smooth muscle contraction (Amano et al., 1996), although the in vitro activity of fasudil is not strictly limited to Rho-kinase. Other Rho-kinase-related protein kinases, such as PKA, PRK2, MSK1, and S6K1, are also inhibited by fasudil, although to a lesser extent (Davies et al., 2000). Fasudil is related to H7, an isoquinoline sulfonamide derivative that is a weak PKC inhibitor (Hidaka et al., 1984) and whose protein kinase binding mode was shown by the cocrystal structure with PKA (Engh et al., 1996). Fasudil has a heptameric homopiperazine ring at the position of the methyl-piperazine ring of H7 (Figure 1). Further derivitization of fasudil led to H-1152P, with two additional methyl groups, one at the isoquinoline ring and the other at the homopiperazine ring (Tanaka et al., 1998). H-1152P has a better inhibitory profile than HA-1077, with a K_0 value for Rho-kinase in the low nanomolar range and a reportedly enhanced selectivity (Tanaka et al., 1998; Sasaki et al., 2002). Rho-kinase may be an important pharmacological target also for cancer because of its role in the phosphorylation of focal adhesion kinase (Sinnett-Smith et al., 2001) and the invasion and migration of cancer cells (for reviews, see Fukata et al., 2001; Amano et al., 2000). Regarding the latter, Itoh et al. (1999) showed that the migration of rat MM1 hepatoma cells was prevented by the Rho-kinase inhibitor Y-27632. As a pyridine derivative, Y-27632 differs in its chemical structure from H inhibitors described above. It has a K_0 of 140 nM for Rho-kinase and 25 μM for PKA (Ishizaki et al., 2000) and is ATP competitive, like the H inhibitors (Trauger et al., 2002; Ikenoya et al., 2002).

Crystal structure analyses of protein kinase inhibitor complexes reveal the intermolecular interactions responsible for ligand binding and thereby enable structure-based rational design and optimization of kinase inhibitors. To date, crystal structures have been determined for some 30 protein kinases, representing less than 6% of the 518 protein kinases in the human genome (Manning et al., 2002). Many of these structures have been complexes with protein kinase inhibitors, but most have shown an inactive state. As a serine-threonine kinase of the AGC group, Rho-kinase possesses a cata-
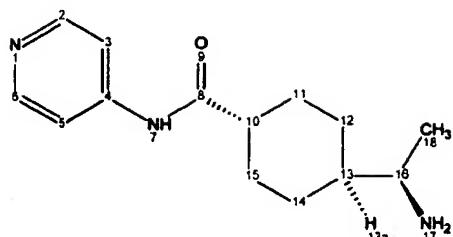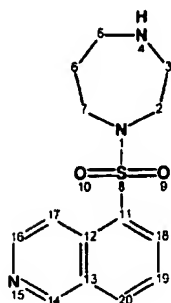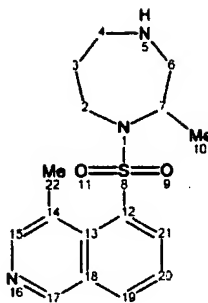
Y-27632

HA-1077   H-1152P

Figure 1. Chemical Structures of the inhibitors Y-27632, HA-1077, and H-1152P

lytic domain closely related to other AGC group kinases, among them PKA, PKB, PKC, and PKG, although no crystal structure of Rho-kinase has been reported. The close relationship between PKA and Rho-kinase and the well established crystallization conditions for PKA make PKA a suitable model system for studying Rho-kinase inhibitors. Furthermore, cocrystallization of PKA with Rho-kinase inhibitors helps identify factors governing cross selectivity of protein kinase inhibitors, a major concern in protein kinase inhibitor design.

The ATP binding site residues conserved between PKA and Rho-kinase include Phe327 (PKA numbering). This residue is a characteristic but not absolutely conserved feature of the AGC group of kinases. It is positioned on the C-terminal polypeptide strand which stretches between the α helical catalytic domain lobe and the C-terminal anchor in the hydrophobic motif. Phe327 shields one side of the ATP pocket and lies adjacent to the adenine of ATP and aromatic groups of ATP-site inhibitors (Prade et al., 1997; Engh et al., 1996). Rho-kinase and PKA differ, however, in eight positions in the ATP binding pocket (Figure 2). Four of their side chains are in close (<4 Å) contact with the inhibitors, corresponding to the following PKA→Rho substitutions: Leu49Ile, Val123Met, Thr183Ala, and Glu127Asp. Because the protein kinase fold is so highly conserved, variations of amino acid residues that line the ATP subsite belong to the most important factors in defining inhibitor selectivity. Here we describe the crystal structures of PKA in complex with HA-1077 (at 2.2 Å resolution), with H-1152P (1.9 Å), and with Y-27632 (2.0 Å) and

analyze the factors governing their relative affinities for PKA and Rho-kinase. The structures identify the binding interactions of the inhibitors in the ATP pocket. The surface areas of the inhibitor/PKA interface correlate well with their inhibitory activities. Furthermore, the specific sequence differences between PKA and Rho-kinase provide an explanation for the observed higher affinity of these molecules for Rho-kinase. On the basis of these structural data, we propose models for the Rho-kinase-specific binding modes that rationalize the roles of the unique combination of amino acid residues found in the Rho-kinase ATP binding pocket. In addition, a second, well ordered H-1152P molecule was observed in a surface region with contact to the phosphoryl group of Thr197 and to Lys189, both from the activation loop, and to Glu86 from Helix C, a region critical for kinase activity and protein-protein interaction.

Results and Discussion

Overall Structure
The PKA complexes with Rho-kinase inhibitors Y-27632 (PKA-Y), fasudil or HA-1077 (PKA-1077), and H-1152P (PKA-1152) were cocrystallized as ternary complexes with the recombinant catalytic subunit of cyclic AMP-dependent protein kinase (PKA) and the pseudo-substrate kinase inhibitor peptide [PKI(5-24)]. All three inhibitor complexes crystallized in the orthorhombic space group $P2_12_12_1$. The PKA-1152 and PKA-Y crystals have similar cell constants (ca. 74.1, 76.6, 81.0) and the same crystal packing arrangement (Table 1). PKA-1077 has slightly different cell constants (70.33, 73.67, 79.08) and different crystal contacts. The inhibitor molecules occupy the ATP binding site; H-1152P binds additionally at a second site bounded by pThr197, helix C residues, and residues from the PKI(5-24) peptide of a symmetry related molecule. Apart from that, no direct contacts exist between any of the inhibitors and PKI(5-24).

Open and Closed Conformations
Ligand-induced conformational changes have been well documented for PKA (Prade et al., 1997; Johnson et al., 2001). Foremost among these are variations in the relative orientations of N- and C-terminal lobes, whose interface creates the ATP binding pocket. The "openness" of the pocket ranges from "closed" for PKA structures with bound ATP or AMPPNP (PDB code 1ATP, 1CDK) in the presence of pseudosubstrate, "closed" or "intermediate" for various inhibitors, to "open" for unliganded PKA (PDB code 1J3H; Akamine et al., 2003). The extent of openness can be quantitatively characterized by using several parameters. One is the occurrence of a hydrogen bonding distance between NE2 of His87 from helix C and pThr197 (O3P) of the activation loop in the closed conformation. By this measure, the structures of PKA-Y and PKA-1152 (Figure 3, green ribbon, 2.5 Å; yellow ribbon, 2.6 Å) represent closed lobe structures, whereas the PKA-1077 structure is—with a 4.6 Å separation—an open structure (Figure 3, red ribbon).

Glycine Loop
The flexibility of the glycine loop is demonstrated by relatively high B factors and by the occurrence of dif-
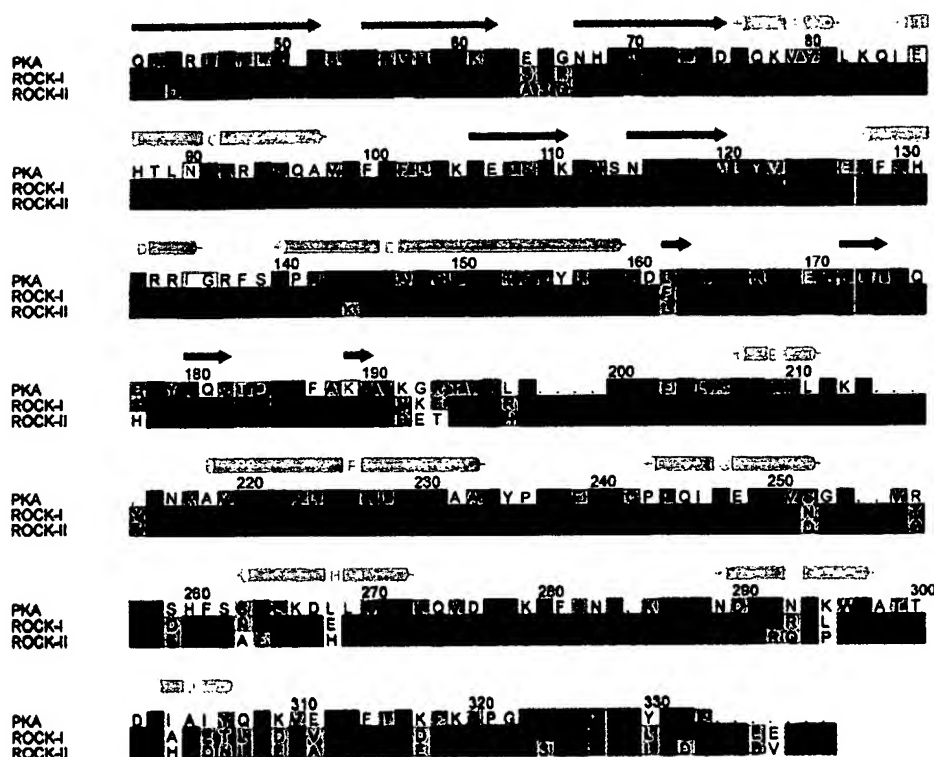
Figure 2. Sequence Alignment of PKA and the Highly Similar Rho Kinase Family Members ROCK-I and ROCK-II

Blue backgrounds indicate identical residues whereas brown indicates conservative exchanges. Secondary structure elements of PKA (from Bossemeyer et al., 1993) are indicated above the PKA numbering. The most highly conserved kinase residues are shown in red letters. Inhibitor contacts are marked with light violet letters and boxes. Additionally, contacts with H-1152P in the second binding site are indicated in green.

ferent positions in all three structures. The differing positions create ATP ligand binding sites that are progressively more open among structures 1CDK (PKA/ PKI(5–24)/MnAMP-PNP) (Bossemeyer et al., 1993), PKA-Y, PKA-1152, and PKA-1077 (3, 4) (Figure 3C, blue, green, yellow, and red ribbon, respectively). There is also evi-

Table 1. Data Collection and Refinement Statistics

	Y-27632	H-1152P	HA-1077
Data Collection			
Space group	P2₁2₁2₁	P2₁2₁2₁	P2₁2₁2₁
Cell (a, b, c) (Å)	74.0, 76.6, 80.7	74.2, 76.4, 81.8	70.3, 73.7, 79.1
Resolution range (Å)	15.8–2.0	10.91–1.9	20–2.2
Completeness (%) [last shell]	97.8 [88.7]	91.8 [56.0]	82.4 [59]
I/σ(I) [last shell]	4.2 [1.4]	7.5 [0.6]	7.5 [1.3]
R$_{sym}$ [last shell]	0.12 [0.50]	0.06 [0.51]	0.10 [0.34]
Refinement			
Number of atoms used in refinement	3104	3245	2914
R factor (%)	18.1	17.9	21.7
Free R factor (%)	22.9	21.7	29.3
Free R value test size (%)	10.1	5.0	5.0
Reflections used	27,774	32,327	16,761
Standard Deviation from Ideal Values			
Bond length (Å)	0.016	0.017	0.021
Bond angles (°)	1.440	1.491	1.83
Temperature Factors			
All atoms	39.4	25.1	24.4
Main chain/side chain atoms PKA	37.6/40.0	22.9/25.5	23.1/25.2
Main chain/side chain atoms PKI	32.8/36.7	21.0/23.9	26.6/29.8
Inhibitor atoms	38.3	33.3	23.2
Solvent molecules	50.3	36.6	25.8
Inhibitor atoms (second)		21.2	
Detergent		43.3	

A

B

C
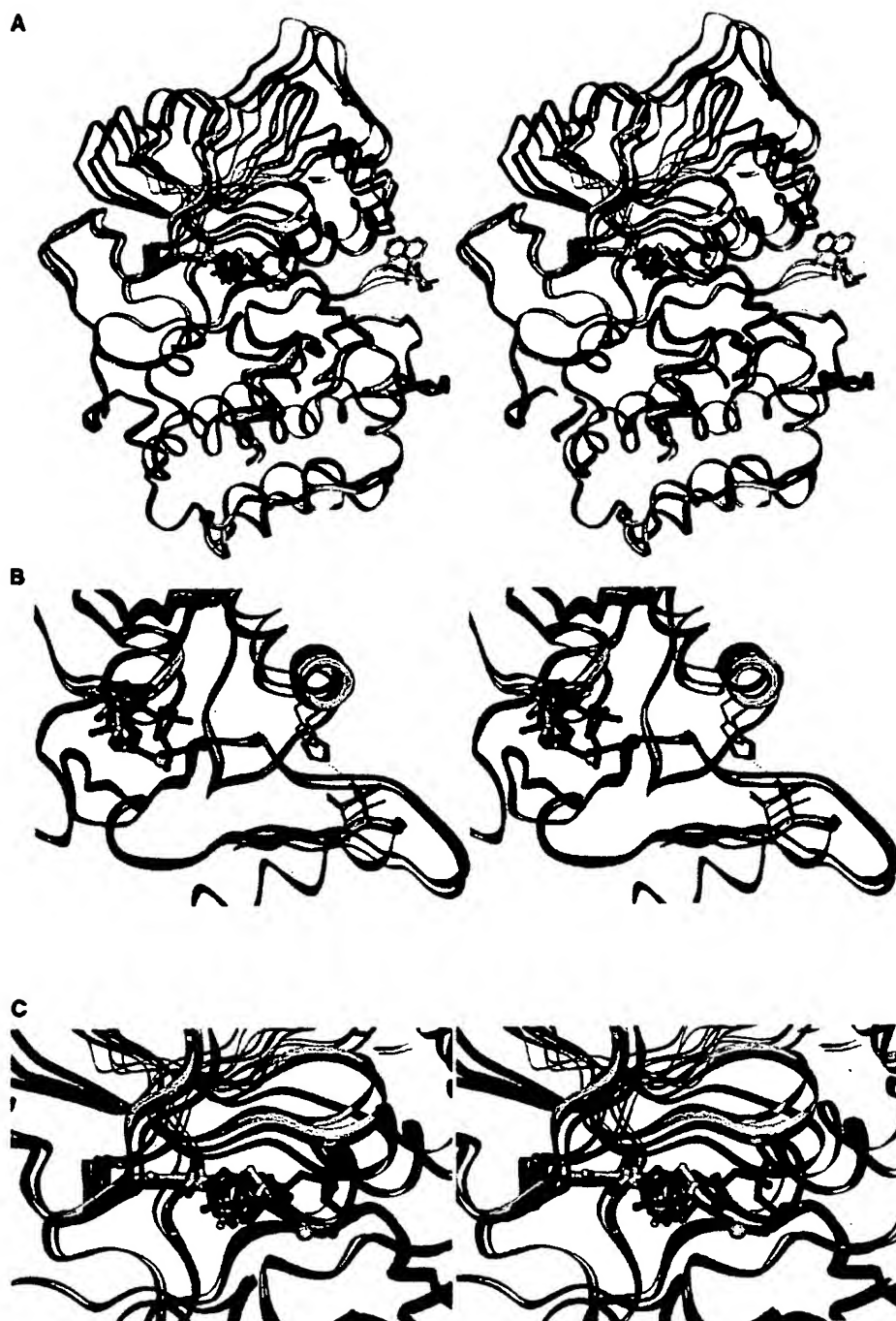
Figure 3. Binding of the Inhibitors to PKA

(A) Open-closed conformations illustrated by an overlay of all three inhibitor structures (Y-27632, green; HA-1077, red; H-1152P, yellow) and the PKA-AMP-PNP (1CDK) complex (blue) for comparison.

(B) In the PKA-HA1077 structure, helix C is further away from the activation loop, and the salt bridge His87-pThr197 is not formed.

(C) A closer view of the binding pocket shows the inhibitor binding modes relative to AMP-PNP and the positions of the flexible glycine-loop. The inhibitor molecules occupy both the adenine and the ribose pocket, but not the triphosphate binding site.

dence for multiple conformations of the glycine flap within a single crystal (data not shown). PKA-Y electron density maps suggest the partial occupancy of a more closed position of the glycine flap (especially involving tum residues Ser53-Phe54-Gly55), similar to that previously observed with the H7 and H8 inhibitor complex structures of PKA (Engh et al., 1996). Because none of the cocrystallized inhibitors occupies this site, they do

not have the structuring effect of the triphosphoryl group of ATP with its contacts to the glycine loop.

Inhibitor Binding

The chemical structures of the three inhibitors are shown in Figure 1. They originate from two different chemical classes but share the general architecture of a planar ring system linked to a saturated ring. In the case of Y-27632, a pyridine ring is connected by an amide to a saturated para-aminoethyl cyclohexane ring. HA-1077 and its derivative H-1152P share the basic scaffold of an isoquinoline ring connected to a homopiperazine ring by a sulfonamide linker. Compared to HA-1077, H-1152P has two additional methyl groups, one at the isoquinoline ring and another at the homopiperazine ring. These two methyl groups are thus responsible for the unique binding properties of the derivative. The planar ring systems occupy the adenine subsite, while the linker and the saturated rings occupy the ribosyl subsite. The triphosphate subsite is not used by any of the inhibitors (Figures 3C and 4).

Figure 4 shows the inhibitors in the ATP pocket and the F_o-F_c electron density maps with the inhibitor atoms omitted contoured at 2.5σ. Y-27632 is well defined in the electron density (Figure 4A), which, however, does not uniquely identify the orientation of the cyclohexane ring chair conformer (see next paragraph). The typical intrinsic flexibility of the seven-membered homopiperazine rings of HA-1077 and H-1152P is reflected in less well defined electron densities in this region (Figures 4B and 4C). The electron density of H-1152P (Figure 4C) has gaps in portions of the homopiperazine ring too, contradicting expectations that the two extra methyl groups should stabilize the ring conformations relative to HA-1077. In contrast, the homopiperazine ring of the H-1152P inhibitor bound outside the catalytic cleft close to Thr197 of the activation loop binds with a clearly defined electron density for the whole inhibitor (Figure 4D).

Binding of Y-27632

With a K_D value of 17.5 ± 3.87 μM by surface plasmon resonance spectroscopy (SPR) and a 25 μM K_i value from previous kinetic data (Uehata et al., 1997), Y-27632 has the weakest PKA inhibition of the compounds studied here (Table 2). For Rho-kinase, however, Y-27632 has a K_i value of 140 nM. This pronounced selectivity for Rho-kinase is further emphasized by data showing that Y-27632 inhibited only one other protein kinase (PRK2) from a panel of 34 kinases with similar potency (Davies et al., 2000).

Despite the relatively weak PKA inhibition, Y-27632 cocrystallized readily and is clearly localized in the electron density, although two orientations of a chair conformer of the cyclohexane ring are possible (Figure 4A). To analyze the binding of Y-27632 to PKA, we considered binding surfaces and hydrophobic (van der Waals), and hydrophilic (H bonds) interactions for both conformations (see Tables 3–5). The buried surface areas (188 or 189 Å^2) and numbers of van der Waals contacts (64 or 67) are similar for the two conformations. The van der Waals contacts are formed to residues from the ATP

binding pocket, especially to the invariable Val57 with 9 or 10 side chain contacts and to the more variable Val123 with 12 contacts. Four contacts are formed to Phe327, the residue characteristic of the AGC kinases that is inserted into the ATP pocket from the C-terminal strand of the kinase. The two conformations differ most at the terminal aminoethyl group, which adopts either one H bond between N17 and the backbone carbonyl oxygen of Thr51 (2.83 Å) (Table 4; Figure 5A), or a H bond with Asn171 (OD1) (2.89 Å) and Asp184 (OD1) (2.93 Å) (Table 4). The pyridine ring in both conformations forms a H bond between pyridine nitrogen atom N1 and backbone nitrogen of Val123 (2.93 Å) (Figure 5A), the hydrogen bond donor at the hinge region between the N- and C lobes that binds to nearly all known ATP-site inhibitors (Engh and Bossemeyer, 2001). Y-27632 also binds via water molecules sandwiched between N7 and the carboxylate of Glu127 and the backbone carbonyl of Leu49.

HA-1077

As described in the introduction, HA-1077, also known as fasudil, is used to treat cerebral vasospasm and works via Rho-kinase inhibition. However, it also inhibits several other kinases in the μM range (Davies et al., 2000). Our SPR data show a K_D value of 5.7 μM for PKA; published data include a K_i value of 1.0 μM (Ikenoya et al., 2002) (Table 2). HA-1077 makes three H bonds to PKA (Figure 5B; Table 4). Like other isoquinoline inhibitors (Engh et al., 1996), one H bond is formed between the isoquinoline N (N15) to the backbone N of Val123 (2.8 Å). The homopiperazine amine (N4) forms H bonds with the backbone carbonyl oxygen of Glu170 (3.25 Å) and the side chain of Glu127 (OE2) (2.69 Å), the latter at the position of the ribose 3'OH group in the ATP-PKA complex (Bossemeyer et al., 1993). A Glu127-inhibitor contact was observed for staurosporine (Prade et al., 1997), but not with the other isoquinoline sulfonamide inhibitors (Engh et al., 1996). A total of 81 van der Waals contacts are formed to the residues of the ATP pocket. Most contacts are to Val123 (13), Val57 (11), and Thr183 (11) (Table 4).

H-1152P

H-1152P is a derivative of HA-1077 with enhanced specificity for Rho-kinase (Sasaki et al., 2002). For PKA, it has a K_D (SPR) or K_i (Ikenoya et al., 2002) value of 1.06 or 0.63 μM, respectively (Table 2). With a K_i of 1.6 nM, H-1152P inhibits Rho-kinase potently (Sasaki et al., 2002; Ikenoya et al., 2002). The H-1152P molecule that binds to the ATP pocket makes only one H bond contact (from the isoquinoline N [N16] to the backbone NH of Val123 [3.0 Å]) (Figure 5C; Table 3). As with the other inhibitors described here, Val57 and Val123 are involved in many van der Waals contacts; in contrast to the other two inhibitors, Leu173 and Leu49 additionally form many contacts (Leu173: 12 with H-1152P versus 2 with HA-1077; and Leu49: 8 with H-1152P versus 2 with Y-27632 and 4 with HA-1077).

In its second binding site close to helix C and the activation segment, H-1152P makes five H bond contacts, three to the Thr197-phosphoryl group in the acti-
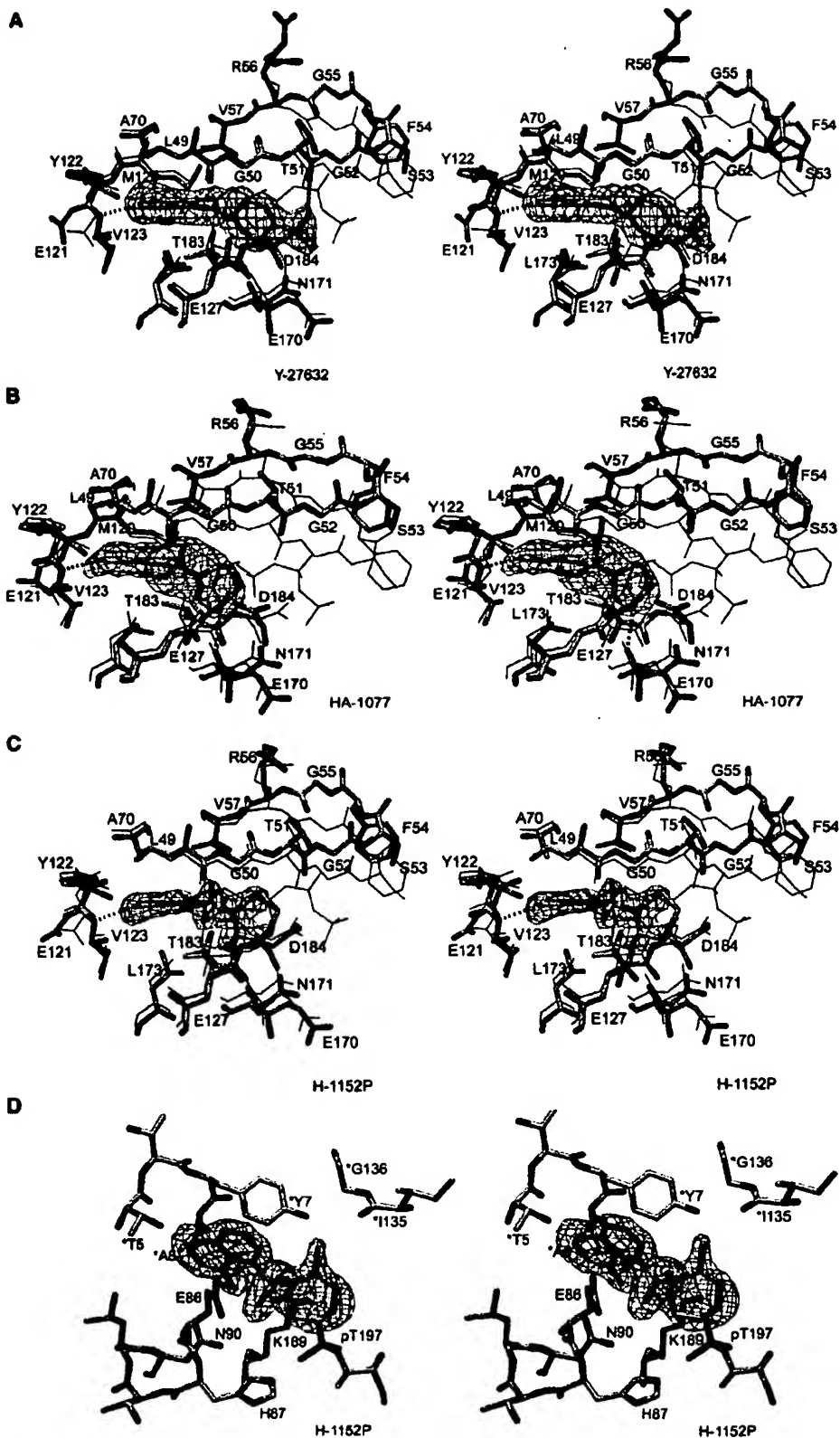
A

Y-27632

Y-27632

B

HA-1077

HA-1077

C

H-1152P

H-1152P

D

H-1152P

H-1152P

Figure 4. Structure of Inhibitor Binding Sites with Electron Density Maps

Shown are the three PKA bound inhibitors with corresponding F_o-F_c electron density maps (inhibitor atoms omitted) contoured at 2.5σ. Amino acid residues in the vicinity of the inhibitors are shown. H bonds between inhibitor atoms and enzyme residues are depicted as dotted lines. The PKA-PKI-AMP-PNP complex is drawn as fine black lines. Inhibitors (A) Y-27632, (B) HA-1077, and (C) H-1152P bind in the ATP pocket. (D) The second H-1152P molecule, which occupies a binding site at the enzyme surface in contact with the activation loop and helix C, is well ordered, indicated by its well defined electron density. (Residues from a symmetry-related molecule are colored yellow.)

Table 2. Inhibitor Binding Properties

Inhibitor	Y-27632	HA-1077	H-1152P
K_D PKA	17.5 ± 3.9 μM	5.7 ± 1.2 μM	1.1 ± 0.1 μM
K_i PKA[a]	25 μM	1.0 μM	0.63 μM
K_i RHO[a]	0.14 μM	0.33 μM	0.0016 μM
Buried surface	188(189)	196.4	215.7
VDW contacts	64(67)	81	96
H bonds	2(3)	3	1

K_D values from surface plasmon resonance spectroscopy (SPR) analysis, Chi² smaller than five, two independent experiments. Inhibition constants correlate well with the buried surface and number of van der Waals (VDW) contacts but not with number of H bonds. [a]K_i values from literature (Ikenoya et al., 2002; Sasaki et al., 2002).

vation loop, one to Lys189 also of the activation loop, and one to Thr5 of PKI(5-24) from a symmetry-related molecule (Figure 5D). The inhibitor is embedded in a network of water molecules, thus making additional contacts via water to Asn90 from helix C and Thr195 from the activation loop. In this activation loop binding site, the inhibitor electron density is well connected and verifies a unique conformation of the homopiperazine ring with no apparent disorder (Figure 4D). Significant van der Waals contacts are made to the side chain of Glu86 from helix C, which changes its side chain conformation (compared to 1CDK) to accommodate the inhibitor. Further binding studies are necessary to determine the relevance of the second binding site in solution.

Binding Specificities of Y-27632, HA-1077, and H-1152P

Comparison with the Mn^{2+}-AMP-PNP complex identifies only small induced-fit movements of ATP pocket residues associated with binding of the three inhibitors. The side chain of Asp184, which chelates a metal ion in the active complex, is oriented toward the opening of the active side cleft in the AMP-PNP complex and in the PKA-Y or PKA-1152 structure. In the PKA-1077 structure, however, Asp184 adopts a different rotamer (Figure 5B), which points toward the homopiperazine

ring, increasing van der Waals contacts and apparently enhancing hydrophobic effect binding. A similar reorientation of this side chain was observed in the H8-inhibitor complex of PKA (Engh et al., 1996), where Asp184 makes an H bond contact to the amide of the inhibitor side chain. Thr183 and Leu173 in the PKA-Y structure apparently have two conformations that were each modeled with an occupancy of 0.50 (data not shown). These two amino acid residues interact with each other by van der Waals contacts which limit their degree of conformational freedom, indicating mutually dependent rotamer conformations and a concerted induced fit movement.

The three inhibitors bind with moderate binding strengths to PKA. Their differing affinities (Table 2) correlate with the different numbers of van der Waals contacts and with the contact surface area between the inhibitors and enzyme residues (buried surface) (Table 2). H-1152P, which has the highest affinity for PKA, also has the highest number of van der Waals contacts and the largest buried surface (215.7 Å²). Y-27632, with the weakest PKA binding, has the smallest total number of van der Waals contacts and a buried surface area of 189.9 Å². A relationship of buried surface areas and affinities of PKA inhibitors has been noted previously (Engh and Bossemeyer, 2002). The simplest measure of hydrophilic binding interactions—the number of inhibitor-protein H bonds—does not correlate with PKA binding affinities. This is typical of enzyme inhibitors and reflects the existence of competing hydrophilic interactions in inhibitor solvation. H-1152P possesses only a single H bond from its isoquinoline ring to Val123 in the hinge region. This H bond to Val123 or its equivalent is nearly universal among protein kinase-inhibitor complexes and exists in all PKA-inhibitor complexes crystallized so far (Narayana et al., 1999; Prade et al., 1997; Engh et al., 1996). Indeed, a survey of ligand binding properties from protein kinase crystal structures in the protein data bank identifies only two inhibitors that lack such an interaction, namely CK2/Emodin (1F0Q) (Battistutta et al., 2000) and p38/BPU (1KV1). All other ligands make one, two, or three H bonds to the hinge polypeptide, i.e., always one to the hinge region backbone amide of the Val123

Table 3. Van der Waals Contacts of the Inhibitors to PKA Enzyme Residues

Residue	Y Chain1	Y Chain2	HA-1077	H-1152P	Interaction via
L49	2	2	4(1p*)	8(1p*)	main chain/side chain
G50	—	1	2	4(1p*)	main chain
T51	3	3	—	5	main chain
V57	9	10	11	12	side chain
A70	4	4	6	7	side chain
M120	1	1	4	4	side chain
E121	2(1p*)	2(1p*)	3(1p*)	3(1p*)	main chain
Y122	6	6	7	6	main chain/side chain
V123	12	12	13	10(1p*)	main chain/side chain
E127	—	—	4	4(2p*)	side chain
E170	2	2	2	4	main chain
N171	6	4	2	2	main chain/side chain
L173	5	6	2	12	side chain
T183	4(1p*)	6(1p*)	11	7	side chain
D184	4	4	4	—	side chain
F327	4	4	6	8	side chain
Total	64(2p*)	67(2p*)	81(2p*)	96(6p*)	

Residues that have side chain contacts with the ATP-site ligands and differ between Rho-kinase and PKA are in bold.
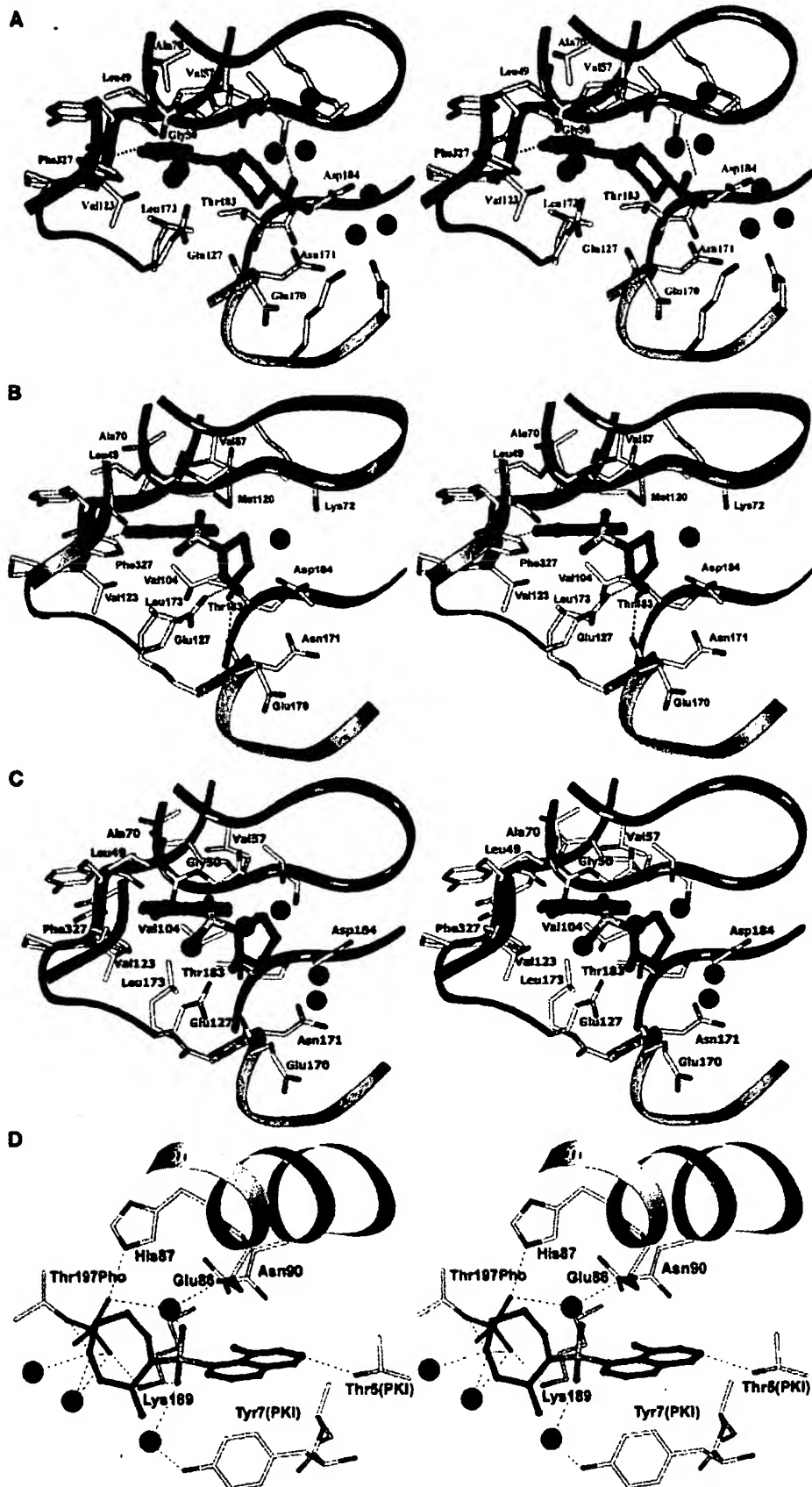
Figure 5. Inhibitor Binding Modes

Binding of Y-27632 (A) and HA-1077 (B) to PKA to the ATP binding site. H-1152P binds in two positions: (C) in the ATP binding site and (D) in a second binding site at the surface interacting with the activation loop and helix C in a crystal contact region.

Table 4. H Bonds between Inhibitor Atoms and PKA Enzyme Residues

H Bonds	Inhibitor Atom	PKA Residue and Atom	Distance (Å)	Interaction via
Y-27632 chair 1	N1	Val123(N)	2.9	main chain
	N17	Thr51(O)	2.8	side chain
Y-27632 chair 2	N1	Val123(N)	2.9	main chain
	N17	Glu171(OD1)	2.9	side chain
	N17	Asp184(OD1)	2.9	side chain
HA-1077	N15	Val123(N)	2.8	main chain
	N4	Glu170(O)	3.3	main chain
	N4	Glu127(OE2)	2.7	side chain
H-1152P	N16	Val123(N)	3.0	main chain

H bonds between inhibitor and PKA atoms are listed together with the distance (in Å) and information about main chain or side chain interaction.

homolog, and, in addition, further contacts to the homologs of the Val123 and/or Glu121 carbonyl atom(s). This interaction is conserved despite the wide chemical diversity of small molecule protein kinase inhibitors. Thus the interaction is critical for good inhibitors, or conversely stated, the kinase is apparently unable to compensate for the desolvation of the Val123NH equivalent group if a potential inhibitor lacks the appropriate hydrogen bond acceptor. Hydrogen bonds from other residues that bind to the adenosine group of ATP appear to be of less importance for protein kinase inhibitor binding. Two H bonds that are formed between the ribosyl hydroxyl groups of AMP-PNP and the Glu127 carboxyl and the Glu170 main chain carbonyl groups have counterparts in the PKA-1077 structure. The presumably doubly protonated secondary amine (N4) of HA-1077 forms hydrogen bonds both to the carboxyl group of Glu127 and to the backbone carbonyl of Glu170. In the case of H-1152P, these contacts are not formed, because contacts between Thr183 and Leu173 of the enzyme and homopiperazine methyl group (C10) of the inhibitor apparently shift the heptamer ring by ca. 1.5 Å in comparison to HA-1077. Consequently, the distances to E170(O) (4.2 Å) and E127 (OD1) (3.57 Å) are too large for tight H bonds. The overlay of the two structures in Figure 6 shows the colocalization of the isoquinoline atoms with respect to the surrounding residues, and the divergent positions of the homopiperazine rings. Although H-1152P makes only one hydrogen bond to the enzyme, the two extra methyl groups increase the number of van der Waals interactions (Table 3) and enlarge the buried surface area, which probably leads to the enhanced affinity of H-1152 in comparison to HA-1077.

The Second Binding Site of H-1152P

The second molecule of H-1152P in PKA-1152P is found in contact with the activation segment and helix C, the two structural elements critical for protein kinase inactivation (Engh and Bossemeyer, 2001), which suggests a potential for activity modulation. Because the residues in contact with this second inhibitor molecule are not conserved between PKA and Rho-kinase, the observed second H-1152P binding site likely appears to be unique for PKA. Further, this site is an important contact region for protein-protein interaction with the regulatory subunits of PKA (Orellana et al., 1993; Gibbs et al., 1992). Occupation of this site with a small molecule derivative could provide a means to abolish negative regulation of PKA by the R subunits. If this site could be explored

more generally as a docking site for small molecules in drug design, other important interactions, for example cyclin binding to cyclin-dependent kinases, could be targeted as well.

Comparison of the Rho-Kinase and PKA Ligand Binding Sites

Although the three inhibitors bind and inhibit PKA, all of them bind Rho-kinase more tightly than PKA. Because of the high conservation of the protein kinase fold, especially for closely related kinases, one can assume that the side chains that are nearest to the inhibitor are the major determinants of selectivity. The sequence alignment of the kinase domains of Rho-kinase and PKA (Figure 2) show either conservation (blue coloring) or conservative exchanges (beige coloring) over large parts of the kinase domain. Rho-kinase has several exchanges relative to PKA, but only four of them make side chain interactions with the inhibitors: Thr183Ala, Leu49Ile, Val123Met, and Glu127Asp. These exchanges very likely are responsible for the effects of the extra methyl groups of H-1152P compared to HA-1077 on specificity toward Rho-kinase. The two methyl groups lead to a 200-fold higher affinity for Rho-kinase (Table 2), but only a 2- to 5-fold higher affinity for PKA, or in other words, cause a 40- to 100-fold increase in selectivity.

The residues nearest to the H-1152P methyl groups are Leu49, Leu173, Thr183, and Phe 327, thus involving directly two of these four PKA to Rho-kinase exchanges, and one residue (Phe 327) specific for most AGC kinases. The Thr183Ala substitution would provide more room for the C10 methyl group and possibly allow more rotamer conformations of Leu173. The interactions of C10 with Thr183 and Leu173 in PKA appear to force the H-1152P homopiperazine away from its position in the PKA-1077 structure (Figure 6), presumably at some energy cost. The exchange of Thr183Ala in Rho-kinase would, however, allow the homopiperazine to retain its preferred binding orientation. Consequently, H-1152P might be able to form hydrogen bonds to both the Glu170 homolog and to the aspartyl residue occupying the Glu127 homologous position in Rho-kinase. Although the side chain of the aspartyl is shorter by one methylene group, this should not affect its ability to hydrogen bond a homopiperazine nitrogen in a position similar to that of HA-1077 in PKA.

The effect of the Leu49Ile exchange is more difficult to evaluate because of the number of possible rotamer
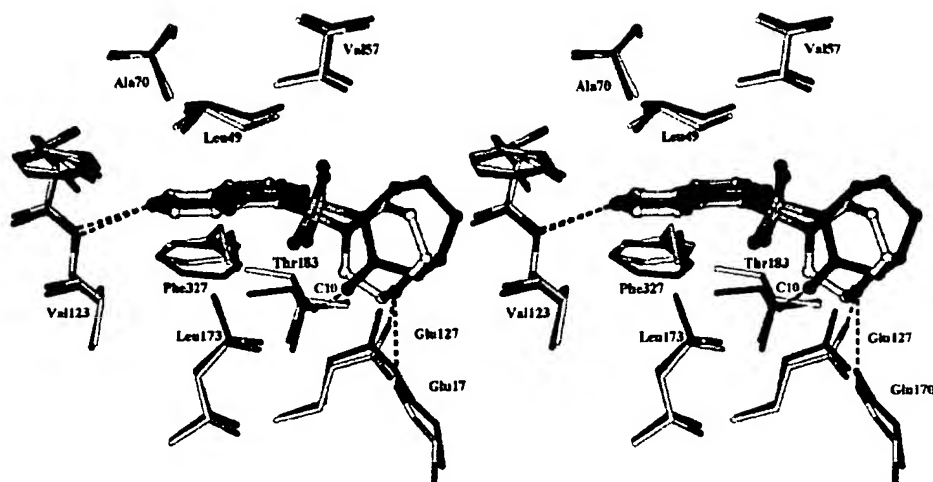
Figure 6. Comparison of HA-1077 and H-1152P

Overlay of HA-1077 and H-1152P demonstrates the colocalization of the isoquinoline atoms with respect to the surrounding residues. Both inhibitor molecules form an H bond to the backbone amide of Val123 in the hinge region. The position of the homopiperazine rings, however, diverge by ca. 1.5 Å. Consequently, H bonds between the homopiperazine nitrogen and Glu127 and Glu170 are formed only in the PKA-1077 complex. The contact between C10 and Thr183, which prevents as a steric clash a HA-1077-like positioning of the H-1152P homopiperazine ring, is shown as a red double arrow.

conformations of the isoleucine residue. Most rotamers of an isoleucine modeled into the Leu49 position increase the number of interactions with the inhibitor or cause steric clashes with the inhibitor isoquinoline sulfonamide moiety. Because of the branching of the isoleucine side chain at the Cβ, in contrast to a leucine residue, the inhibitor binding pocket is narrowed in the expected binding region of the isoquinoline methyl and sulfonamide groups, also close to the Phe327 homolog; this appears to favor H-1152P binding. It is likely that the isoquinoline methyl group of H-1152P then additionally contributes to a productive interaction by a mutual increase in the number of van der Waals interactions with the isoleucine side chain.

How or even whether the Val123Met exchange might affect binding selectivity is unclear. A relatively large number of van der Waals contacts (Table 3) are formed to all three inhibitors. A methionine residue is found at this position in several kinases with known structures, including Erk, p38, Src, and Abl. In all these cases, the methionine side chain is oriented away from the adenosine subsite, providing little contact beyond the Cγ atom. By analogy, this methionine side chain therefore is not likely to be a major factor in H-1152P specificity for Rho-kinase. In addition, a large number of van der Waals contacts are found with the residue Phe327, which is conserved in most members of the AGC group of protein kinases. Phe327 makes attractive additional interactions with the isoquinoline extra methyl group of H-1152P in PKA, compared to HA-1077.

Taken together, the higher affinities of HA-1077 and H-1152P for Rho-kinase—and the especially strong binding of the H-1152P derivative to Rho-kinase—can be explained largely by three factors: the Thr183Ala exchange and the concomitant relaxation of the steric clash between the inhibitor C10 methyl group and Thr183 and Leu173 (Figure 6). This in turn allows the

inhibitor to bind with the optimal geometry and hydrogen bonding pattern as observed for HA-1077 in PKA. Further, the exchange Leu49Ile presumably optimizes the van der Waals interactions—i.e., inhibitor fit—because of the position of the branch in the side chain. Whether additional effects arise from the Val123Met exchange remains to be seen. Last but not least, the AGC-kinase typical Phe327 residue makes attractive contacts with all inhibitors, but especially with the C22 extra methyl group of H-1152P.

The higher affinity of Y-27632 for Rho-kinase is more difficult to rationalize based on sequence considerations. One determinant is probably the Leu49Ile exchange. The shorter branched methyl group is likely to provide additional van der Waals interactions with three different parts of the inhibitor molecule, thereby increasing the overall binding surface area and improving the quality of the fit. The absence of steric clashes in the region of Thr183 (and Glu127), however, obscures analysis of possible contributions of the corresponding exchanges at these positions to the higher affinity of Y-27632 in Rho-kinase. Regarding the Val123Met exchange, the likelihood that it is oriented away from the inhibitor as discussed above leads to the conclusion that Rho-specific interactions with the Met side chain are possible but unlikely. A similar compound, Y-30141, which differs from Y-27632 by a pyrrolopyridine ring replacing the pyridine ring, has a similar inhibitory profile, but a 10-fold higher affinity for Rho-kinases (Ishizaki et al., 2000). Its selectivity, i.e., the ratios of the IC50 for Rho-kinase to that for other kinases, however, is about 10-fold lower. In the binding pocket, the extra pyrrolidine group is likely to make one additional hinge region contact with its proton donor in the five ring, either to the carbonyl of Glu121 (PKA numbering) or, if rotated 80°, to the carbonyl of Val123. The higher affinity can also be explained by the larger surface of the planar double

Table 5. Conservation of Residues in the Binding Pocket that Differ between PKA and Rho-Kinase

Residue in PKA	PKA	No.*	%	Rho kinase	No.*	%	Contact
49	Leu	241	49.1	Ile	186	37.9	**side chain/backbone**
51	Thr	18	3.7	Arg	71	14.5	backbone only
123	Val	76	15.5	Met	123	25.1	**side chain/backbone**
127	Glu	76	15.5	Asp	158	32.2	**side chain**
170	Glu	140	28.5	Asp	59	12.0	backbone only
183	Thr	76	15.5	Ala	142	28.9	**side chain**

Shown are residues in contact with the inhibitors that differ between PKA and Rho-kinase according to the alignment from www.kinase.com (Manning et al., 2002). The total number of kinases in the alignment is 491. The number (No.*) as well as percentage (%) of kinases with the same corresponding residue (numbering according to PKA) to PKA and Rho-kinase, respectively, were calculated. Contacts to the inhibitor via main chain or side chain are indicated. Residues that have side chain contacts with the ATP-site ligands are in bold.

ring compared to the single ring of Y-27632. These additional interactions can be assumed to increase the binding potency. The drop in selectivity can be explained if one assumes that the interactions which determine the selectivity for these Y-class inhibitors remain the same for both inhibitors and thus are less relevant in the case of the better binding Y-30141.

Selectivity of the Inhibitors for Rho-Kinase Relative to Other Kinases

We have argued above that many of the interactions with residues which differ between Rho-kinase and PKA explain why HA-1077, H-1152P, and Y-27632 bind more tightly to Rho-kinase than to PKA. The amino acid residues in question are, however, common in the kinase family. From the available kinetic data, at least HA-1077 and Y-27632 show selectivity for only a few kinases (less data is available for H-1152P). The question arises whether selectivity arises from a unique combination of specific amino acid residues or simply from the sum of a small number of individual interactions that can be considered independently of one another.

Using a sequence alignment of 491 human kinases (see e.g., www.kinase.com; Manning et al., 2002), we built a database to calculate the frequency of certain amino acid residues and of their combinations. Table 5 shows the degree of conservation for the residues that are different between PKA and Rho-kinase. Either isoleucine and leucine is found at the Leu49 position in most kinases, with leucine more frequent than isoleucine. Also, an alanine in the Thr183 position (28.9%) is common (and more common than threonine with 15.5%). Relatively high frequencies are found also for Rho-kinase side chains of methionine in the Val123 position (25.1%) and aspartic acid at the Glu127 position (32.2%). While these residues are common when considered individually, the combination of all four is nearly unique. Only 6 out of 491 kinases possess the same combination, 3 from the subgroup of cell cycle related kinases (CRK7, CCRK, and CHED), and 3 tyrosine kinases, MUSK, MET and RON.

If we consider additionally the AGC characteristic residue Phe327, the combination of inhibitor binding side chains seen in Rho-kinase becomes truly unique. Phe327, located on a C-terminal strand that stretches across the catalytic cleft, interacts with its aromatic side chain with the adenosine moiety of ATP, as well as with

all kinase inhibitors cocrystallized with PKA so far. The three inhibitors in this study make four (Y-27632), six (HA-1077), or eight (H-1152P) van der Waals contacts to Phe327. Sequence alignments of PKA versus ROCK-I or ROCK-II indicate that Rho-kinase also has a phenylalanine residue in a position homologous to Phe327 (Figure 2). The crystal structure of AGC kinase PKB shows residue Phe439 in a position identical to Phe327 in PKA (Yang et al., 2002). More distantly related kinases, however, do not have a corresponding C-terminal strand with a recognizably equivalent aromatic side chain (although other strands, domains, or subunits may contribute a similar chain). Thus, the combination of all five residues, Ile (Leu49), Ala (Thr183), Asp (Glu127), Met (Val123), and Phe (Phe327), is an exclusive feature of Rho-kinase. It should be noted that these residues are also among the ones with the largest numbers of contacts to the inhibitors, especially to H-1152P (Table 3). And, while the individual residues exchanges may be relatively conserved, in combination they generate a uniquely shaped inhibitor binding pocket with unique electronic properties, rationalizing the selectivity of Rho-kinase for certain protein kinase inhibitors, such as HA-1077, H-1152P, and Y-27632.

Conclusions

The one common feature of all protein kinases is ATP binding at a highly conserved ATP binding site with highly conserved binding interactions. The highest degree of conservation is seen with the catalytic residues that are absolutely conserved across the entire protein kinase family. The tertiary structure that forms the ATP binding site is apparently highly conserved in the active state of the protein, but this conclusion depends upon extrapolation from the still relatively few active structures that have been solved. The primary sequences are mostly highly conserved at the residues that form the triphosphoryl binding site, presumably because this represents the catalytic site. Conserved features of the adenosine binding site are restricted to the backbone contacts of the hinge region and to a generally hydrophobic or aromatic environment surrounding adenine; residues at positions homologous to Val57 and Ala70 in PKA are additionally conserved as small hydrophobic residues. Otherwise, there is considerable variability in sequence and, when considering inactive forms, in structure among protein kinases. Physiological

roles for this variability are generally recognized only for those cases where specific events such as phosphorylation are seen to modulate activity. Most protein kinases bind ATP with low micromolar binding constants, consistent with the need for exchange of ATP, ADP, and unbound states. Thus, sequence and structural variability at the ATP binding pocket has few known physiological roles regarding ATP binding, but is crucial for the selectivity of nonphysiological, high affinity ATP-site ligands, such as low molecular weight protein kinase inhibitors.

Crystallographic studies of enzyme-inhibitor complex structures provide information directly relevant to the drug design tasks of optimizing potency and selectivity. For protein kinases, these tasks are complicated by several factors. First, the substrate binding sites are relatively flexible, so that individual structures do not fully characterize an enzyme. Secondly, as discussed above, the natural substrates generally bind weakly, so that tight binding inhibitors are not obviously derivable from substrates. Third, the similarity of the ATP binding sites of active protein kinases means that inhibitors are likely to bind many of the ca. 600 kinases other than the target kinase.

The development of potent and selective kinase inhibitors and their success as therapeutics has demonstrated that problems anticipated with protein kinases as targets can be overcome. The process of optimization of such inhibitors can be improved. Of the inhibitors described here, only H-1152P was specifically designed to target Rho-kinase. The crystal structures, however, show how they bind and identify the probable determinants of Rho-kinase selectivity. This information focuses strategies for chemical synthesis and should improve the overall efficiency in achieving desired inhibition profiles. Cocrystal structures of Rho-kinase with inhibitors are needed to verify and possibly refine the model. Verification of the model would also verify the approach of using PKA as a surrogate for Rho-kinase crystallization, which might remain a preferable approach if Rho-kinase crystallization proves difficult, or if only inactive conformations of Rho-kinase will be crystallizable.

Experimental Procedures

Protein Expression and Purification
Recombinant bovine Cα catalytic subunit of cAMP-dependent protein kinase (which differs from the human protein at two positions: Asn32Ser and Met63Lys) was soluble expressed in E. coli BL21(DE3) cells and then purified via affinity chromatography and ion exchange chromatography as previously described (Engh et al., 1996). Threefold phosphorylated protein was used for crystallization of Y-27632 and H-1152P, whereas 4-fold phosphorylated protein successfully formed cocrystals with HA-1077.

Crystallization
Y-27632 and HA-1077 were purchased from Calbiochem. Y-27632, HA-1077, and H-1152P were cocrystallized with PKA and PKI(5-24) at 75 mM LiCl, 25 mM MesBisTris (pH 6.4). Hanging drop vapor diffusion against 15% methanol as precipitant was used to obtain ca. 100 × 100 × 500 μm crystals.

Biacore Sensor Chip Preparation
Proteins used for Biacore analysis were dialyzed two times with the 400-fold volume of 50 mM MOPS (pH 6.8), 10 mM MgCl$_2$, and 50 mM KCl (Gassel et al., 2003). Coupling of PKA to a CM5 Biasensor

chip via amine group linkage was achieved using standard coupling procedures (Löfås and Johnsson, 1990). Briefly, CM5 sensor chips were activated by injecting 35 μl of a 1:1 mixture of N-ethyl-N'-[dimethylamino]carbodiimide/N-hydroxysuccinimide at 5 μl/min. After diluting the proteins in 10 mM sodium acetate (pH 5.5), PKA (with HSA as a control) was coupled to the CM5 sensor chip by injecting a 50 μM solution of the protein selected with a flow rate of 5 μl/min until 11,000 RU was reached.

Generation of Kinetic Binding Data
Kinetic studies with a range of analyte concentrations were determined at a flow rate of 10 μl/min by allowing 300 s for association and 900 s for dissociation. Analytes were diluted in MilliQ water or running buffer (50 mM MOPS [pH 7.4], 50 mM KCl, and 10 mM MgCl$_2$). Kinetic data were analyzed with BIAevaluation 3.0 software. For each binding curve, the response obtained using the HSA cell as control was subtracted. Due to the small signals (up to 40 RU), the steady-state affinity model was used to determine the K_i of the different small molecular weight compounds. Goodness of fit (measured as χ^2) was less than 5 for binding of the low molecular weight compounds. All binding experiments were repeated two times, and biosensor chips coupled at different times yielded surfaces with identical binding affinities. The binding affinities of H-1152P, HA-1077, and Y-27632 to PKA were similar to the K_i values reported in different studies (Sasaki et al., 2002; Uehata et al., 1997) and citations therein, using enzymatic assays.

Data Collection and Structure Determination
Diffraction data were measured at 4°C in a sealed capillary on an image plate detector (Mar research) or Bruker X1000 area detector using a copper target Rigaku Rotaflex X-ray generator and graphite crystal K$_\alpha$ monochromator. In each case one crystal was sufficient to obtain a complete data set. The data were processed with the programs MOSFLM and SCALA or ASTRO and SAINT. All crystals have an orthorhombic symmetry (P2$_1$2$_1$2$_1$) with similar cell constants (Table 1). The structures were determined by molecular replacement using the CCP4 program package (www.ccp4.ac.uk/main/html). As a starting model we chose a PKA structure in a closed conformation (our unpublished data). Refmac 5.1.24 was used for refinement, while MOLOC was used (www.moloc.ch) for graphical evaluation and model building.

Surface Calculations
Buried surfaces were calculated with the program Insight II (Accelrys). The total surface of the isolated inhibitor and the accessible surface of the inhibitor in the complex were calculated. The difference is the buried surface.

Sequence Alignment and Homology Model Building
Sequences were aligned using the ClustalW server from http://www.ebi.ac.uk/clustalw/. The homology model was calculated by the SWISS-MODEL Protein Modelling Server (http://www.expasy.ch/swissmod/SWISS-MODEL.html).

References

Akamine, P., Madhusudan, Wu, J., Xuong, N.H., Eyck, L.F.T., and Taylor, S.S. (2003). Dynamic features of cAMP-dependent protein kinase revealed by apoenzyme crystal structure. J. Mol. Biol. 327, 159–171.

Amano, M., Ito, M., Kimura, K., Fukata, Y., Chihara, K., Nakano, T., Matsuura, Y., and Kaibuchi, K. (1996). Phosphorylation and activa-

tion of myosin by Rho-associated kinase (Rho-kinase). J. Biol. Chem. 271, 20246–20249.

Amano, M., Fukata, Y., and Kaibuchi, K. (2000). Regulation and functions of Rho-associated kinase. Exp. Cell Res. 261, 44–51.

Battistutta, R., Sarno, S., De Moliner, E., Papinutto, E., Zanotti, G., and Pinna, L.A. (2000). The replacement of ATP by the competitive inhibitor emodin induces conformational modifications in the catalytic site of protein kinase CK2. J. Biol. Chem. 275, 29618–29622.

Bossemeyer, D., Engh, R.A., Kinzel, V., Ponstingl, H., and Huber, R. (1993). Phosphotransferase and substrate binding mechanism of the cAMP-dependent protein kinase catalytic subunit from porcine heart as deduced from the 2.0 A structure of the complex with Mn2+ adenylyl imidodiphosphate and inhibitor peptide PKI(5–24). EMBO J. 12, 849–859.

Davies, S.P., Reddy, H., Caivano, M., and Cohen, P. (2000). Specificity and mechanism of action of some commonly used protein kinase inhibitors. Biochem. J. 351, 95–105.

Engh, R.A., and Bossemeyer, D. (2001). The protein kinase activity modulation sites: mechanisms for cellular regulation—targets for therapeutic intervention. Adv. Enzyme Regul. 41, 121–149.

Engh, R.A., and Bossemeyer, D. (2002). Structural aspects of protein kinase control: role of conformational flexibility. Pharmacol. Ther. 93, 99–111.

Engh, R.A., Girod, A., Kinzel, V., Huber, R., and Bossemeyer, D. (1996). Crystal structures of catalytic subunit of cAMP-dependent protein kinase in complex with isoquinolinesulfonyl protein kinase inhibitors H7, H8, and H89. Structural implications for selectivity. J. Biol. Chem. 271, 26157–26164.

Fukata, Y., Amano, M., and Kaibuchi, K. (2001). Rho-Rho-kinase pathway in smooth muscle contraction and cytoskeletal reorganization of non-muscle cells. Trends Pharmacol. Sci. 22, 32–39.

Gassel, M., Breitenlechner, C.B., Ruger, P., Jucknischke, U., Schneider, T., Huber, R., Bossemeyer, D., and Engh, R.A. (2003). Mutants of protein kinase a that mimic the ATP-binding site of protein kinase B (AKT). J. Mol. Biol. 329, 1021–1034.

Gibbs, C.S., Knighton, D.R., Sowadski, J.M., Taylor, S.S., and Zoller, M.J. (1992). Systematic mutational analysis of cAMP-dependent protein kinase identifies unregulated catalytic subunits and defines regions important for the recognition of the regulatory subunit. J. Biol. Chem. 267, 4806–4814.

Hidaka, H., Inagaki, M., Kawamoto, S., and Sasaki, Y. (1984). Isoquinolinesulfonamides, novel and potent inhibitors of cyclic nucleotide dependent protein kinase and protein kinase C. Biochemistry 23, 5036–5041.

Ikenoya, M., Hidaka, H., Hosoya, T., Suzuki, M., Yamamoto, N., and Sasaki, Y. (2002). Inhibition of Rho-kinase-induced myristoylated alanine-rich C kinase substrate (MARCKS) phosphorylation in human neuronal cells by H-1152, a novel and specific Rho-kinase inhibitor. J. Neurochem. 81, 9–16.

Ishizaki, T., Uehata, M., Tamechika, I., Keel, J., Nonomura, K., Maekawa, M., and Narumiya, S. (2000). Pharmacological properties of Y-27632, a specific inhibitor of Rho-associated kinases. Mol. Pharmacol. 57, 976–983.

Itoh, K., Yoshioka, K., Akedo, H., Uehata, M., Ishizaki, T., and Narumiya, S. (1999). An essential part for Rho-associated kinase in the transcellular invasion of tumor cells. Nat. Med. 5, 221–225.

Johnson, D.A., Akamine, P., Radzio-Andzelm, E., Madhusudan, and Taylor, S.S. (2001). Dynamics of cAMP-dependent protein kinase. Chem. Reviews 101, 2243–2270.

Löfås, S., and Johnsson, B. (1990). A novel hydrogel matrix on gold surfaces in surface plasmon resonance sensors for fast and efficient covalent immobilization of ligands. J. Chem. Soc. Chem. Commun. 21, 1526–1528.

Manning, G., Whyte, D.B., Martinez, R., Hunter, T., and Sudarsanam, S. (2002). The protein kinase complement of the human genome. Science 298, 1912–1934.

Matsui, T., Amano, M., Yamamoto, T., Chihara, K., Nakafuku, M., Ito, M., Nakano, T., Okawa, K., Iwamatsu, A., and Kaibuchi, K. (1996). Rho-associated kinase, a novel serine threonine kinase, as a puta-

tive target for the small GTP binding protein Rho. EMBO J. 15, 2208–2216.

Narayana, N., Diller, T.C., Koide, K., Bunnage, M.E., Nicolaou, K.C., Brunton, L.L., Xuong, N.H., Ten Eyck, L.F., and Taylor, S.S. (1999). Crystal structure of the potent natural product inhibitor balanol in complex with the catalytic subunit of cAMP-dependent protein kinase. Biochemistry 38, 2367–2376.

Ono-Saito, N., Niki, I., and Hidaka, H. (1999). H-series protein kinase inhibitors and potential clinical applications. Pharmacol. Ther. 82, 123–131.

Orellana, S.A., Amieux, P.S., Zhao, X., and McKnight, G.S. (1993). Mutations in the catalytic subunit of the cAMP-dependent protein kinase interfere with holoenzyme formation without disrupting inhibition by protein kinase inhibitor. J. Biol. Chem. 268, 6843–6846.

Prade, L., Engh, R.A., Girod, A., Kinzel, V., Huber, R., and Bossemeyer, D. (1997). Staurosporine-induced conformational changes of cAMP-dependent protein kinase catalytic subunit explain inhibitory potential. Structure 5, 1627–1637.

Sasaki, Y., Suzuki, M., and Hidaka, H. (2002). The novel and specific Rho-kinase inhibitor (S)-(+)-2-methyl-1-[(4-methyl-5-isoquinoline) sulfonyl]-homopiperazine as a probing molecule for Rho-kinase-involved pathway. Pharmacol. Ther. 93, 225–232.

Shimokawa, H., Iinuma, H., Kishida, H., Nakashima, M., and Kato, K. (2001). Antianginal effect of fasudil, a Rho-kinase inhibitor, in patients with stable effort angina: a multicenter study. Circulation 104, 2843.

Sinnett-Smith, J., Lunn, J.A., Leopoldt, D., and Rozengurt, E. (2001). Y-27632, an inhibitor of Rho-associated kinases, prevents tyrosine phosphorylation of focal adhesion kinase and paxillin induced by bombesin: dissociation from tyrosine phosphorylation of p130(CAS). Exp. Cell Res. 266, 292–302.

Tanaka, H., Ohshima, N., Takagi, M., Komeima, K., and Hidaka, H. (1998). Novel vascular relaxant, Hmn-1152: its molecular mechanism of action. Naunyn-Schmied. Arch. Pharmacol. 358, P3740.

Trauger, J.W., Lin, F.F., Turner, M.S., Stephens, J., and LoGrasso, P.V. (2002). Kinetic mechanism for human Rho-Kinase II (ROCK-II). Biochemistry 41, 8948–8953.

Uehata, M., Ishizaki, T., Satoh, H., Ono, T., Kawahara, T., Morishita, T., Tamakawa, H., Yamagami, K., Inui, J., Maekawa, M., and Narumiya, S. (1997). Calcium sensitization of smooth muscle mediated by a Rho-associated protein kinase in hypertension. Nature 389, 990–994.

Yang, J., Cron, P., Good, V.M., Thompson, V., Hemmings, B.A., and Barford, D. (2002). Crystal structure of an activated Akt/protein kinase B ternary complex with GSK3-peptide and AMP-PNP. Nat. Struct. Biol. 9, 940–944.

Accession Numbers

Atomic coordinates have been deposited in the Protein Data Bank with accession numbers 1Q8T, 1Q8U, and 1Q8W.

REVIEWS

GLIVEC (STI571, IMATINIB), A RATIONALLY DEVELOPED, TARGETED ANTICANCER DRUG

Renaud Capdeville, Elisabeth Buchdunger, Juerg Zimmermann and Alex Matter

In the early 1980s, it became apparent that the work of pioneers such as Robert Weinberg, Mariano Barbacid and many others in identifying cancer-causing genes in humans was opening the door to a new era in anticancer research. Motivated by this, and by dissatisfaction with the limited efficacy and tolerability of available anticancer modalities, a drug discovery programme was initiated with the aim of rationally developing targeted anticancer therapies. Here, we describe how this programme led to the discovery and continuing development of Glivec (Gleevec in the United States), the first selective tyrosine-kinase inhibitor to be approved for the treatment of a cancer.

LEUKAEMIA
Leukaemia is an uncontrolled proliferation of one type of white blood cell (leukocyte).

Novartis Oncology, Novartis Pharma AG, S-27 2.033, CH-4002 Basel, Switzerland. Correspondence to R.C. e-mail: renaud.capdeville@pharma.novartis.com

Until the early 1980s, drug discovery programmes for cancer were focused almost exclusively on DNA synthesis and cell division, and resulted in agents such as antimetabolites, alkylating agents and microtubule destabilizers. These drugs showed efficacy, but at the price of high toxicity due to lack of selectivity. Also, resistance was frequently observed after initial stabilization or regression of the disease. The discovery of cancer-causing genes, later called oncogenes, represented a radical departure — all of a sudden, genes were identified that were uniquely associated with cancerous cells. The molecular epidemiology of these genes was established over many years of studying clinical tumour samples, but as described below, it was clear at the outset that chronic myelogenous LEUKAEMIA (CML) — a haematological stem-cell disorder that is characterized by excessive proliferation of cells of the myeloid lineage — represented a particularly interesting case.

Target selection: BCR–ABL

CML is characterized by a reciprocal translocation between chromosomes 9 and 22 (REF. 1). The shortened version of chromosome 22, which is known as the Philadelphia chromosome, was discovered by Nowell and Hungerford[2], and provided the first evidence of a specific genetic change associated with human cancer.

The molecular consequence of this inter-chromosomal exchange is the creation of the *BCR–ABL* gene, which encodes a protein with elevated tyrosine-kinase activity. The demonstration that *Bcr–Abl* as the sole oncogenic event could induce leukaemias in mice[3–5] has established *BCR–ABL* as the molecular pathogenic event in CML. As the tyrosine-kinase activity of BCR–ABL is crucial for its transforming activity[6], the enzymatic activity of this deregulated gene could plausibly be defined as an attractive drug target for addressing BCR–ABL-positive leukaemias.

For the first time, a drug target was identified that clearly differed in its activity between normal and leukaemic cells. It was conceivable that this enzyme could be approached with classical tools of pharmacology, as its activity — the transfer of phosphate from ATP to tyrosine residues of protein substrates — could clearly be described and measured in biochemical as well as cellular assays. Furthermore, cell lines that were derived from human leukaemic cells with the same chromosomal abnormality were available. Such cell lines were instrumental for *in vitro* and animal studies, which laid the groundwork for the clinical trials. So, the essential tools were assembled to go forward with the aim of identifying potent and selective inhibitors of the ABL tyrosine kinase.
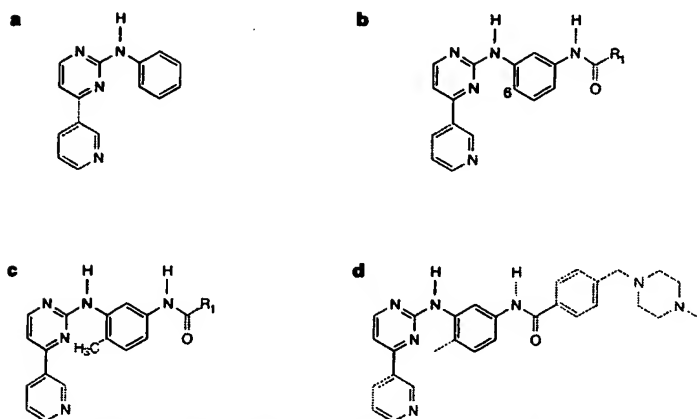
Figure 1 | Summary of the chemical optimization. The core structure of the lead compound, a phenylamino derivative, is indicated in black. a | The addition of a 3'-pyridyl group (blue) at the 3'-position of the pyrimidine enhanced the cellular activity. b | An amide group (red) attached to the phenyl ring provided activity against tyrosine kinases. c | A 'flag methyl' (purple) attached to the diaminophenyl ring abolished the undesirable protein-kinase-C inhibitory activity. d | The final attachment of an N-methyl piperazine moiety (green) markedly increased the solubility and oral bioavailability.

Medicinal chemistry

The starting point for every medicinal-chemistry project is a lead compound with a given pharmacological activity. However, the biological activity of a molecule must be complemented by other properties that make the molecule a good drug — it is estimated that a large proportion of molecules fails in late stages of drug development due to drug–drug interactions or poor ADME (absorption, distribution, metabolism and excretion) features. Not detecting these liabilities early in the drug discovery process can be extremely costly and time consuming. On the basis of physical and calculated properties for known drugs, criteria for 'drug-likeness' have been established[7].

In the case of Glivec, a lead compound was identified in a screen for inhibitors of protein kinase C (PKC). This compound — a phenylaminopyrimidine derivative — had promising 'lead-like' properties[8] and a high potential for diversity, allowing simple chemistry to be applied to produce compounds with more potent activity or selectivity. Strong PKC inhibition in cells was obtained with derivatives bearing a 3'-pyridyl group at the 3'-position of the pyrimidine (FIG. 1a). During the optimization of this structural class, it was observed that the presence of an amide group on the phenyl ring provided inhibitory activity against tyrosine kinases, such as the BCR–ABL kinase (FIG. 1b). At this point, a key observation from analysis of structure–activity relationships was that a substitution at position 6 of the diaminophenyl ring abolished PKC inhibitory activity completely. Indeed, although the introduction of a simple 'flag-methyl' led to loss of activity against PKC, the activity against protein tyrosine kinases was retained or even enhanced (FIG. 1c). However, the first series of selective inhibitors that was prepared originally showed poor oral bioavailability

and low solubility in water. The attachment of a highly polar side chain (an N-methylpiperazine) was found to improve markedly both solubility and oral bioavailability. To avoid the mutagenic potential of aniline moieties, a spacer was introduced between the phenyl ring and the nitrogen atom. The best compound from this series was a methylpiperazine derivative that was originally named STI571 (imatinib, now known as Glivec or Gleevec), which was selected as the most promising candidate for clinical development[9,10] (FIG. 1d).

Docking studies[11] and X-ray crystallography[12] showed that binding of Glivec occurs at the ATP-binding site. Analysis of the crystal structure[12] showed that Glivec inhibits the ABL kinase by binding with high specificity to an inactive form of the kinase. The need for the kinase to adopt this unusual conformation, which favours binding, might contribute to the high selectivity of the compound. Unexpectedly, these analyses indicated that the N-methylpiperazine group (added to increase drug solubility) also interacted strongly with ABL by means of hydrogen bonds to the backbone carbonyl group of isoleucine (Ile)360 and histidine (His)361.

In an in vitro screen against a panel of protein kinases, the compound was found to inhibit the autophosphorylation of essentially three kinases: BCR–ABL, c-KIT and the platelet-derived growth factor (PDGF) receptor (TABLE 1). More recently, activity against ARG kinase has also been reported[13].

Pharmacological profile

In collaboration with Brian Druker, the selective inhibitory activity of Glivec was shown at the cellular level on the constitutively active p210[BCR–ABL] tyrosine kinase[14]. Subsequently, a similar inhibitory activity was also shown on other ABL fusion proteins, such as p185[BCR–ABL] (REFS 15,16) and TEL (ETV6)–ABL[15]. The inhibition of autophosphorylation of BCR–ABL was closely related to the antiproliferative activity of Glivec. Incubation with submicromolar concentrations of Glivec selectively induced APOPTOSIS in BCR–ABL-positive cell lines, and induced cell killing in primary leukaemia cells from patients with Philadelphia-chromosome-positive (Ph+) CML and acute lymphoblastic leukaemia[14,16-20].

In in vivo experiments, once daily intraperitoneal treatment with 2.5–50 mg kg^{-1} of Glivec, started one week after injecting BCR–ABL-transformed 32D cells into SYNGENEIC mice, caused dose-dependent inhibition of tumour growth[14]. In nude mice implanted with KU812 cells, oral treatment with 160 mg kg^{-1} daily in three divided doses for 11 consecutive days was associated with continuous blockage of p210[BCR–ABL] tyrosine phosphorylation, and resulted in tumour-free survival of the animals[20]. The antitumour effect of Glivec was specific for BCR–ABL-expressing cells, as no growth inhibition occurred in mice that were given injections of U937, a BCR–ABL-negative myeloid cell line. Recently, Glivec was shown to be orally active in a mouse model of CML, based on retroviral p210[BCR–ABL]

APOPTOSIS
Programmed cell death.

SYNGENEIC MODEL
An animal model in which the injected tumour cells are derived from the same animal species as the host animal.

transduction of transplanted bone marrow. Survival of animals was significantly prolonged, together with a marked improvement in peripheral-white-blood-cell counts and splenomegaly[21].

Table 1 | **Cellular profile of Glivec**

Assay	IC$_{50}$ (μM)
Inhibition of autophosphorylation	
v-ABL	0.1–0.3
p210[BCR-ABL]	0.25
p185[BCR-ABL]	0.25
TEL–ABL	0.35
TEL–ARG	0.5
PDGF receptor	0.1
TEL–PDGF receptor	0.15
c-KIT	0.1
FLT3	> 10
c-FMS and v-fms	> 10
EGF receptor	> 100
c-ERBB2	> 100
Insulin receptor	> 100
IGF-1 receptor	> 100
v-SRC	> 10
JAK2	> 100
Inhibition of MAPK activation	
PDGF dependent	0.1–1
SCF dependent	0.1–1
Inhibition of AKT activation	
SCF dependent	0.1–1
Inhibition of IP release	
PDGF induced	0.25
Inhibition of c-FOS mRNA expression	
PDGF induced	0.3–1
EGF, FGF or PMA induced	> 100
*Antiproliferative activity**	
32D, MO-7e, BaF3 cells	> 10
BCR-ABL-transfected 32D, MO-7e, BaF3 cells	< 1
BCR-ABL-positive human leukaemia lines‖	0.1–1
BaF3 TEL-ARG	0.5
BALB/c 3T3 v-SIS (PDGF autocrine)	0.3
BaF3 TEL-PDGF receptor	< 1
U-87 human glioma‡	~1.5
U-343 human glioma‡	~1.5
MO-7e, SCF stimulated	~0.1
H526 human SCLC, SCF stimulated§	0.8
Human GIST882 line¶	< 1
Human mast-cell leukaemia line HMC-1#	0.01–0.1

Glivec concentrations that cause 50% inhibition (IC$_{50}$) are given[13–20,47,48,53,54,61,63,66]. EGF, epidermal growth factor; FGF, fibroblast growth factor; FLT3, fms-related tyrosine kinase 3; IGF-1, insulin-like growth factor-1; IP, inositol phosphate; MAPK, mitogen-activated protein kinase; PDGF, platelet-derived growth factor; PMA, phorbol 12-myristate 13-acetate; SCF, stem-cell factor; SCLC, small-cell lung cancer. *Antiproliferative experiments were carried out in 10% fetal calf serum, except for those that were carried out in ‡5% human-platelet poor plasma or under §serum-free conditions. ‖K562, KU812, MC-3, MBA-1, KBM-5, Z-33, Z-119, Z-181. ¶Expresses the activating KIT mutation K642E (lysine 642 to glutamic acid). #Expresses the activating KIT mutation V560G (valine 560 to glycine).

Fundamental phenotypic features in BCR–ABL-positive cells involve resistance to apoptosis, enhanced proliferation and altered adhesion properties. The impact of Glivec on some known downstream signalling molecules of BCR–ABL has been examined. A link between constitutive activation of STAT5 (signal transducer and activator of transcription 5) and enhanced viability of BCR–ABL-transformed cells has been shown[22,23]. Glivec had a profound inhibitory effect on STAT5 activation *in vitro* and *in vivo*[21–23]. Furthermore, inhibition of the BCR–ABL kinase activity by Glivec in BCR–ABL-expressing cell lines and fresh leukaemic cells from CML patients induced apoptosis by suppressing the capacity of STAT5 to activate the expression of the anti-apoptotic protein BCL-X$_L$[23]. The adaptor molecule CRKL is a prominent target of BCR–ABL, and its tyrosine phosphorylation has been a useful marker of BCR–ABL kinase activity[24]. As expected, a decrease in tyrosine phosphorylation of CRKL has been observed in Glivec-treated cell lines, and has also served as an indicator of BCR–ABL kinase activity in patients (see below).

There is increasing evidence that cell-cycle regulation is disturbed in BCR–ABL-positive cells; however, the underlying molecular mechanisms are poorly understood. Recently, BCR–ABL has been shown to promote cell-cycle progression and activate cyclin-dependent kinases by interfering with the regulation of the cell-cycle inhibitory protein p27 (REF. 25). Glivec prevented downregulation of p27 levels in BCR–ABL-expressing cells[25,26].

The effects of Glivec on cytoskeletal changes and adhesion have been investigated using BCR–ABL-transfected fibroblasts[27]. Glivec was shown to restore normal architecture and to increase adhesion in this model of BCR–ABL expression.

Clinical development in CML

Because of the three known targets of Glivec, many potential cancers can be speculated to be good candidates for clinical testing of this new drug. However, in most cancers, tumorigenesis is complex and involves the disruption of multiple genes and signalling pathways. By contrast, CML can be considered as one of the few examples of a malignancy in which a single signalling-pathway defect is thought to cause the disease. In addition, in contrast to most of the solid tumours, for which the measurement of tumour response is complex, pharmacodynamic response in CML can be measured easily using blood leukocyte count as the end point. For these reasons, CML was selected as the first indication for Phase I clinical testing.

Clinically, CML is a chronic disease that evolves through three successive stages, from the chronic phase to the end stage of blast crisis that resembles acute leukaemia (FIG. 2). Overall, the median survival time of patients with newly diagnosed CML is approximately 5–6 years with an interferon-based treatment regimen. The first trial with Glivec was a Phase I study in patients with chronic-phase, and subsequently also with blast-phase, CML. In this trial, patients were treated with doses
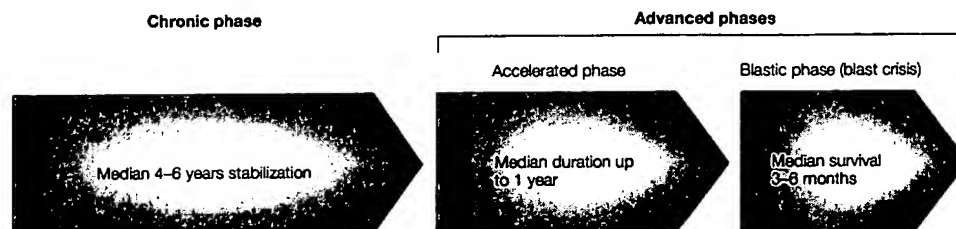
Figure 2 | Clinical course of chronic myelogenous leukaemia.

ranging from 25 to 1,000 mg per day, and no maximal tolerated dose was identified, despite a trend for a higher frequency of GRADE III–IV ADVERSE EVENTS at doses of 750 mg or higher. On the other hand, a clear dose–response relationship with respect to efficacy was described in patients with chronic-phase CML. At doses of 300 mg or higher, 98% of the patients achieved a complete haematological response, and trough serum levels were above the concentrations required for *in vitro* activity[28,29]. Subsequently, a mathematical modelling of the relationship between dose and response, as measured by leukocyte counts after four weeks of therapy, confirmed that doses of 400 mg and higher were optimal in inducing a haematological response[30] (FIG. 3). In addition, effective inhibition of the BCR–ABL kinase was documented in patient samples by inhibition of the phosphorylation status of the downstream target CRKL[27]. From this study, doses ranging from 400 mg (for chronic-phase patients) to 600 mg (for advanced-phase CML) were recommended for subsequent studies.

Subsequently, three large multinational studies have been carried out in 532 patients with late chronic-phase CML in whom previous interferon therapy had failed[31], in 235 patients with accelerated-phase CML[32], and in 260 patients with myeloid blast crisis[33]. Treatment was given at a dose of 400 mg in the chronic-phase trial and 600 mg in the two other studies. The results of these three studies indicated that the rate of both haematological and cytogenetic response increased as the treatment was started earlier in the course of the disease (FIG. 4). Importantly, the achievement of a haematological and/or cytogenetic response was associated with improved survival and progression-free survival[31–33]. In the chronic-phase study, in which patients started treatment within a median of 32 months after their initial diagnosis, the estimated probability of being free of progression at 18 months was 89.2%[31]. The most frequently reported adverse events were mild nausea, vomiting, oedema and muscle cramps. However, rare but serious adverse events, such as liver

GRADE III–IV ADVERSE EVENTS
For each adverse event that is associated with a specific treatment, grades are assigned and defined using a scale from 0 to V. Grade III, severe and undesirable adverse event; grade IV, life-threatening or disabling adverse event.
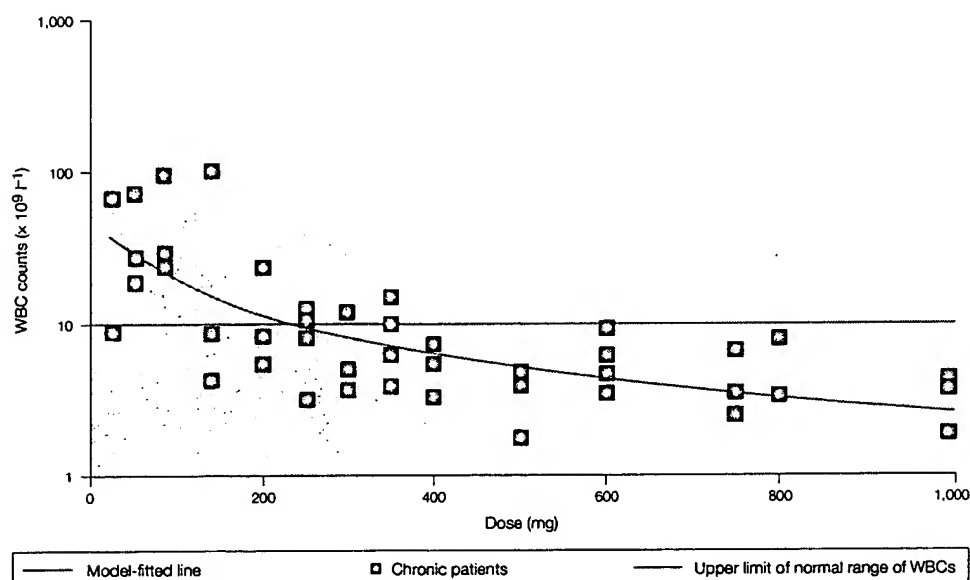
Figure 3 | Dose–response relationship of Glivec in CML (Phase I study). Using the leukocyte (white blood cell; WBC) count after 28 days of treatment as a pharmacodynamic marker, the relationship between dose and response was modelled using an E_{max} model, which makes the assumption that once the maximal effect is achieved (E_{max}), increasing the dose further does not translate into additional benefit. The data indicate that at doses of 400 mg per day or higher, all the patients are predicted to achieve a reduction of their leukocyte counts within normal range below 10×10^9 l^{-1}. Adapted with permission from REF. 30 © (2001) American Society of Clinical Oncology. CML, chronic myelogenous leukaemia.

toxicity or fluid-retention syndromes, were also reported. Neuropaenias and thrombopaenias were more common in patients with advanced disease, which indicates that haematological toxicity might be related more to an underlying compromised bone-marrow reserve than to toxicity of the drug itself through inhibition of c-KIT-driven haematopoiesis. Taken together, these findings have established Glivec as a safe and effective therapy in all stages of CML, and were the basis for marketing approval by the FDA on 10 May 2001 — less than three years after the start of the first Phase I study (FIG. 5).

Resistance. In CML blast crisis, even though the rate of haematological responses with Glivec is high, these responses are usually short lived, and most patients will ultimately develop resistance and undergo disease pro-gression. A prerequisite to optimally develop strategies to prevent or overcome this resistance is to get a good understanding of the potential mechanisms of resis-tance in these patients.

On the basis of preclinical and clinical data that are available at present, several potential mechanisms of resistance have been described, which are summarized in BOX 1. They can be categorized into two main groups: mechanisms whereby BCR–ABL is reactivated and cell proliferation remains dependent on BCR–ABL sig-nalling, and mechanisms whereby the BCR–ABL protein remains inhibited by Glivec, but alternative signalling pathways become activated.

BCR–ABL overexpression and *BCR–ABL* gene ampli-fication has been shown in p210^BCR–ABL-transformed mouse haematopoietic Ba/F3 cells that are resistant to Glivec[34,35], as well as in human *BCR–ABL*-positive leukaemia lines LAMA84 and AR230 (REFS 35,36).

In treated patients, there is now increasing evidence that amplification of the *BCR–ABL* gene and mutations in the BCR–ABL kinase domain are two common mechanisms of resistance to Glivec. The occurrence of these mechanisms was first reported by Sawyers' group[37]. In a study of 11 patients with blast crisis and overt clinical resistance when treated with Glivec, 3 had amplification of the *BCR–ABL* gene and 6 had a point mutation in the ABL kinase domain, which resulted in a T315I (threonine 315 to isoleucine) amino-acid sub-stitution. Following this initial report, the T315I muta-tion as well as further mutations in the ABL kinase domain have been reported by various invest-igators[38–41]. Even though these mutations vary in their type and frequency, it is speculated that they might all lead to a reactivation of BCR–ABL-driven signal trans-duction. To understand the molecular mechanism by which such mutations might cause resistance to Glivec, current studies are using X-ray crystallography to analyse the three-dimensional structure of a complex between the drug and the human c-ABL kinase domain. Glivec binds to an unusual, inactive confor-mation of ABL with the amino terminus of the activa-tion loop, which contains the highly conserved DFG (asparagine-phenylalanine-glycine) motif, folded into the ATP-binding site[42]. This conformation has been
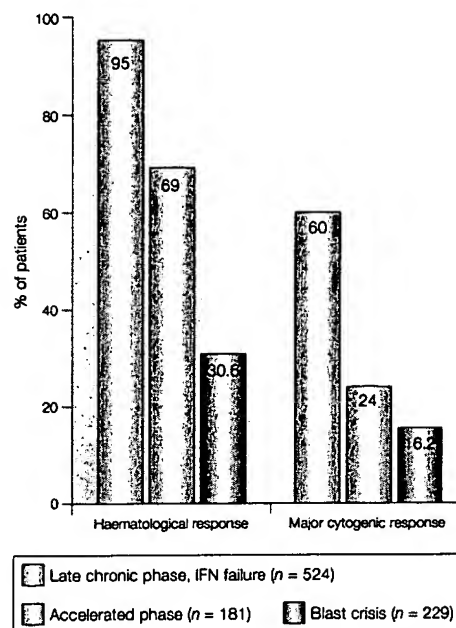
Figure 4 | Haematological and cytogenetic response in CML: Phase II data. In all studies, results are expressed as the percentage of responding patients among the patients for whom the diagnosis of the correct phase of chronic myelogenous leukaemia (CML) was confirmed after a central review of the data. A major cytogenetic response combines both complete (0% Ph+ metaphases) and partial (1–35% Ph+) responses. Haematological response was defined as complete haematological response (CHR) in the chronic-phase study, and as either a CHR, a marrow response or a return to chronic phase (RTC) in the advanced-phase studies, all to be confirmed after at least four weeks. In the chronic-phase study, CHR was defined as white blood cells <10 x 10^9 l^-1, platelets <450 x 10^9 l^-1, myelocytes and metamyelocytes <5% in blood, no blasts and promyelocytes in blood, basophils <20% and no extramedullary involvement. In advanced-phase studies, CHR was defined as neutrophils = 1.5 x 10^9 l^-1, platelets = 100 x 10^9 l^-1, no blood blasts, marrow blasts <5% and no extramedullary disease. A marrow response was defined by the same criteria as for CHR, but with neutrophils = 1 x 10^9 l^-1 and platelets = 20 x 10^9 l^-1. An RTC was defined as <15% blasts in marrow and blood, <30% blasts and promyelocytes in marrow and blood, <20% basophils in blood and no extramedullary disease. IFN, interferon; Ph+, Philadelphia chromosome positive.
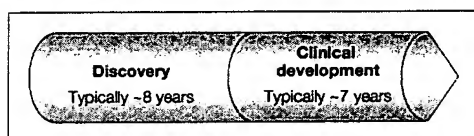
observed by Kuriyan and co-workers[12] in a complex between mouse c-Abl and a Glivec analogue, and can-not bind ATP. The knowledge of the crystal structure allows a better understanding of the decreased sensi-tivity of mutated BCR–ABL to Glivec, and can be a powerful tool in the design of new BCR–ABL inhibitors that maintain inhibitory activity against these mutated kinases.

Resistance to Glivec might also be related to phar-macokinetic factors. Glivec is a substrate of the multi-drug-resistance-associated P-glycoprotein (PgP).

Glivec development timeline

1990 – Lead compound identified in a screen for inhibitors of PKC.

1996 – *In vivo* activity shown in *BCR–ABL*-transformed cells in syngeneic mice.

June 1998 – First patient with CML treated.

June 2000 – Phase III trials initiated.

May 2001 – Approved by the FDA for CML.

November 2001 – Approved in Europe and Japan for CML.

Discovery

Clinical development

1992 – First batch of Glivec synthesized.

June 1999 – Phase II trials initiated.

February 2001 – NDA submitted to FDA for CML.

February 2002 – Approved by the FDA for GIST.

Typical development timeline

Discovery
Typically ~8 years

Clinical development
Typically ~7 years

Figure 5 | **Key points in the discovery and development of Glivec.** The clinical development was particularly rapid, as can be seen by comparison with the typical drug discovery and development times shown in the inset. An NDA for Glivec was submitted just two years and nine months after treatment of the first patient with CML, and FDA approval was given less than three months after application. CML, chronic myelogenous leukaemia; GIST, gastrointestinal stromal tumour; NDA, new drug application; PKC, protein kinase C.

Accordingly, the uptake of Glivec was reduced in Glivec-resistant LAMA84 cells in association with an overexpression of the PgP protein. Sensitivity to Glivec was recovered when cells were treated with the PgP inhibitor verapamil[35]. At clinically relevant concentrations of Glivec, binding to plasma proteins is approximately 95%, mostly to albumin and α1-acid glycoprotein (AGP). It has been suggested that a potential mechanism of resistance might relate to this high binding to increased levels of AGP, which would lead to insufficient availability of free drug for antileukaemic activity[43]. However, the clinical significance of this hypothesis is uncertain, in particular in view of the finding that AGP purified from CML patients failed to block the effect of Glivec on the proliferation of leukaemic cells[44].

Recently, Hofmann *et al.*[45] studied a small group of patients with Ph+ acute lymphoblastic leukaemia who were resistant to Glivec by using DNA-microarray expression profiling. They described an association between the occurrence of resistance to Glivec and upregulation of genes encoding proteins such as Bruton tyrosine kinase and two ATP synthetases (ATP5A1 and ATP5C1), and downregulation of other genes, such as the pro-apoptotic gene *BAK1* and the cell-cycle-control gene *INK4B*[45] (also known as *p15*). This is the first report to identify dysregulation of genes

that are unrelated to BCR–ABL signalling, and further studies will be necessary to fully assess the significance of these findings and their relevance to CML patients.

Current and future development in CML

The activity of Glivec in patients with newly diagnosed CML is being further investigated by a large randomized Phase III study to compare first-line therapy with Glivec against standard interferon in combination with low-dose cytarabine. This study, known as the 'IRIS' study (International Randomized study of Interferon versus STI571), has enrolled 1,106 patients. The results of an interim analysis with a median follow-up of 14 months indicate a better tolerability and a superior efficacy of first-line Glivec compared with interferon and low-dose cytarabine in terms of cytogenetic response, haematological response and, more importantly, time to progression to accelerated phase or blast crisis[46].

Preclinical studies have shown that the combination of Glivec with various anticancer agents might have synergistic effects. Consequently, several Phase I/II studies are evaluating the feasibility of combining Glivec with interferon, polyethylene glycol (PEG)ylated interferon, cytarabine and other single-agent or combination chemotherapy regimens, in patients with either chronic-phase or advanced CML.

Box 1 | **Mechanisms of resistance to Glivec in CML**

BCR–ABL-dependent mechanisms (cells remain dependent on BCR–ABL signalling)

• Amplification of *BCR–ABL* gene

• Mutations in BCR–ABL kinase domain prevent correct binding of Glivec

• Efflux of Glivec (for example, by PgP-associated MDR protein)

• Protein binding of Glivec (for example, to circulating AGP)

BCR–ABL-independent mechanisms (BCR–ABL is inactivated)

• Activation of signalling pathways downstream of BCR–ABL

• Activation of leukaemogenic pathways unrelated to BCR–ABL

AGP, α1-acid glycoprotein; CML, chronic myelogenous leukaemia; MDR, multidrug resistant; PgP, P-glycoprotein.

c-KIT is another target

In addition to various oncogenic forms of the BCR–ABL tyrosine kinase, Glivec also inhibits the receptor for stem-cell factor (SCF) — c-KIT, a member of the type III group of receptor kinases. Preclinical studies have established that the drug blocks c-KIT autophosphorylation, as well as SCF-stimulated downstream signalling events, such as activation of the mitogen-activated protein kinases (MAPKs) ERK1 and ERK2, and AKT (also known as protein kinase B)[47,48].

Development in c-KIT-positive GISTs. Gastrointestinal stromal tumours (GISTs) represent a rare subset of soft-tissue sarcomas that involve the gastrointestinal tract and are thought to be derived from the interstitial cells of Cajal. Scientific rationale for the use of Glivec in the treatment of these tumours comes from the landmark work of Hirota *et al.*[49], who first identified somatic gain-of-function mutations in the *c-KIT* gene in patients with GIST. Oncogenic *c-KIT* mutations in GISTs have been localized to the extracellular domain, kinase domains 1 and 2 and predominantly in the juxtamembrane domain of the c-KIT protein[50-52]. As c-KIT serves as a phenotypic marker of GISTs and has a key role in their pathogenesis, it provides an ideal target for molecular-based therapy. The first evidence that Glivec might inhibit GIST cells that express mutated *c-KIT* was obtained from studies in a mast-cell leukaemia line expressing a mutated *c-KIT* similar to that found in GISTs[48,53]. Furthermore, Glivec rapidly and completely abolished constitutive phosphorylation of c-KIT in the human cell line GIST882, which expresses an activating *c-KIT* mutation in the first part of the cytoplasmic split-tyrosine-kinase domain, and inhibited proliferation in this GIST line[54]. Similarly, a primary GIST cell culture that expressed a *c-KIT* exon 11 juxtamembrane mutation was also inhibited by Glivec[54].

As reported recently, a pronounced tumour response was first observed in a single patient with progressing GIST[55]. Following this case report, the high level of efficacy of Glivec in GIST has been shown in two subsequent Phase I (REF. 56) and Phase II studies (REF. 57). Two large Phase III studies are being carried out at present to compare the effectiveness of two doses of Glivec (400 mg or 800 mg daily). On the basis of the Phase II data, the FDA approved the use of Glivec for GISTs on 1 February 2002.

AUTOCRINE
Describes an agent secreted from a cell that acts on the cell in which it is produced.

PARACRINE
Describes an agent secreted from a cell that acts on other cells in the local environment.

Other c-KIT-expressing tumours. In human systemic mastocytosis, most cases show a point mutation in codon 17 of *c-KIT*, which results in a D816V (aspartic acid 816 to valine) amino-acid substitution in the kinase-2 domain of c-KIT. Interestingly, this mutated c-KIT is resistant to inhibition by Glivec[53,58].

Expression of c-KIT and SCF has been reported in a retrospective small-cell lung cancer (SCLC) series, indicating that SCLC growth might involve an AUTOCRINE loop. Inhibition of c-KIT activation by transfection of a dominant-negative *c-KIT* gene results in loss of growth-factor independence[59,60]. Furthermore, the c-KIT/PDGF-receptor inhibitor AG1296 inhibits growth of SCLC cells in serum-containing medium[60]. In H526 SCLC cells, pretreatment with Glivec inhibited SCF-mediated c-KIT activation with an IC_{50} (half-maximal inhibitory concentration) of 0.1 μM (REF. 61). The compound also blocked downstream signal transduction, as evidenced by inhibition of SCF-mediated activation of MAPK and AKT, and potently inhibited SCF-mediated growth in serum-free medium, with a marked increase in apoptosis. Glivec also inhibited the growth of SCLC cell lines in a dose-dependent fashion when grown in serum-containing medium; however, the average IC_{50} was in the range of 5 μM (REFS 61,62).

Although *c-KIT* expression has been documented in various other human tumours, including acute myelogenous leukaemia, ovarian and testicular cancer, it will be important to determine the activation status of the receptor and its importance in the pathogenesis (for a review, see REF. 58). Furthermore, it needs to be explored whether pharmacological inhibition of PARACRINE or autocrine activation of this kinase will be successful therapeutically. Exploratory clinical studies are continuing at present in patients with *c-KIT*-expressing SCLC and acute myelogenous leukaemia.

PDGF receptor as a target

The third target of Glivec is the PDGF-receptor tyrosine kinase. Cellular studies have shown potent inhibition of the two structurally similar PDGF-α and PDGF-β receptors (PDGFR-α and PDGFR-β), as well as blockade of PDGF-mediated cellular events[47,63]. PDGF is a connective-tissue-cell mitogen with *in vivo* functions that include embryonal development, wound healing and control of interstitial-fluid pressure in soft connective tissue. There is increasing evidence that the PDGF ligand–receptor system also has an important role in tumorigenesis[64]. Paracrine and/or autocrine activation of the PDGFR kinase has been postulated in numerous malignancies, and the presence of PDGF autocrine loops is most well documented in gliomas[65]. Glivec inhibited the *in vitro* and *in vivo* growth of cells with autocrine PDGF signalling, including the formation of tumours by the human glioblastoma lines U343 and U87, which had been injected into the brains of nude mice[66]. The inhibitory effects were mediated predominantly through promotion of growth arrest rather than apoptosis.

Autocrine PDGFR activation is also well documented in tumour cells of dermatofibrosarcoma protuberans (DFSP), a highly recurrent, infiltrative skin tumour that is characterized by a chromosomal rearrangement involving chromosomes 17 and 22. The resulting fusion-gene product collagen I, α1 polypeptide (COL1A1)–PDGF-β triggers the autocrine stimulation of the PDGFR[67]. COL1A1–PDGFβ-transformed fibroblasts, as well as primary DFSP and giant-cell fibrosarcoma cell cultures, were inhibited by Glivec in vitro and in vivo[67–69]. The main mechanism by which Glivec affected DFSP tumour growth was through induction of apoptosis[69]. Preliminary data indicate that Glivec might also be active in patients with DFSP[70].

Relatively little is known about the ligand-independent activation of PDGFR. However, rearrangement of PDGFRβ has been described in chronic myeloproliferative diseases. The best known of these is the t(5;12) chromosomal translocation in chronic myelomonocytic leukaemia (CMML), in which PDGFRβ, which is located on chromosome 5, is fused to the TEL gene on chromosome 12. Transformation of haematopoietic cells occurs through oligomerization of the TEL–PDGFR-β fusion protein, which causes ligand-independent constitutive activation of the PDGFR kinase[71]. Glivec inhibited the growth of cells expressing TEL–PDGFRβ[15], and in transgenic mice that expressed the TEL–PDGFRβ, treatment with Glivec inhibited tumour formation and prolonged survival of the animals[72]. A remarkable haematological and complete cytogenetic response has been observed in two patients with chronic myeloproliferative disorders associated with a t(5;12) translocation — one of them with a well-characterized TEL–PDGFR fusion gene and the second with a rearranged PDGFR gene with an as yet unidentified partner gene[73]. Other exploratory clinical trials are being carried out in gliomas and in prostate cancer.

Targeting the tumour microenvironment

An alternative strategy to influence tumour growth is to interfere with the tumour stroma and microvasculature. Paracrine PDGF signalling in the connective-tissue tumour stroma has been described in various types of solid tumour[64]. Several lines of evidence indicate a role for PDGF in the regulation of interstitial fluid pressure (IFP)[74–76]. As most solid tumours have an increased IFP, pharmacological reduction might be a way to increase the uptake of anticancer drugs into tumours[77]. Recent experiments have shown that Glivec significantly reduced tumour IFP in subcutaneously growing PROb rat-colon carcinomas, and a concomitant increase in trans-capillary transport of a radiolabelled tracer compound into the tumour interstitium was observed[78]. These effects were mediated by inhibition of the expression of PDGFR on blood vessels and stromal cells, as tumour epithelial cells in this tumour model do not express PDGFRs.

The angiogenic activity that has been described for PDGF might not only be explained by its direct effects on capillary endothelial cells, pericytes and smooth-muscle cells[79], but might also be influenced indirectly through paracrine action on PDGF-responsive stromal and perivascular cells, which are a principal source of vascular endothelial growth factor (VEGF)[80]. PDGF has also been shown to induce the expression of VEGF in endothelial cells, which in turn causes an autocrine VEGF loop[81]. Anti-angiogenic activity of Glivec has been shown in vitro through inhibition of serum-stimulated capillary sprouting from rat aorta, and in vivo in a subcutaneous implant model in which the drug inhibited PDGF- and also VEGF- and basic fibroblast growth factor (bFGF)-stimulated vascularization[82]. Blockade of PDGFR signalling by Glivec has also been shown to inhibit angiogenesis and tumour growth in an experimental model of bone metastasis[83]. Glivec treatment of nude mice injected with PC-3MM human prostate-cancer cells into the tibia inhibited tumour-cell growth and induced apoptosis, both in tumour cells and tumour-associated endothelial cells. The effects were pronounced when mice were treated with the combination of Glivec and taxol. Interestingly, immunohistochemical studies showed that tumour cells growing in the bone (but not those in surrounding musculature) expressed high levels of PDGF-α, PDGF-β, PDGFR-α and PDGFR-β. Tumour-associated endothelial cells within the bone also expressed PDGFR-α and PDGFR-β. These data indicate that inhibition of the PDGFR in combination with chemotherapy might provide a new approach for the treatment of bone metastasis.

Conclusion

The discovery and development of Glivec has shown that is possible to produce rationally designed, molecular-targeted drugs for the treatment of a specific cancer. The research programme has also clearly shown that it is possible to define in vitro and animal models with high predictive quality, as the results of the subsequent clinical studies have largely corroborated the preclinical findings. The predictive quality was achieved in this particular case by using models with identical genetic abnormalities as those found in man. The case of Glivec also shows that compounds that do not only affect one, but two or more targets (which is frequently the case), can be beneficial in allowing several diseases with differing molecular abnormalities to be addressed, without paying too high a price in terms of toxicity.

The clinical data available so far in CML, GIST and chronic myeloproliferative disorders that involve rearrangement of the PDGFR gene indicate that the inhibition of BCR–ABL, c-KIT and PDGFRs can be achieved with Glivec in humans, and translated into clinically meaningful patient benefit. Providing clinical 'proof of concept', these data validate the initial hypothesis of this programme, and underscore the importance of rationally selecting the target diseases to be considered in the early phases of development of a molecule such as Glivec.

Beyond these reasonably well-understood malignancies, Glivec could have potential in the treatment of other malignancies that involve any of these signalling

pathways, or through targeting of the tumour micro-environment. However, most human cancers are likely to be heterogeneous with regard to molecular abnormalities, such as oncogene activation, and involve multiple signalling pathways in addition to either c-KIT and/or the PDGFR. Consequently, careful attention will have to be paid in designing clinical trials in these more complex indications as to how patients should be selected on the basis of the expression or activation of the molecular target in their tumour, as far as is technically feasible. This point has been crucial in the successful outcome of the CML, GIST and CMML trials. The activity of Glivec in more common cancers with multiple and more complex molecular abnormalities remains to be determined, and is the objective of continuing research in diseases such as SCLC, prostate cancer and gliomas. The potential activity of the combination of Glivec with other signal-transduction inhibitors or anticancer agents is also being investigated.

1. Rowley, J. D. A new consistent abnormality in chronic myelogenous leukaemia identified by quinacrine fluorescence and giemsa staining. Nature 243, 290–293 (1973).
2. Nowell, P. C. & Hungerford, D. A. A minute chromosome in human chronic granulocytic leukemia. Science 132, 1497 (1960).
3. Daley, G. Q., Van Etten, R. A. & Baltimore, D. Induction of chronic myelogenous leukemia in mice by the p210bcr/abl gene of the Philadelphia chromosome. Science 247, 824–830 (1990).
4. Kelliher, M. A. et al. Induction of chronic myelogenous leukemia in mice by the v-Abl and Bcr/Abl. Proc. Natl Acad. Sci. USA 87, 6649–6653 (1990).
5. Heisterkamp, N. et al. Acute leukaemia in Bcr/Abl transgenic mice. Nature 344, 251–253 (1990).
6. Lugo, T. G. et al. Tyrosine kinase activity and transformation potency of Bcr-Abl oncogene products. Science 247, 1079–1082 (1990).
7. Lipinsky, C. A. Drug-like properties and the causes of poor solubility and poor permeability. J. Pharmacol. Toxicol. Methods 44, 235–249 (2001).
8. Teague, S. et al. The design of leadlike combinatorial libraries. Angew. Chem. Int. Edn Eng. 38, 3743–3748 (1999).
9. Zimmermann, J. et al. (Phenylamino)pyrimidine (PAP) derivatives: a new class of potent and highly selective PDGF-receptor autophosphorylation inhibitors. Bioorg. Med. Chem. Lett. 6, 1221–1226 (1996).
10. Zimmermann, J. et al. Potent and selective inhibitors of the ABL-kinase: phenylaminopyrimidine (PAP) derivatives. Bioorg. Med. Chem. Lett. 7, 187–192 (1997).
11. Zimmerman, J., Furet, P. & Buchdunger, E. STI571. A new treatment modality for CML. ACS Symp. Ser. 796, 245–259 (2001).
12. Schindler, T. et al. Structural mechanism for STI571 inhibition of Abelson tyrosine kinase. Science 289, 1938–1942 (2000).
The first description of the structural interactions between Glivec and ABL using crystallographic studies. Provided an important insight into potential mechanisms of resistance.
13. Okuda, K. et al. ARG tyrosine kinase activity is inhibited by STI571. Blood 97, 2440–2448 (2001).
14. Druker, B. J. et al. Effects of a selective inhibitor of the Abl tyrosine kinase on the growth of Bcr-Abl positive cells. Nature Med. 2, 561–566 (1996).
The first study to document the strong efficacy of Glivec in in vitro and in vivo models of BCR-ABL-positive leukaemias.
15. Carroll, M. et al. CGP 57148, a tyrosine kinase inhibitor, inhibits the growth of cells expressing BCR-ABL, TEL-ABL, and TEL-PDGFR fusion proteins. Blood 90, 4947–4952 (1997).
16. Beran, M. et al. Selective inhibition of cell proliferation and BCR-ABL phosphorylation in acute lymphoblastic leukemia cells expressing Mr 190,000 BCR-ABL protein by a tyrosine kinase inhibitor (CGP 57148). Clin. Cancer Res. 4, 1661–1672 (1998).
17. Gambacorti-Passerini, C. et al. Inhibition of the ABL kinase activity blocks the proliferation of BCR/ABL+ leukemic cells and induces apoptosis. Blood Cells Mol. Dis. 23, 380–394 (1997).
18. Deininger, M. et al. The tyrosine kinase inhibitor CGP57148B selectively inhibits the growth of BCR–ABL-positive cells. Blood 90, 3691–3698 (1997).
19. Dan, S., Naito, M. & Tsuruo, T. Selective induction of apoptosis in Philadelphia chromosome-positive chronic myelogenous leukemia cells by an inhibitor of BCR-ABL tyrosine kinase, CGP 57148B. Cell Death Differ. 5, 710–715 (1998).

20. Le Coutre, P. et al. In vivo eradication of human BCR/ABL-positive leukemia cells with an ABL kinase inhibitor. J. Natl Cancer Inst. 91, 163–168 (1999).
21. Wolff, N. C. & Ilaria, R. L. Establishment of a murine model for therapy-treated chronic myelogenous leukemia using the tyrosine kinase inhibitor STI571. Blood 98, 2808–2816 (2001).
22. Sillaber, C. et al. STAT5 activation contributes to growth and viability in Bcr/Abl-transformed cells. Blood 95, 2118–2125 (2000).
23. Horita, M. et al. Blockade of the Bcr-Abl kinase activity induces apoptosis of chronic myeloid leukemia cells by suppressing signal transducer and activator of transcription 5-dependent expression of BCL-X. J. Exp. Med. 191, 977–984 (2000).
24. Oda, T. et al. Crkl is the major tyrosine-phosphorylated protein in neutrophils from patients with chronic myelogenous leukemia. J. Biol. Chem. 269, 22925–22928 (1994).
25. Jonuleit, T. et al. Bcr-Abl kinase downregulates cyclin-dependent kinase inhibitor p27 in human and murine cell lines. Blood 98, 1933–1939 (2000).
26. Gesbert, F. et al. BCR/ABL regulates expression of the cyclin dependent kinase inhibitor p27Kip1 through the PI3K/AKT pathway. J. Biol. Chem. 50, 39223–39230 (2000).
27. Gaston, I. et al. Abl kinase but not PI3-kinase links to the cytoskeletal defects in Bcr-Abl transformed cells. Exp. Hematol. 28, 77–86 (2000).
28. Druker, B. J. et al. Activity of a specific inhibitor of the BCR-ABL tyrosine kinase in the blast crisis of chronic myeloid leukemia and acute lymphoblastic leukemia with the Philadelphia chromosome. N. Engl. J. Med. 344, 1038–1042 (2001).
The first clinical results with Glivec in CML, documenting a high level of efficacy, low level of toxicity and describing the dose–response relationship. These results confirm the crucial role of BCR–ABL in the pathophysiology of CML.
29. Druker, B. J. et al. Efficacy and safety of a specific inhibitor of the BCR–ABL tyrosine kinase in chronic myeloid leukemia. N. Engl. J. Med. 344, 1031–1037 (2001).
30. Peng, B. et al. Clinical investigation of the PK/PD relationship for Glivec (STI571): a novel inhibitor of signal transduction. Proc. Am. Soc. Clin. Oncol. 20, 280 (2001).
31. Kantarjian, H. et al. Hematologic and cytogenetic responses to imatinib mesylate in chronic myelogenous leukemia. N. Engl. J. Med. 346, 645–652 (2002).
32. Talpaz, M. et al. Glivec™ (imatinib mesylate) induces durable hematologic and cytogenetic responses in patients with accelerated phase chronic myeloid leukemia: results of a Phase 2 study. Blood 99, 1928–1937 (2002).
33. Sawyers, C. et al. Imatinib induces hematologic and cytogenetic responses in patients with chronic myeloid leukemia in myeloid blast crisis: results of a Phase II study. Blood 99, 3530–3539 (2002).
34. Weisberg, E. & Griffin, J. Mechanism of resistance to the Abl tyrosine kinase inhibitor STI571 in BCR/ABL transformed hematopoietic cell lines. Blood 95, 3498–3505 (2000).
35. Mahon, F. et al. Selection and characterization of BCR-ABL positive cell lines with differential sensitivity to the tyrosine kinase inhibitor STI571: diverse mechanisms of resistance. Blood 96, 1070–1079 (2000).
36. Le Coutre, P. et al. Induction of resistance to the Abelson inhibitor STI571 in human leukemic cells through gene amplification. Blood 95, 1758–1766 (2000).
37. Gorre, M. E. et al. Clinical resistance to STI-571 cancer therapy caused by BCR–ABL gene mutation or amplification. Science 293, 876–880 (2001).
This study describes potential mechanisms of resistance in CML in clinical samples from treated patients.

38. Gorre, M. E. et al. Roots of clinical resistance to STI-571 cancer therapy. Science 293, 2163a (2001).
39. Barthe, C. et al. Roots of clinical resistance to STI-571 cancer therapy. Science 293, 2163a (2001).
40. Hochhaus, A. et al. Roots of clinical resistance to STI-571 cancer therapy. Science 293, 2163a (2001).
41. Von Bubnoff, N. et al. BCR–ABL gene mutations in relation to clinical resistance of Philadelphia-chromosome-positive leukaemia to STI571: a prospective study. Lancet 359, 487–491 (2002).
42. Manley, P. W. et al. Molecular interactions between Gleevec™ and isoforms of the c-Abl kinase. Proc. Am. Assoc. Cancer Res. 4196 (2002).
43. Gambacorti-Passerini, C. et al. α1 Acidic glycoprotein (AGP) binds, inhibits and causes in vivo resistance of human BCR–ABL+ leukemic cells to STI571. J. Natl Cancer Inst. 92, 1641–1650 (2000).
44. Jorgensen, H. G. et al. α1-Acid glycoprotein expressed in the plasma of chronic myeloid leukemia patients does not mediate significant in vitro resistance to STI571. Blood 99, 713–715 (2002).
45. Hofmann, W. K. et al. Relation between resistance of Philadelphia-chromosome-positive acute lymphoblastic leukaemia to the tyrosine kinase inhibitor STI571 and gene-expression profiles: a gene-expression study. Lancet 359, 481–486 (2002).
46. Druker, B. STI571 (Gleevec/Glivec, imatinib) versus interferon (IFN)+ cytarabine as initial therapy for patients with CML: results of a randomized study. Proc. Am. Soc. Clin. Oncol. 1 (2002).
47. Buchdunger, E. et al. The Abl protein-tyrosine kinase inhibitor, STI571, inhibits in vitro signal transduction mediated by c-Kit and PDGF receptors. J. Pharmacol. Exp. Ther. 295, 139–145 (2000).
48. Heinrich, M. C. et al. Inhibition of c-kit receptor tyrosine kinase activity by STI571, a selective tyrosine kinase inhibitor. Blood 96, 925–932 (2000).
49. Hirota, S. et al. Gain of function mutations of c-Kit in human gastrointestinal stromal tumors. Science 279, 577–580 (1998).
This study establishes the importance of c-KIT signalling in the pathogenesis of GIST tumours.
50. Lasota, J. et al. Mutations in exons 9 and 13 of Kit gene are rare events in gastrointestinal stromal tumors. A study of two hundred cases. Am. J. Pathol. 157, 1091–1095 (2000).
51. Lux, M. L. et al. Kit extracellular and kinase domain mutations in gastrointestinal stromal tumors. Am. J. Pathol. 156, 791–795 (2000).
52. Rubin, B. P. et al. Kit activation is a ubiquitous feature of gastrointestinal stromal tumors. Cancer Res. 61, 8118–8121 (2001).
53. Heinrich, M. C. et al. STI571 inhibits the kinase activity of wild type and juxtamembrane c-Kit mutants but not the exon 17 D816V mutations associated with mastocytosis. Blood 96, 4459 (2000).
54. Tuveson, D. A. et al. STI571 inactivation of the gastrointestinal stromal tumor c-KIT oncoprotein: biological and clinical implications. Oncogene 20, 5054–5058 (2001).
55. Joensuu, H. et al. Effect of the tyrosine kinase inhibitor STI571 in a patient with metastatic gastrointestinal stromal tumor. N. Engl. J. Med. 344, 1052–1056 (2001).
A proof-of-concept report of the efficacy of Glivec in KIT-expressing GIST, and rationale for further development in this indication, as well as in other solid tumours that express KIT.
56. Van Oosterom, A. T. et al. Safety and efficacy of imatinib (STI571) in metastatic gastrointestinal stromal tumors, a phase I study. Lancet 358, 1421–1423 (2001).

57. Blanke, C. D. et al. Evaluation of the safety and efficacy of an oral molecularly-targeted therapy, STI571, in patients with unresectable or metastatic gastrointestinal stromal tumors (GISTs) expressing c-KIT (CD117). Proc. Am. Soc. Clin. Oncol. 20, 1 (2001).

58. Heinrich, M. C. et al. Inhibition of Kit kinase activity: a novel molecular approach to the treatment of Kit-positive malignancies. J. Clin. Oncol. 20, 1692–1703 (2002). **An excellent review of KIT as a target for anticancer therapy.**

59. Krystal, G. W., Hines, S. & Organ, C. Autocrine growth of small cell lung cancer mediated by co-expression of c-kit and stem cell factor. Cancer Res. 56, 370–376 (1996).

60. Krystal, G. W., Carlson, P. & Litz, J. Induction of apoptosis and inhibition of small cell lung cancer growth by the quinoxaline tyrophostins. Cancer Res. 57, 2203–2208 (1997).

61. Krystal, G. W. et al. The selective tyrosine kinase inhibitor STI571 inhibits small cell lung cancer growth. Clin. Cancer Res. 6, 3319–3326 (2000).

62. Wang, W. L. et al. Growth inhibition and modulation of kinase pathways of small cell lung cancer lines by the novel tyrosine kinase inhibitor STI571. Oncogene 19, 3521–3528 (2000).

63. Buchdunger, E. et al. Effects of a selective inhibitor of the Abl tyrosine-kinase in vitro and in vivo by a 2-phenylaminopyrimidine derivative. Cancer Res. 56, 100–104 (1996).

64. Östman, A. & Heldin, C. H. Involvement of platelet-derived growth factor in disease: development of specific antagonists. Adv. Cancer Res. 80, 1–38 (2001).

65. Nistér, M. et al. Differential expression of platelet-derived growth factor receptors in human malignant glioma cell lines. J. Biol. Chem. 266, 16755–16763 (1991).

66. Kilic, T. et al. Intracranial inhibition of platelet-derived growth factor-mediated glioblastoma cell growth by an orally active kinase inhibitor of the 2-phenylaminopyridine class. Cancer Res. 60, 5143–5150 (2000).

67. Shimizu, A. et al. The dermatofibrosarcoma protuberans-associated collagen type 1α/platelet-derived growth factor (PDGF) B-chain fusion gene generates a transforming protein that is processed to functional PDGF-BB. Cancer Res. 59, 3719–3723 (1999).

68. Greco, A. et al. Growth inhibitory effect of STI571 on cells transformed by the COL1A/PDGFB rearrangement. Int. J. Cancer 92, 354–360 (2001).

69. Sjöblom, T. et al. Growth inhibition of dermatofibrosarcoma protuberans tumors by the platelet-derived growth factor receptor antagonist STI571 through induction of apoptosis. Cancer Res. 61, 5778–5783 (2001).

70. Awan, R. A. et al. Patients with metastatic sarcoma arising from dermatofibrosarcoma protuberans (DFSP) may respond to imatinib (STI571, Gleevec). Proc. Am. Soc. Clin. Oncol. 1637 (2002).

71. Jousset, C. et al. A domain of TEL conserved in a subset of ETS proteins defines a specific oligomerization interface essential to the mitogenic properties of the TEL–PDGFRβ oncoprotein. EMBO J. 16, 69–82 (1997).

72. Tomasson, M. H. et al. TEL/PDGFβR induces hematologic malignancies in mice that respond to a specific tyrosine kinase inhibitor. Blood 93, 1707–1714 (1999).

73. Apperley, J. F. et al. Chronic myeloproliferative diseases with t(5;12) and a PDGFRB fusion gene: complete cytogenetic remission with STI571. Blood 98, 726A (2001). **A proof-of-concept study of the efficacy of Glivec in a PDGFR-driven malignancy.**

74. Gullberg, D. et al. β1 Integrin-mediated collagen gel contraction is stimulated by PDGF. Exp. Cell Res. 186, 264–272 (1990).

75. Rodt, S. A. et al. A novel physiologic role for platelet-derived growth factor-BB in rat dermis. J. Physiol. (Lond.) 495, 193–200 (1996).

76. Heuchel, R. et al. Platelet-derived growth factor receptor regulates interstitial fluid homeostasis through phosphatidylinositol-3 kinase signaling. Proc. Natl Acad. Sci. USA. 20, 11410–11415 (1999).

77. Jain, R. K. Delivery of molecular medicine to solid tumors. Science 271, 1079–1080 (1996).

78. Pietras, K. et al. Inhibition of platelet-derived growth factor receptors reduces interstitial hypertension and increases transcapillary transport in tumors. Cancer Res. 61, 2929–2934 (2001).

79. Hellström, M. et al. Role of PDGF-B and PDGFR-β in recruitment of vascular smooth muscle cells and pericytes during embryonic blood vessel formation in the mouse. Exp. Cell Res. 186, 264–272 (1999).

80. Reinmuth, N. et al. Induction of VEGF in perivascular cells defines a potential paracrine mechanism for endothelial cell survival. FASEB J. 15, 1239–1241 (2001).

81. Wang, D. et al. Induction of vascular endothelial growth factor expression in endothelial cells by platelet-derived growth factor through the activation of phosphatidylinositol 3-kinase. Cancer Res. 59, 1464–1472 (1999).

82. Buchdunger, E., O'Reilly, T. & Wood, J. Pharmacology of imatinib (STI571). Eur. J. Cancer (in the press).

83. Uehara, H. et al. Blockade of PDGF-R signaling by STI571 inhibits angiogenesis and growth of human prostate cancer cells in the bone of nude mice. Proc. Am. Assoc. Cancer Res. 2192 (2001).

Online links

DATABASES

The following terms in this article are linked online to:

Cancer.gov:
http://www.cancer.gov/cancer_information/
acute lymphoblastic leukaemia | acute myelogenous leukaemia | chronic myelogenous leukaemia | ovarian cancer | prostate cancer | small-cell lung cancer | testicular cancer

LocusLink:
http://www.ncbi.nlm.nih.gov/LocusLink/
ABL | Abl | AGP | AKT | albumin | ARG kinase | ATP5A1 | ATP5C1| BAK1 | BCL-X₁ | BCR | Bcr | bFGF | Bruton tyrosine kinase | COL1A1 | CRKL | EGF receptor | c-ERBB2 | ERK1 | ERK2 | FGF | c-FMS | v-fms | IGF-1 receptor | INK4B | insulin receptor | JAK2 | c-KIT | p27 | PDGF-α | PDGF-β | PDGFR-α | PDGFR-β | P-GP | PKC | SCF | v-SRC | STAT5 | TEL | VEGF

Medscape DrugInfo:
http://promini.medscape.com/drugdb/search.asp
cytarabine | Glivec | interferon | taxol | verapamil

FURTHER INFORMATION

FDA: http://www.fda.gov/default.htm
Access to this interactive links box is free online.

Discovery of the Pyrrolo[2,1-f][1,2,4]triazine Nucleus as a New Kinase Inhibitor Template

John T. Hunt,*,§ Toomas Mitt,§,‡ Robert Borzilleri,§ Johnni Gullo-Brown,† Joseph Fargnoli,† Brian Fink,§ Wen-Ching Han,§ Steven Mortillo,† Gregory Vite,§ Barri Wautlet,† Tai Wong,† Chiang Yu,† Xiaoping Zheng,§ and Rajeev Bhide§

Departments of Oncology Chemistry, and Oncology Drug Discovery, Bristol-Myers Squibb Pharmaceutical Research Institute, P. O. Box 4000, Princeton, New Jersey 08543-4000

Received February 4, 2004

The pyrrolo[2,1-f][1,2,4]triazine nucleus was identified as a novel kinase inhibitor template which effectively mimics the well-known quinazoline kinase inhibitor scaffold. Attachment of a 4-((3-chloro-4-fluorophenyl)amino) substituent to the template provided potent biochemical inhibitors of the tyrosine kinase activity of EGFR, as well as inhibition of cellular proliferation of the human colon tumor cell line DiFi. Attachment of a 4-((3-hydroxy-4-methylphenyl)amino) substituent provided potent inhibitors of VEGFR-2 which also showed effects on the VEGF-dependent proliferation of human umbilical vein endothelial cells. Biological activity was maintained with substitution at positions 5 or 6, but not 7, suggesting that the former positions are promising sites for introducing side chains which modulate physicochemical properties. Preliminary inhibition studies with varying ATP concentrations suggest that, like the quinazoline-based kinase inhibitors, the pyrrolotriazine-based inhibitors bind in the ATP pocket.

Introduction

In the past decade, efforts aimed at the discovery of therapeutically useful inhibitors of protein kinases have intensified. These efforts have resulted in the identification of a variety of templates which, depending upon the nature of attached substituents, provide selective inhibition both within and across different protein kinase families.[1,2] One of these privileged scaffolds is the quinazoline nucleus 1 (Figure 1), which has served as the core template for a variety of ATP-competitive kinase inhibitors.[3] The leading examples of reversible quinazoline-based inhibitors are the clinically approved anticancer agent Iressa (**1a**, ZD1839) and OSI 774/CP 358,774 (**1b**, Tarceva), which is in Phase III clinical trials for cancer.[4,5] Both compounds are inhibitors of the receptor tyrosine kinase (RTK) activity of the epidermal growth factor receptor (EGFR/HER1), with relative selectivity for EGFR inhibition provided by the substituted aniline at position 4 and substituted alkoxy groups at positions 6 and 7. Two quinazoline-based drug candidates, one reversible (GW-572016/GW2016) and one irreversible (CI1033), which target both EGFR and the related RTK HER2 have been advanced into clinical trials.[6,7] Outside of the HER family, clinical compounds based on the quinazoline scaffold which target vascular endothelial growth factor receptor-2 (VEGFR-2/KDR) have been advanced into clinical trials.[8] Additionally, there are reports of other quinazoline-based RTK inhibitors, including compounds which target the tyrosine kinase activity of the platelet-derived growth factor receptor (PDGFR).[9]

With respect to the structure–activity relationships for kinase inhibition by quinazolines, the nitrogen at
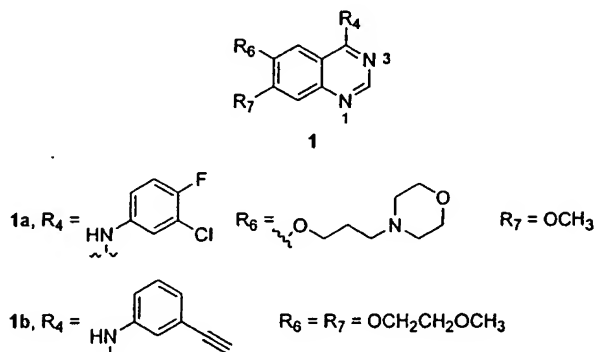
Figure 1. Structures of Iressa (**1a**) and Tarceva (**1b**), quinazoline-based inhibitors of the tyrosine kinase activity of EGFR.

position 3 is important to EGFR inhibitory potency, but the nitrogen at position 1 is an even more important contributor.[10] Electron-donating substituents on the quinazoline ring improve potency, as do specifically substituted C4-anilines. For VEGFR-2 inhibition, the key pharmacophores of the quinazoline inhibitors are reported to be N-1 and specifically substituted C4-anilines.[11]

The search for novel analogues of the quinazoline template has generated kinase inhibitors containing a variety of carbon-fused heterocycles, where the potential for maintaining key pharmacophores is intact.[1] For example, the effects on EGFR inhibition of replacing the fused benzene of the quinazoline ring system with each of the isomeric pyridines has been studied.[12] Because of the substantial prior art with 6,6-fused analogues of quinazolines, we were intrigued by the possibility that insertion of a nitrogen at a ring-fusion position could generate novel quinazoline mimics. In addition, the aza-fusion would mandate a 5,6-ring system. It has been generally found that substitution at positions 6 and 7 on the fused benzene ring of quinazoline-based kinase inhibitors is well tolerated, and these positions are often
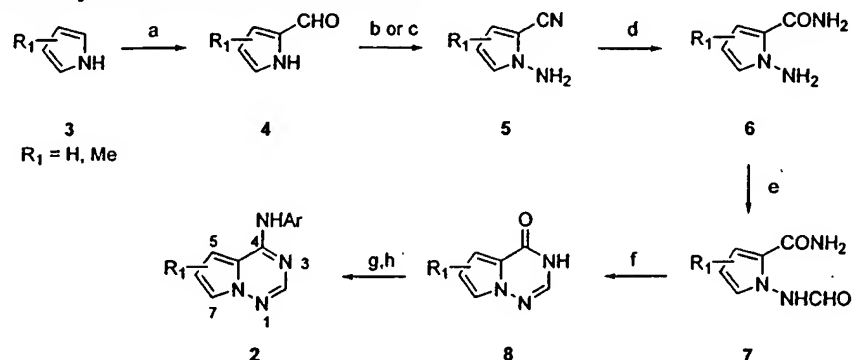
---

* To whom correspondence should be addressed. Tel: (609) 252-4989. Fax: (609) 252-6171. E-mail: john.hunt@bms.com.
§ Department of Oncology Chemistry.
† Department of Oncology Drug Discovery.
‡ Deceased March 7, 2004.

Scheme 1. Synthesis of Pyrrolotriazine Kinase Inhibitors[a]

[a] (a) DMF, POCl$_3$, 1,2-dichloroethane; (b) hydroxylamine-O-sulfonic acid, KOH, water; (c) O-mesitylenesulfonylhydroxylamine, NaH, CH$_2$Cl$_2$; (d) KOH; (e) HCO$_2$H, NaOAc; (f) NaOMe, MeOH; (g) POBr$_3$; (h) 3-chloro-4-fluoro-phenylamine or 5-amino-2-methylphenol, acetonitrile.

utilized to vary physical and pharmacokinetic properties of drug candidates. Replacement of the carbon-fused ring with a nitrogen-fused ring would allow the fused six-member ring to be replaced with a five-member ring, allowing attachment of side chains to 3 positions, each of which projects into space with a different geometry than quinazoline 6- or 7-substituents.

In this report, we describe our initial progress on aza-fused kinase inhibitors based on the quinazoline nucleus. In particular, we describe preliminary synthetic and structure—activity relationships of pyrrolo[2,1-f][1,2,4]-triazine inhibitors 2 of VEGFR-2 and EGFR.

Chemistry. The initial pyrrolotriazine targets were prepared according to a reported procedure (Scheme 1) through the intermediacy of the requisite pyrrolotriazi-nones 8.[13] The methyl-substituted 2-formylpyrroles 4 were prepared from the pyrroles 3 by reaction with phosphorus oxychloride and DMF in yields ranging from 18 to 89%. An isomeric mixture of 2-formyl-3-meth-ylpyrrole and 2-formyl-4-methylpyrrole in a 4:1 ratio was produced from the formylation of 3-methylpyrrole. Amination of this mixture with hydroxylamine O-sulfonic acid produced both N-amination as well as transformation of the aldehyde to the nitrile to form 5 (isomeric mixture of R$_1$ = 3-methyl and 4-methyl) in 20% overall yield. The same set of transformations produced 5 (R$_1$ = 5-methyl) in 65% yield by treatment of 5-methyl-2-formylpyrrole with O-mesitylenesulfonyl-hydroxylamine (MSH) in DMF followed by NaH. For 2-formyl-3,4-dimethylpyrrole, transformation to 5 (R$_1$ = 3,4-dimethyl) was produced by a two-step reaction se-quence involving treatment with aqueous hydroxyla-mine O-sulfonic acid (37% yield) and subsequent N-amination by treatment with MSH followed by NaH (94% yield). Hydrolysis of the isomeric mixture of 1-amino-2-cyano-3-methylpyrrole and 1-amino-2-cyano-4-methylpyrrole with aqueous KOH at room temperature produced 1-amino-2-aminocarbonyl-4-methylpyrrole (6, R$_1$ = 4-methyl, 61% yield), leaving the 1-amino-2-cyano-3-methylpyrrole unreacted and separable. The 1-amino-2-cyano-5-methylpyrrole was similarly hydrolyzed to 6 (R$_1$ = 5-methyl) in 94% yield. Hydrolysis of the pure 1-amino-2-cyano-3-methylpyrrole was achieved with KOH in aqueous ethanol at reflux to form 6 (R$_1$ = 3-methyl) in 82% yield. Formylation of the 1-amino group to form 7 in yields ranging from 76 to 89% was achieved with formic acid and sodium acetate. In the

case of the dimethyl isomer 6 (R$_1$ = 3,4-dimethyl), heating at 65 °C in a mixture of formic acid and sodium acetate led directly to the cyclized product 8 (R$_1$ = 5,6-dimethyl). For the remaining compounds, cyclization was achieved with sodium methoxide in methanol in 53—80% yields. Activation of the 4-position was gener-ally achieved with phosphorus oxybromide, and reaction with the requisite anilines in acetonitrile provided the target compounds in two step yields ranging from 19 to 49%. In the case of compound 10, activation was achieved with phosphorus oxychloride, and the two-step yield was 85%.

Biological Testing. Kinase inhibition assays were performed in standard fashion, using the entire cyto-plasmic sequences of EGFR and VEGFR-2 fused to glutathione S-transferase (GST-HER1, GST-VEGFR-2). Activity was determined by quantitation of the amount of radioactive phosphate transferred to the poly(Glu$_4$/Tyr) substrate. Enzyme assays to shed light on the ATP-competitive nature of the inhibitors were performed at ATP concentrations of 1 and 10 μM. Cellular assays for EGFR activity measured the ability of compounds to inhibit proliferation of DiFi human colon tumor cells or to inhibit proliferation of human umbilical vein endo-thelial cells (HUVECs) driven by EGF. Cellular assays for VEGFR-2 activity measured the ability of compounds to inhibit proliferation of HUVECs driven by the mito-gen VEGF.

Structure—Activity Relationships. To ascertain whether the pyrrolo[1,2,4]triazine nucleus was capable of affording potent kinase inhibitors, we focused on two kinases for which a variety of potent quinazoline inhibi-tors are known, namely EGFR and VEGFR-2. For these studies, we selected key C4-anilino side chains which have been shown in analogous quinazoline inhibitors to provide potent inhibition of the kinase activity of these RTKs. These side chains were the 4-(3-chloro-4-fluorophenyl)amino group, present in the clinical EGFR inhibitor Iressa, and the 4-(3-hydroxy-4-methylphenyl)-amino group, a representative side chain present in a potent preclinical series of VEGFR-2 inhibitors.[4,11] The initial analogues prepared contained an otherwise un-substituted pyrrolo[1,2,4]triazine, as well as substitution patterns with a single methyl group at either the 5-, 6-, or 7-positions.

Attachment of the (3-chloro-4-fluorophenyl)amino Iressa side chain to the 4-position of the unsubstituted

Table 1. Enzymatic and Cellular Activity of Pyrrolotriazine Kinase Inhibitors

compd	R4	R5	R6	R7	biochemical IC50 (µM)		cellular IC50 (nM)	
					VEGFR-2	EGFR	HUVEC: VEGF/EGF	DiFi
9	A	H	H	H	>10	0.118	>2500/345	1840
10	A	Me	H	H	>10	0.100	>2500/602	3060
11	A	H	Me	H	>2	0.151	>2500/509	1600
12	A	H	H	Me	>2	3.25	>2500/>2500	>10000
13	B	H	H	H	1.44 ± 0.95	0.51	360/ND[a]	>10000
14	B	Me	H	H	0.066	0.346	98 ± 88/270	>10000
15	B	H	Me	H	0.405	0.654	213 ± 89/644	>10000
16	B	H	H	Me	>10	29.4	477 ± 92/101	>10000
17	B	Me	Me	H	0.023	0.200	310/ND	>10000

[a] ND = not determined.

pyrrolo[1,2,4]triazine nucleus afforded compound **9**, which was a relatively potent inhibitor (IC50 = 118 nM) of the tyrosine kinase activity of EGFR (Table 1). For an initial analogue, this potency compares favorably to the reported IC50 value for Iressa (23 nM).[4] Appendage of a methyl group to either the 5- or 6-position of the pyrrolotriazine provided analogues **10** and **11**, respectively, which showed inhibitory potency similar to the unsubstituted compound **9**. The 7-methyl analogue **12** was substantially poorer as an inhibitor of EGFR, suggesting that this RTK makes close contacts with the pyrrolo[1,2,4]triazine nucleus in the region around the 7-position. Keeping in mind the slightly different vectors produced by the 7-pyrrolotriazine and 8-quinazoline substituents, these data are consistent with the observation that 8-substituents in the quinazoline-based EGFR inhibitors do not generally lead to improved biochemical potency.[10]

Attachment of the (3-hydroxy-4-methylphenyl)amino substituent to the 4-position of the unsubstituted nucleus afforded compound **13** which was a moderately potent inhibitor of the tyrosine kinase activity of both VEGFR-2 and EGFR. Incorporation of a 5-methyl group provided analogue **14** which showed slightly increased inhibition of EGFR but substantially increased inhibition of VEGFR-2. The 6-methyl analogue **15** was intermediate at inhibiting VEGFR-2 and roughly equivalent to the parent **13** against EGFR. Again, the 7-methyl analogue **16** was dramatically poorer as an inhibitor of both EGFR and VEGFR-2, indicating that each of these RTKs has steric requirements which are quite stringent in this area of the inhibitor. Interestingly, the 5,6-dimethyl analogue **17** was the most potent inhibitor identified of the tyrosine kinase activity of VEGFR-2, with an IC50 value of 23 nM. Improvements in potency with the modestly electron-donating methyl groups in this series parallel findings that the strongly electron-donating 6- and 7-alkoxy groups provide increased inhibitory potency in the quinazoline-based EGFR inhibitors.[10]

To gain some insight into the kinetic mechanism of enzyme inhibition by this new class of inhibitors, IC50 values against EGFR were determined for a selected compound in the presence of different concentrations of ATP. The IC50 value for **9** against EGFR increased

from 0.118 ± 0.013 µM to 1.11 ± 0.23 µM when the ATP concentration in the assay was raised from 1 µM to 10 µM. While far from conclusive, these preliminary data support the presumption that the pyrrolotriazine-based inhibitors are likely to be ATP competitive, a finding which would not be surprising, considering the fact that the quinazoline-based inhibitors from which the corresponding pyrrolotriazine inhibitors were derived are known to be ATP-competitive inhibitors.[14,11,15]

Cellular assays were undertaken to explore whether this new inhibitor class was capable of providing inhibitors of the cellular functions of the EGFR and VEGFR-2 receptors. Compounds were tested for their ability to inhibit the proliferation of the human colon adenocarcinoma cell line DiFi, which overexpresses EGFR and is known to be sensitive to EGFR inhibitors. Compounds were also tested for their ability to inhibit the proliferation of human umbilical vein endothelial cells (HUVECs) driven by either of the mitogens EGF or VEGF. In the DiFi tumor cell line, each of the submicromolar inhibitors of EGFR (**9, 10, 11**) demonstrated inhibition of cellular proliferation in the low micromolar range, while the cellular IC50 value was greater than 10 µM for the less potent EGFR biochemical inhibitor **12**. In accord with their biochemical potencies, none of the EGFR selective compounds **9, 10, 11** or **12** inhibited the proliferation of HUVECs driven by VEGF. Again in accord with their biochemical potencies, the submicromolar EGFR inhibitors **9, 10** and **11** inhibited the proliferation of HUVECs driven by EGF with submicromolar potencies.

The cellular behavior of the compounds with the phenol side chain, which were biochemical inhibitors of both VEGFR-2 and EGFR, was less easily interpretable. Several analogues (**13, 14, 15, 17**) which displayed submicromolar IC50 values for EGFR inhibition inhibited HUVEC proliferation driven by EGF, but these compounds did not inhibit the cellular proliferation of DiFi cells. Unexpectedly, all of the compounds with the phenolic side chain (**13–17**) were moderate to potent inhibitors of HUVEC proliferation, regardless of the mitogen employed or the potency of the analogue against VEGFR-2 or EGFR. For example, the inhibition of HUVEC proliferation by **14** is not unexpected,

considering that it is a submicromolar inhibitor of both VEGFR-2 and EGFR. On the contrary, the inhibition of VEGF- or EGF-driven HUVEC proliferation by **16** is completely unexpected, considering that it is a very poor inhibitor of both VEGFR-2 and EGFR. At the present time, we have no explanation for the behavior in the HUVEC proliferation assay of the pyrrolotriazines containing the phenolic side chain. Despite some inconsistencies in the cellular behavior of the phenol derivatives, both chemical series demonstrated sufficient cellular activity to showcase the potential value of RTK inhibitors derived from the pyrrolo[1,2,4]triazine nucleus.

Conclusions

A search for novel kinase inhibitor templates identified the pyrrolo[1,2,4]triazine nucleus as one which effectively mimics the well-known quinazoline kinase inhibitor template. Attachment of C4-substituents which were known from quinazoline-based compounds to confer inhibitory activity against the kinase activity of EGFR or VEGFR-2 provided potent pyrrolotriazine-based inhibitors of these receptor tyrosine kinases. Initial structure—activity studies identified positions 5 and 6 as ones which tolerated substitution, while substitution at the 7-position led to substantial loss of inhibitory activity. Confirming the importance of this new class of kinase inhibitors, many of the compounds were also shown to have substantial activity in cellular assays. Future reports will detail the application of the pyrrolo[1,2,4]triazine nucleus to the design of potent and selective inhibitors of a variety of kinases, and the demonstration of inhibitor efficacy in preclinical disease models.

Experimental Section

In Vitro Kinase Assays. Recombinant proteins that consisted of the entire cytoplasmic sequences of HER1 (GST-HER1) and VEGFR-2 (GST-VEGFR-2) fused to glutathione S-transferase were prepared by expression in Sf9 insect cells of the fusion cDNA. The protein was isolated by affinity chromatography using glutathione-Sepharose. Kinase assays were performed in 96-well microtiter plates using the synthetic polymer poly(Glu4/Tyr) (Sigma Chemicals) as a phosphoacceptor substrate. Test compounds were dissolved in DMSO and diluted with water/1% DMSO. Final concentration of DMSO in assay solutions was 0.5%, which was shown to have no effect on kinase activity. Assay conditions were (VEGFR-2; HER1): total volume (50 μL; 50 μL), enzyme (7.5 ng; 10 ng), substrate (75 μg/mL; 100 μg/mL), ATP (2.5 μM and 0.04 μCi of [γ-^{33}P]-ATP; 1 μM and 0.15 μCi of [γ-^{33}P]ATP), kinase buffer (20 mM Tris, pH 7.0, 0.5 mM DTT, 25 μg/mL BSA, 1.5 mM MnCl2; 50 mM Tris, pH 7.5, 0.5 mM DTT, 0.1 mg/mL BSA, 10 mM MnCl2), reaction conditions (27 °C, 1 h; 28 °C, 1 h), assay quench (50 μL of 30% trichloroacetic acid on ice; 10 μL of buffer consisting of 2.5 mg/mL BSA and 300 mM EDTA, followed by immediate precipitation with 110 μL of 10% TCA on ice for 30 min). The precipitates were transferred to 96-well UniFilter GF/C plates (Packard Instrument Co.) using a Filtermate universal harvester. The amount of phosphorylated substrate was quantitated using a TopCount 96-well liquid scintillation counter (PerkinElmer Life Sciences). Dose—response curves were generated to determine the concentration of inhibitor required to inhibit 50% of kinase activity (IC50). For VEGFR-2, compounds were dissolved in dimethyl sulfoxide (DMSO) to a concentration of 10 mM and were evaluated at six concentrations diluted 4-fold, each in triplicate. For HER1, compounds were dissolved in 100% DMSO and diluted into 2× the final concentration with water/1% DMSO prior to assay.

Cell Based Assays. HUVEC Proliferation Assay. Primary human umbilical vein endothelial cells (HUVECs) were purchased from Clonetics and not used beyond Passage 3 for mitogen-stimulated proliferation assays. For compound assessment, cells were plated in 100 μL minimal growth medium (Cellgro) and 1.0% fetal bovine serum, heat-inactivated in 96-well collagen IV-coated plates (Becton-Dickinson) at a density of 2 × 10³ per well in a 37 °C/5% CO₂ environment. After 24 h, growth factor and test compound at various dilutions were added to each well in a final volume of minimal growth media that contained either VEGF (Peprotech) at 80 ng/mL, EGF (Clonetics) at 5 ng/mL, or no growth factors. After 48 h, 0.5 μCi of ³H-thymidine (Amersham) was added in a volume of 20 μL minimal media, and the cells were incubated for 24 h. Plates were washed once in PBS. Upon removal of PBS, trypsin (Cellgro) was added to cells which were subsequently harvested onto glass fiber filters (Perkin-Elmer Life Sciences) using an automated harvester (Brandel Model# MWX RI-192TI). Incorporated tritium was quantified using a beta counter (Wallac Microbeta). Dose—response curves were generated to determine the IC50, which is defined as the concentration of drug required to inhibit 50% of tritium incorporation when compared to untreated mitogen-stimulated cells.

DiFi Cell Proliferation Assay. Inhibition of cell proliferation was assessed by the MTS assay using a CellTiter 96 Aqueous Non-Radioactive Proliferation Assay kit (Promega). Cells were inoculated into 96-well microtiter plates and incubated at 37 °C, 5% CO₂, 95% air, and 100% relative humidity for 24 h prior to addition of drug. At the time of drug addition, one plate of the cell line was processed using the above kit to represent a measurement of the cell population at the time of drug addition (A_{0h}). Following drug addition, the plates were incubated for an additional 72 h before processing to measure the cell population (A_{72h} and A_c represent cell populations at 72h in the presence and absence of drug, respectively). Each compound was tested at eight different concentrations in triplicate in addition to control sample without any additions. Growth inhibition of 50% (IC50) is calculated from $[(A_{72h} - A_{0h})/(A_c - A_{0h})] \times 100 = 50$, which is the drug concentration resulting in a 50% reduction in the net increase in cell population (as measured by MTS staining) of control cells during the drug incubation. Analysis of the data was done in Excel using a four-parameter logistic equation to calculate an IC50 with data fitted using the Levenburg Marquardt algorithm.

General Chemical Procedures. Proton NMR (¹H NMR) and carbon NMR (¹³C NMR) spectra were obtained on JEOL Eclipse 400 and 500 or Bruker Avance 400 MHz spectrometers and are reported relative to tetramethylsilane (TMS) reference. Low resolution mass spectra were obtained on a Finnigan SSQ 700 spectrometer; high-resolution mass spectra were obtained on a Micromass LCT spectrometer; LC/MS was performed on a ThermoFinnigan LCQ Advantage system (Micromass). Analytical and preparative HPLC were performed on YMC columns (A-302, S-5, 120A ODS, 4.6 × 150 mm; SH-345-15, S-15, 120A ODS, 20 × 500 mm; ODA S 5m 4.6 × 500 mM) with acetonitrile:water gradients containing 0.1% trifluoroacetic acid. Chromatography was performed under flash conditions using EM Science silica 0.040—0.063 mm particle size. THF was either distilled from Na/benzophenone or obtained from EM Science Drisolv bottles. Solutions were dried with magnesium sulfate unless otherwise noted.

2-Methyl-5-[(6-methylpyrrolo[2,1-*f*][1,2,4]triazin-4-yl)-amino]phenol (15). To 3.15 mL (41 mmol) of DMF at 0 °C under argon was added dropwise 3.81 mL (41 mmol) of phosphorus oxychloride. The cooling bath was removed and stirring was continued for 15 min. The solution was diluted with 9 mL of 1,2-dichloroethane and again cooled to 0 °C. A solution of 3.0 g (37 mmol) of 3-methylpyrrole in 9 mL of 1,2-dichloroethane was added dropwise. The mixture was heated to reflux for 15 min and cooled to 0 °C, and a solution of 16.2 g (203 mmol) of sodium acetate in 45 mL of water was added with vigorous stirring. The mixture was heated at reflux for 20 min and allowed to cool to room temperature. The aqueous

layer was separated and extracted twice with methylene chloride. The combined organic layers were washed with sat $NaHCO_3$ until neutral, and dried, and the solvent was removed to yield a dark oily solid which was purified by flash chromatography (10% EtOAc:hexane) to afford 3.6 g (89%) of a 4:1 mixture of 2-formyl-3-methylpyrrole and 2-formyl-4-methylpyrrole (isomers of **4**, R_1 = Me) as a pale yellow solid. The isomeric mixture was aminated as previously described to form a 2:1 mixture of 1-amino-2-cyano-3-methylpyrrole and 1-amino-2-cyano-4-methylpyrrole (isomers of **5**, R_1 = Me) in 50% yield.[13] The mixture of nitriles was hydrolyzed as described to form 1-amino-2-aminocarbonyl-4-methyl-pyrrole (**6**, R_1 = 4-Me) as well as unreacted 1-amino-2-cyano-3-methylpyrrole, which were separated by flash chromatography (10% EtOAc:hexane). The conversion of 1-amino-2-cyano-3-methylpyrrole to 1-amino-2-aminocarbonyl-3-methyl-pyrrole (**6**, R_1 = 3-Me) was accomplished by performing the hydrolysis in aqueous ethanol at reflux for 2 h. Conversion of 1-amino-2-aminocarbonyl-4-methyl-pyrrole to 6-methyl-pyrrolo[2,1-*f*][1,2,4]triazin-4(3*H*)-one (**8**, R_1 = 6-Me) in 71% overall yield was performed as described.[13] A mixture of 23 mg (0.15 mmol) of 6-methyl-pyrrolo[2,1-*f*][1,2,4]triazin-4(3*H*)-one and 0.1 g of phosphorus oxybromide was heated at 60 °C for 20 min under argon. A melt was initially obtained which solidified on continued heating. Ice was added to the solid with vigorous stirring. The mixture was extracted twice with ethyl acetate. The combined extracts were washed with sat $NaHCO_3$ and brine and dried, and the solvent was removed to afford 25 mg of crude 4-bromo-6-methyl-pyrrolo[2,1-*f*][1,2,4]triazine as a yellow solid. A solution of this material and 20 mg (0.165 mmol) of 3-hydroxy-4-methylaniline in 0.5 mL of acetonitrile was stirred overnight at room temperature under argon. The mixture was evaporated to dryness, and the residue was diluted with EtOAc. Sufficient sat $NaHCO_3$ was added to generate the free base. The organic layer was separated and washed with brine and dried and the solvent removed. The residual solid was subjected to flash chromatography (25% EtOAc:hexanes) to yield 11 mg (0.04 mmol, 29%) of **15** as a tan solid. ^1H NMR (400 MHz, DMSO-d_6) δ 9.56 (s, 1H), 9.38 (s, 1H), 7.91 (s, 1H), 7.55 (s, 1H), 7.39 (d, 1H, J = 1.3 Hz), 7.12 (dd, 1H, J = 1.8, 8.1 Hz), 7.02 (d, 1H, J = 8.1 Hz), 6.97 (s, 1H), 2.26 (s, 3H), 2.10 (s, 3H). HRMS for $C_{14}H_{13}N_4O$ (M − H), Calcd: 253.1090, Found: 253.1094.

4-(2-Chloro-4-fluorophenylamino)-pyrrolo[2,1-*f*][1,2,4]-triazine (9). ^1H NMR (400 MHz, $CDCl_3$) δ 8.04 (s, 1H), 7.91 (dd, 1H, J = 2.8, 6.6 Hz), 7.65 (s, 1H), 7.50 (ddd, 1H, J = 3.3, 7.1, 9.3 Hz), 7.16 (t, 1H, J = 8.8 Hz), 6.92 (br s, 1H), 6.73 (dd, 1H, J = 2.8, 4.4 Hz), 6.61 (d, 1H, J = 4.4 Hz). ^{13}C NMR (125 MHz, acetone-d_6) δ 154.2 (d, J = 244.2 Hz), 152.2, 146.6, 136.3, 123.2, 121.5 (d, J = 7.6 Hz), 119.9 (d, J = 20.4 Hz), 119.4, 116.6 (d, J = 22.9 Hz), 114.5, 111.2, 101.0. HRMS for $C_{12}H_9N_4$-FCl (M + H). Calcd: 263.0510, Found: 263.0500.

4-(2-Chloro-4-fluorophenylamino)-5-methyl-pyrrolo-[2,1-*f*][1,2,4]triazine (10). ^1H NMR (125 MHz, $CDCl_3$/CD_3-OD) δ 7.70 (s, 2H), 7.42 (s, 1H), 7.36−7.34 (m, 1H), 7.29−7.06 (m, 1H), 6.43 (s, 1H), 2.53 (s, 3H). ^{13}C NMR (125 MHz, $CDCl_3$/CD_3OD) δ 156.3, 154.3, 152.8, 145.0, 133.6, 125.0, 122.6, 121.0, 118.6, 116.6, 116.4, 113.6, 113.3, 111.3, 13.3. HRMS for $C_{13}H_{11}N_4FCl$ (M + H), Calcd: 276.0578, Found: 276.0599.

4-(2-Chloro-4-fluorophenylamino)-6-methyl-pyrrolo-[2,1-*f*][1,2,4]triazine (11). ^1H NMR (400 MHz, $CDCl_3$) δ 8.00 (s, 1H), 7.91 (dd, 1H, J = 2.8, 6.6 Hz), 7.50 (m, 2H), 7.16 (t, 1H, J = 8.8 Hz), 6.76 (br s, 2H), 6.42 (s, 1H), 2.33 (s, 3H). ^{13}C NMR (125 MHz, acetone-d_6) δ 154.4 (d, J = 244.2 Hz), 151.4, 145.9, 136.4, 123.0, 122.4, 121.3 (d, J = 7.6 Hz), 119.8 (d, J = 20.4 Hz), 118.4, 116.5 (d, J = 22.9 Hz), 114.4, 101.3, 11.5. HRMS for $C_{13}H_{11}N_4FCl$ (M + H), Calcd: 277.0656, Found: 277.0657.

4-(2-Chloro-4-fluorophenylamino)-7-methyl-pyrrolo-[2,1-*f*][1,2,4]triazine (12). ^1H NMR (400 MHz, $CDCl_3$) δ 8.10 (s, 1H), 7.93 (dd, 1H, J = 2.5, 6.1 Hz), 7.50 (ddd, 1H, J = 3.1, 4.0, 7.1 Hz), 7.16 (t, 1H, J = 8.7 Hz), 6.84 (br s, 1H), 6.58 (d, 1H, J = 4.6 Hz), 6.53 (d, 1H, J = 4.1 Hz), 2.55 (s, 3H). ^{13}C NMR (125 MHz, $CDCl_3$) δ 154.9 (d, J = 246.7 Hz), 151.9, 146.4,

134.6, 128.4, 124.1, 121.6 (d, J = 5.1 Hz), 121.1 (d, J = 17.8 Hz), 116.5 (d, J = 20.4 Hz), 113.6, 110.8, 99.4, 10.8. HRMS for $C_{13}H_{11}N_4FCl$ (M + H), Calcd: 277.0659, Found: 277.0657.

2-Methyl-5-(pyrrolo[2,1-*f*][1,2,4]triazin-4-ylamino)phenol (13). ^1H NMR (400 MHz, CD_3OD) δ 7.83 (s, 1H), 7.57 (dd, 1H, J = 1.6, 2.3 Hz), 7.31 (d, 1H, J = 1.6 Hz), 7.06 (d, 1H, J = 8.06 Hz), 6.96 (m, 2H), 6.69 (dd, 1H, J = 2.6, 4.3 Hz), 2.18 (s, 3H). ^{13}C NMR (125 MHz, CD_3OD) δ 156.8, 154.2, 148.1, 138.1, 131.6, 122.7, 119.9, 116.1, 115.1, 111.9, 110.9, 102.5, 15.8. HRMS for $C_{13}H_{12}N_4O$, Calcd: 240.1011, Found: 240.1014.

2-Methyl-5-[(5-methylpyrrolo[2,1-*f*][1,2,4]triazin-4-yl)-amino]phenol (14). ^1H NMR (400 MHz, DMSO-d_6) δ 9.35 (s, 1H), 8.24 (s, 1H), 7.82 (s, 1H), 7.61 (d, 1H, J = 2.5 Hz), 7.24 (d, 1H, J = 2.0 Hz), 7.02 (d, 1H, J = 8.1 Hz), 6.96 (dd, 1H, J = 2.0, 8.1 Hz), 6.63 (d, 1H, J = 2.4 Hz), 2.60 (s, 3H), 2.10 (s, 3H). HRMS for $C_{14}H_{13}N_4O$ (M − H), Calcd: 253.1090, Found: 253.1084.

2-Methyl-5-[(7-methylpyrrolo[2,1-*f*][1,2,4]triazin-4-yl)-amino]phenol (16). ^1H NMR (400 MHz, DMSO-d_6) δ 9.53 (s, 1H), 9.36 (s, 1H), 8.00 (s, 1H), 7.43 (d, 1H, J = 1.9 Hz), 7.12 (dd, 1H, J = 1.9, 8.1 Hz), 7.10 (d, 1H, J = 4.3 Hz), 7.02 (d, 1H, J = 8.1 Hz), 6.53 (d, 1H, J = 4.3 Hz), 2.44 (s, 3H), 2.10 (s, 3H). HRMS for $C_{14}H_{13}N_4O$ (M − H), Calcd: 253.1090, Found: 253.1094.

5-[(5,6-Dimethylpyrrolo[2,1-*f*][1,2,4]triazin-4-yl)amino]-2-methylphenol (17). ^1H NMR ($CDCl_3$, 400 MHz) δ 7.74 (s, 1H), 7.34 (s, 1H), 7.06 (d, 1 H, J = 8 Hz), 6.96 (d, 1H, J = 2 Hz), 6.65 (dd, 1H, J = 2, 8 Hz), 2.48 (s, 3H), 2.17 (s, 3H), 2.05 (s, 3H). HRMS for $C_{15}H_{16}N_4O$, Calcd: 268.1324, Found: 268.1330.

References

(1) Garcia-Echeverria, C.; Traxler, P.; Evans, D. B. ATP Site-Directed Competitive and Irreversible Inhibitors of Protein Kinases. *Med. Res. Rev.* **2000**, *20*, 28−57.

(2) Dumas, J. Protein Kinase Inhibitors: Emerging Pharmacophores 1997−2000. *Expert Opin. Ther. Pat.* **2001**, *11*, 405−429.

(3) Ward, W. H. J.; Cook, P. N.; Slater, A. M.; Davies, D. H.; Holdgate, G. A. et al. Epidermal Growth Factor Receptor Tyrosine Kinase: Investigation of Catalytic Mechanism, Structure-Based Searching and Discovery of a Potent Inhibitor. *Biochem. Pharmacol.* **1994**, *48*, 659−666.

(4) Barker, A. J.; Gibson, K. H.; Grundy, W.; Godfrey, A. A.; Barlow, J. J. et al. Studies Leading to the Identification of ZD1839 (Iressa™): An Orally Active, Selective Epidermal Growth Factor Receptor Tyrosine Kinase Inhibitor Targeted to the Treatment of Cancer. *Bioorg. Med. Chem.* **2001**, *11*, 1911−1914.

(5) Moyer, J. D.; Barbacci, E. G.; Iwata, K. K.; Arnold, L.; Boman, B. et al. Induction of Apoptosis and Cell Cycle Arrest by CP-358, 774, an Inhibitor of Epidermal Growth Factor Receptor Tyrosine Kinase. *Cancer Res.* **1997**, *57*, 4838−4848.

(6) Kim, T. E.; Murren, J. R. Lapatinib Ditosylate. *IDrugs* **2003**, *6*, 886−893.

(7) Smaill, J. B.; Rewcastle, G. W.; Loo, J. A.; Greis, K. D.; Chan, O. H. et al. Tyrosine Kinase Inhibitors. 17. Irreversible Inhibitors of the Epidermal Growth Factor Receptor: 4-(Phenylamino)-quinazoline- and 4-(Phenylamino)pyrido[3,2-*d*]pyrimidine-6-acrylamides Bearing Additional Solubilizing Functions. *J. Med. Chem.* **2000**, *43*, 1380−1397.

(8) Hennequin, L. F.; Stokes, E. S. E.; Thomas, A. P.; Johnstone, C.; Ple, P. A. et al. Novel 4-Anilinoquinazolines with C-7 Basic Side Chains: Design and Structure Activity Relationship of a Series of Potent, Orally Active, VEGF Receptor Tyrosine Kinase Inhibitors. *J. Med. Chem.* **2002**, *45*, 1300−1312.

(9) Matsuno, K.; Nakajima, T.; Ichimura, M.; Giese, N. A.; Yu, J.-C. et al. Potent and Selective Inhibitors of PDGF Receptor Phosphorylation. 2. Synthesis, Structure Activity Relationship, Improvement of Aqueous Solubility, and Biological Effects of 4-[4-(N-Substituted (thio)carbamoyl)-1-piperazinyl]-6,7-dimethoxy-quinazoline Derivatives. *J. Med. Chem.* **2002**, *45*, 4513−4523.

(10) Rewcastle, G. W.; Denny, W. A.; Bridges, A. J.; Zhou, H.; Cody, D. R. et al. Tyrosine Kinase Inhibitors. 5. Synthesis and Structure−Activity Relationships for 4-[(Phenylmethyl)amino]-

and 4-(Phenylamino)quinazolines as Potent Adenosine 5'-Triphosphate Binding Site Inhibitors of the Tyrosine Kinase Domain of the Epidermal Growth Factor Receptor. *J. Med. Chem.* **1995**, *38*, 3482–3487.

(11) Hennequin, L. F.; Thomas, A. P.; Johnstone, C.; Stokes, E. S. E.; Ple, P. A. et al. Design and Structure–Activity Relationship of a New Class of Potent VEGF Receptor Tyrosine Kinase Inhibitors. *J. Med. Chem.* **1999**, *42*, 5369–5389.

(12) Rewcastle, G. W.; Palmer, B. D.; Thompson, A. M.; Bridges, A. J.; Cody, D. R. et al. Tyrosine Kinase Inhibitors. 10. Isomeric 4-[(3-Bromophenyl)amino]pyrido[d]-pyrimidines Are Potent ATP Binding Site Inhibitors of the Tyrosine Kinase Function of the Epidermal Growth Factor Receptor. *J. Med. Chem.* **1996**, *39*, 1823–1835.

(13) Patil, S. A.; Otter, B. A.; Klein, R. S. Synthesis of Pyrrolo[2,1-*f*][1, 2, 4]triazine Congeners of Nucleic Acid Purines via the N–Amination of 2-Substituted Pyrroles [1]. *J. Heterocycl. Chem.* **1994**, *31*, 781–786.

(14) Fry, D. W.; Kraker, A. J.; McMichael, A.; Ambroso, L. A.; Nelson, J. M. et al. A Specific Inhibitor of the Epidermal Growth Factor Receptor Tyrosine Kinase. *Science* **1994**, *265*.

(15) Stamos, J.; Sliwkowski, M. X.; Eigenbrot, C. Structure of the Epidermal Growth Factor Receptor Kinase Domain Alone and in Complex with a 4-Anilinoquinazoline Inhibitor. *J. Biol. Chem.* **2002**, *277*, 46265–46272.

Tyrosine Kinase Inhibitors. 14. Structure–Activity Relationships for Methyl-amino-Substituted Derivatives of 4-[(3-Bromophenyl)amino]-6-(methylamino)-pyrido[3,4-d]pyrimidine (PD 158780), a Potent and Specific Inhibitor of the Tyrosine Kinase Activity of Receptors for the EGF Family of Growth Factors

Gordon W. Rewcastle,[†] Donna K. Murray,[†] William L. Elliott,[‡] David W. Fry,[‡] Curtis T. Howard,[‡]
James M. Nelson,[‡] Billy J. Roberts,[‡] Patrick W. Vincent,[‡] H. D. Hollis Showalter,[‡] R. Thomas Winters,[‡] and William A. Denny*[,†]

*Cancer Society Research Laboratory, Faculty of Medicine and Health Science, The University of Auckland,
Private Bag 92019, Auckland, New Zealand, and Parke-Davis Pharmaceutical Research, Division of Warner-Lambert
Company, 2800 Plymouth Road, Ann Arbor, Michigan 48106-1047*

The 4-[(3-bromophenyl)amino]pyrido[3,4-d]pyrimidine PD 158780 is a very potent in vitro inhibitor of the tyrosine kinase activity of the epidermal growth factor receptor (EGFR) (IC$_{50}$ 0.08 nM), and other members of the *erbB* family, by competitive binding at the ATP site of these signal transduction enzymes. A series of analogues of PD 158780 bearing solubilizing functions off the 6-methylamino substituent were prepared by reaction of the 6-fluoro derivatives with appropriate amine nucleophiles. These were evaluated for their ability to inhibit the tyrosine phosphorylating action of EGF-stimulated full-length EGFR enzyme and for inhibition of autophosphorylation of the EGFR in A431 human epidermoid carcinoma cells in culture. The most effective analogues were those bearing weakly basic substituents through a secondary amine linkage, which proved water-soluble (>10 mM) and potent (IC$_{50}$s generally <1 nM). No clear SAR could be discerned for these compounds with respect to amine base strength or the distance of the cationic center from the chromophore, suggesting that 6-substituents are in a favorable area of bulk tolerance in the enzyme binding site. More distinct SAR emerged for the ability of the compounds to inhibit EGFR autophosphorylation in A431 cells, where analogues bearing lipophilic weak bases were preferred. Representative analogues were evaluated for antitumor effectiveness against four in vivo tumor models. Significant in vivo activity was observed in estrogen-dependent MCF-7 breast and A431 epidermoid tumors. Marginal activity was seen in an EGFR-transfected tumor model, suggesting that while this cell line requires EGF for clone formation in soft agar, other growth factors may be able to replace EGF in vivo. Also, no activity was seen against the SK-OV-3 ovarian cancer model, which is known to express other EGF receptor family members (although it is not clear whether these are absolutely required for growth in vivo). While substantial growth delays were seen in A431 and MCF-7 tumor models, the treated tumors remained approximately the same size throughout therapy, suggesting that the compounds are cytostatic rather than cytotoxic under these test conditions. It remains to be determined if more prolonged therapy has cytotoxic effects in vivo, resulting in net tumor cell kill.

The epidermal growth factor receptor (EGFR) has become an important enzyme target for cancer chemotherapy.[1–3] It plays a central role in growth signaling[4,5] and is overexpressed in a significant proportion of human tumors.[6,7] A major step forward in the development of EGFR-targeted drugs was the discovery of the 4-anilinoquinazoline class of compounds.[8–12] These are potent and selective inhibitors of the tyrosine kinase activity of the EGFR via competitive binding at the ATP site of the enzyme. Potent inhibition of the enzyme is associated with small lipophilic electron-withdrawing groups at the 3-position of the aniline ring and with electron-donating groups at the 6- and/or 7-positions of the quinazoline.[9–11] For example, 1 has an IC$_{50}$ of 0.025 nM for inhibition of substrate phosphorylation by the isolated EGFR enzyme.[9] Two examples of this class (2 and 3) that exemplify these structure–activity relationships (SAR) are reported to be in clinical trial.[13,14]
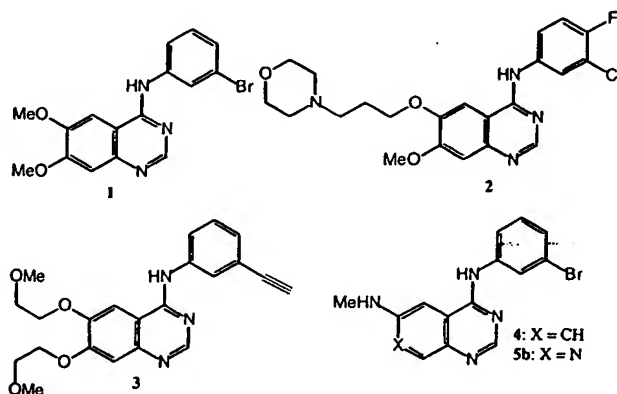
We have recently shown[15] that related 4-(3-bromoanilino)pyrido[d]pyrimidines are also potent and selective inhibitors of both substrate phosphorylation by the isolated EGFR enzyme and its autophosphorylation in cells. The most potent subclass of this series of regioi-

somers was the pyrido[3,4-*d*]pyrimidines, and in particular the 6-methylamino derivative **5b** (PD 158780). This compound had an IC_{50} of 0.008 nM for inhibition of substrate phosphorylation,[15] compared with an IC_{50} of 7 nM for the corresponding 6-(methylamino)quinazoline analogue (**4**).[11]

A detailed study[16] of **5b** showed that it was a competitive inhibitor of the EGFR with respect to ATP and inhibited EGFR autophosphorylation in A431 human epidermoid carcinoma cells with an IC_{50} of 13 nM. While the onset of inhibition was immediate, recovery of receptor autophosphorylation was slow, requiring 8 h to complete. Compound **5b** was also active against other members of the EGFR family, with IC_{50}s of 49 and 52 nM respectively for inhibition of heregulin-stimulated autophosphorylation in SK-BR-3 and MDA-MB-453 breast carcinomas. SK-BR-3 cells express EGFR, *erbB2*, and *erbB3*, while MDA-MB-453 expresses *erbB2*, *erbB3*, and *erbB4*; heregulin is a specific ligand for *erbB4* but also binds and activates heterodimers of *erbB3*, *erbB2*, and *erbB4*.[16-18] Studies of the inhibition of clone formation in soft agar of a series of transformed fibroblasts and established human breast carcinoma lines confirmed that **5b** had good activity against members of the EGFR family, while not influencing the function of related tyrosine kinases.[16] The above properties of **5b** make it an attractive lead compound for further development.

The broad SAR reported for the 4-anilinoquinazolines and pyrido[*d*]pyrimidines as EGFR inhibitors are consistent[19] with the compounds binding to the ATP site of the EGFR. In this model,[19] the N-1 atom accepts an H-bond from Met-769 and N-3 from the side chain of Thr-766 on strand 5 deep in the binding cleft, and the anilino side chain binds in an adjacent hydrophobic pocket. This pocket is exceptionally large in the EGFR, formed in part by three additional sulfur-containing amino acids (Cys-751, Met-769, and Met-742). This binding model suggests that the only positions on the model where substantial property-modulating groups can be placed are the 6- and 7-positions of the bicyclic chromophore, which are situated at the entrance of the adenine binding cleft. We have shown previously[20] that a variety of bulky side chains on the 7-position of pyrido-[4,3-*d*]pyrimidines are acceptable, but show a distinct SAR.

In this paper we report the synthesis and evaluation of a series of 6-substituted pyrido[3,4-*d*]pyrimidines, representing analogues of **5b** substituted on the 6-methylamino group. We also compare SAR for these compounds with that of the related 7-substituted pyrido-[4,3-*d*]pyrimidines for inhibition of isolated EGFR. Selected analogues were also evaluated for autophosphorylation in A431 cells and in vivo against a range of human tumor xenografts in nude mice.

Chemistry

The 6-substituted 4-(phenylamino)pyrido[4,3-*d*]pyrimidines of Table 1 were prepared by the general method of Scheme 1. Activation of the known[21] 6-fluoropyrido-[3,4-*d*]pyrimidin-4(3*H*)-one (**11**) with $SOCl_2$/DMF gave 4-chloro-6-fluoropyrido[3,4-*d*]pyrimidine (**12**), and reaction of this with appropriate 3-substituted anilines gave the key intermediates **13–16**. Displacement of the

Scheme 1[a]

11 → 12 →

13: X = Br
14: X = Cl
15: X = CF_3
16: X = Me

compounds 5-9 of Table 1
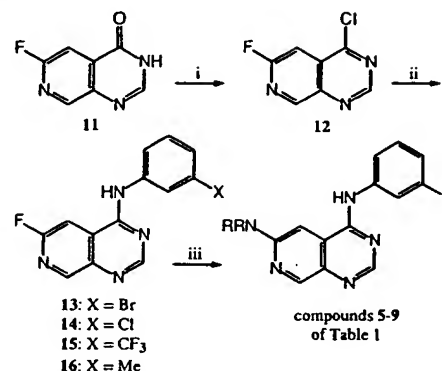
[a] (i) $SOCl_2$/dichloroethane/DMF/reflux/2.5 h; (ii) 3-X-aniline/2-propanol/reflux/45 min; (iii) RRNH/DMSO/85-95 °C/2 h–5 d.

Scheme 2[a]

13 → 17 → 10n
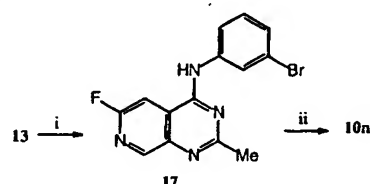
[a] (i) $MeNO_2$/DBU/DMSO/25 °C/24 h; (ii) 4-(2-aminoethyl)morpholine/DMSO/80 °C/22 h.

Scheme 3[a]

18 → 19 → 20
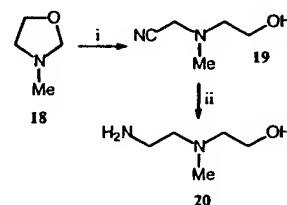
[a] (i) aqueous HCN; (ii) $LiAlH_4$.

6-fluorine atom from these intermediates with amine nucleophiles was normally conducted in DMSO at 80–95 °C for 1–5 days (in a pressure vessel for the more volatile amines) followed by purification by direct recrystallization or chromatography (method A). With amino acid nucleophiles, it was necessary to preform the sodium salts prior to reaction (method B).[20]

The 2-methyl derivative **10n** was prepared by reaction of **13** with nitromethane to give **17** followed by fluorine displacement with 4-(2-aminomethyl)morpholine (Scheme 2). Most of the required amines were commercially available. 2-[(2-Aminoethyl)methylamino]ethanol was prepared by the general method of Kohn et al.[22] (Scheme 3).

Results and Discussion

The structures of the 6-substituted 4-(phenylamino)-pyrido[3,4-*d*]pyrimidines studied (**5–10**) are recorded in Table 1. Inhibition of tyrosine phosphorylation of a random tyrosine/glutamic acid copolymer (Sigma) by EGF-stimulated full-length EGFR enzyme isolated from A431 cells was measured by a filter binding assay.[8] At least two complete dose–response curves were determined for each compound, and averaged IC_{50}s are listed in Table 1. Most compounds were also evaluated for their ability to inhibit autophosphorylation of the EGF receptor in A431 human epidermoid carcinoma cells.

Table 1. Structural and Biological Properties of 6-Substituted 4-(Phenylamino)pyrido[3,4-d]pyrimidines

compounds 5–9   10n
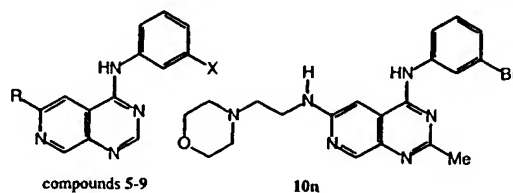
no.	R	X	mp (°C)	solubility[a] (nM)	IC$_{50}$ (nM) enzyme[b]	IC$_{50}$ (nM) autophos[c]
5a	NH$_2$	Br	ref 13		0.13	16
5b	NHMe	Br	ref 13	0.10	0.008	13
5c	NMe$_2$	Br	ref 13	0.06	0.006	21
5d	NHCH$_2$CH$_2$OH	Br	209–210	0.02	0.19	
5e	N(Me)CH$_2$CH$_2$OH	Br	236–237	0.11	0.22	
5f	NHCH$_2$CH(OH)CH$_2$OH	Br	186.5–188	0.21	0.18	
5 g	N(Me)CH$_2$CH(OH)CH$_2$OH	Br	159–160	0.18	0.56	
5h	NH(CH$_2$)$_2$NMe$_2$	Br	250–252	>48	1.1	43
5i	NH(CH$_2$)$_3$NMe$_2$	Br	160–161	30	1.2	16
5j	NH(CH$_2$)$_4$NMe$_2$	Br	176–177	38	1.8	19
5k	NHCH$_2$CH(OH)CH$_2$NEt$_2$	Br	189–192	36	4.6	28
5l	NH(CH$_2$)$_2$N(Me)CH$_2$CH$_2$OH	Br	182–189	>45	1.7	27
5m	N(Me)(CH$_2$)$_2$NMe$_2$	Br	260–262	39	8.1	46
5n	NH(CH$_2$)$_2$morpholinyl	Br	267 dec	10	0.65	7.9
5o	NH(CH$_2$)$_3$morpholinyl	Br	177–178	>44	1.0	5.9
5p	NH(CH$_2$)$_3$NMepiperazinyl	Br	182–183	32	3.9	8.9
5q	NH(CH$_2$)$_2$N(CH$_2$CH$_2$OH)$_2$	Br	210–211	36	0.93	71
5r	NH(CH$_2$)$_3$N(CH$_2$CH$_2$OH)$_2$	Br	205–207	20	0.35	230
5s	NHCH$_2$(3-pyridyl)	Br	260–262	12	1.5	13
5t	NHCH$_2$CH$_2$(2-pyridyl)	Br	170–171.5	17	1.2	8.1
5u	NH(CH$_2$)$_2$(4-imidazolyl)	Br	200–201	15	0.78	6.3
5v	NH(CH$_2$)$_3$(1-imidazolyl)	Br	195.5–197	23	1.7	9.1
5w	4-Mepiperazinyl	Br	219.5–222	2.5	6.4	102
5x	NHCH$_2$COOH	Br	234–239	5	0.28	
5y	N(Me)CH$_2$COOH	Br	225–227	44	0.44	
5z	NH(CH$_2$)$_2$COOH	Br	276–280	38	0.27	449
6b	NHMe	H	ref 13		9	
7b	NHMe	Cl	185.5–187		0.19	
8b	NHMe	CF$_3$	172–173		1.1	
9a	NH$_2$	Me	235.5–237	0.4	3.1	
9b	NHMe	Me	189–190		0.45	23
9c	NMe$_2$	Me	239–241	0.02	2.8	
9n	NH(CH$_2$)$_2$morpholinyl	Me	168–170	>40	1.5	20
9o	NH(CH$_2$)$_3$morpholinyl	Me	200–203	>35	1.8	
9u	NH(CH$_2$)$_2$(4-imidazolyl)	Me	207–209	>30	1.3	
10n	NH(CH$_2$)$_2$morpholinyl[d]	Br	>260		117	

[a] Solubility in water at 20 °C, determined by HPLC (see text). Values are for the hydrochloride or dihydrochloride salt form of amines and the sodium salt form of acids. [b] IC$_{50}$, concentration of drug (nM) to inhibit the phosphorylation of a random tyrosine/glutamic acid copolymer by EGFR (prepared from human A431 carcinoma cell vesicles by immunoaffinity chromatography). See Experimental Section for details. Values are the averages from at least two independent dose–response curves; variation was generally ±15%. [c] IC$_{50}$s for inhibition of autophosphorylation of EGFR in A431 cells in culture. Values are the average of two experiments; see Experimental Section for details. [d] 2-Me analogue.

Compound aqueous solubilities were determined by HPLC following sonication for 30 min at 20 °C. Lactate buffer (0.05 M) was used for compounds with neutral side chains and water for hydrochloride salts of amines and sodium salts of acids.

The initial set of 6-methylamino compounds (6b, 7b, 8b, and 9b) was prepared to compare with 5b and evaluate SAR for the anilino side-chain substituent. A number of small lipophilic substituents have been used at the 3′-position in anilinoquinazolines[9,12–14] and corresponding pyrido[4,3-d]pyrimidines,[23] including Cl, CF$_3$, Me, and ethynyl. We have previously shown[11] that the 3′-Br derivative was the most potent enzyme-inhibitory analogue in the anilinoquinazoline series, and this proved also to be the case with the pyrido[3,4-d]-pyrimidines. The 3′-Br analogue 5b (IC$_{50}$ 0.008 nM) proved by far to be the most potent inhibitor of the isolated enzyme, and we focused mainly on this sub-

stituent in developing the 6-substituted series, although a small number of 3-Me analogues were also prepared for comparison purposes.

Compounds 5d–g, bearing hydroxyl substituents, although considerably less potent than the parent 5b against the isolated enzyme, retained acceptable levels of inhibition (IC$_{50}$s <1 nM). However, they did not show improved aqueous solubility over 5b. In contrast, all but one of the basic analogues 5h–w had aqueous solubilities of ≥10 mM; the exception was 5w, with a rigid, directly attached piperazine substituent. All of the weak bases were evaluated for inhibition of isolated enzyme and of autophosphorylation. Compounds 5h,m compared the utility of a secondary versus tertiary amine linkage; the tertiary amine 5m was less effective against isolated enzyme, but no difference was seen in the autophosphorylation assay. Because of this result, and a more extensive evaluation of this aspect (which

showed no advantage) in the related pyrido[4,3-*d*]-pyrimidines,[20] tertiary amine linkages were not investigated further.

For the 14 compounds with NH-linked amine side chains (5h−l, 5n−v), no clear SAR emerges for inhibition of substrate phosphorylation by the isolated enzyme (Table 1). These 6-substituents vary in amine base strength (from about pK_a 7 to 10), the distance of the cationic center from the chromophore (from 3 to 5 atoms), and the overall lipophilicity of the side chain (containing from one to two additional OH groups). However, nearly all of have IC$_{50}$ values of around 1 nM, varying by less than 10-fold (except for two outliers, 5k,p, by less than 5-fold). There is no variation with positioning of the cation (5h−j), with side-chain lipophilicity (for example, 5h,q), or with base strength (several examples). This is in contrast to the 7-subsstituted pyrido[4,3-*d*]pyrimidines,[20] where IC$_{50}$s between analogues with cationic side chains varied by about 100-fold, improving with distance from the chromophore and for weak bases. While the modeling studies[19] show that both 6- and 7-substituents are in an area of bulk tolerance in the binding site, at the entrance of the ATP pocket, the above results suggest that 6-substituents are in a more favorable environment.

There were clear SARs for the ability of the basic compounds to inhibit EGFR autophosphorylation in A431 cells (Table 1). The hydrophilic OH-containing analogues, and especially the diols 5q,r, were relatively inactive, despite high potency against the isolated enzyme. This is almost certainly due to poor cellular uptake characteristics. With the exception of the (CH$_2$)$_2$-NMe$_2$ analogue 5h, where the cationic charge is positioned closest to the chromophore, all the other NH-linked analogues were at least as potent as the parent 5b. Overall, the weaker bases (e.g., 5u) appeared to show better activity. A small series of analogous 3′-methyl derivatives with amine side chains was also studied (compounds 9n,o,u) but these were less active than their 3′-Br analogues in both assays, as shown previously[12,23−25] in several series of related EGFR inhibitors. The 2-methyl compound 10n was prepared to check bulk tolerance at this position, but it showed very poor activity, as suggested both from previous studies with 4-anilinoquinazolines[11] and from the binding model.[19]

Three anionic derivatives (5x−z) were also examined. These were more potent than any of the amine analogues against the isolated enzyme, but 5z showed very poor activity in the cell-based autophosphorylation assay. A similar result was seen for the 7-substituted pyrido[4,3-*d*]pyrimidines[20] and is again attributed to poor cellular uptake.

From the above results, three compounds (5h,k, n), which represent the range of structural variations studied, were selected for comparison with the parent 5b in xenograft assays in vivo. They all had much better aqueous solubility than 5b and showed acceptable activity in the two screening assays (IC$_{50}$s for inhibition of the isolated enzyme of ∼1 nM and IC$_{50}$s comparable to that of the parent 5b for inhibition of autophosphorylation). Like 5b,[16] all showed an ability to shut down both EGF and heregulin-stimulated receptor autophos-

Table 2. Inhibition (IC$_{50}$ Values, μM) of EGF-Dependent Verus Heregulin-Dependent Tyrosine Autophosphorylation

no.	EGF[a]	heregulin[b]
5b	13	52
5h	43	379
5k	28	1100
5n	7.9	219

[a] EGF-dependent receptor autophosphorylation in A431 cells. [b] Heregulin-dependent receptor autophosphorylation in MDA-MB-453 cells.

Table 3. Selectivity of Inhibition of Isolated EGFR Over Other Receptor Tyrosine Kinases by Selected Analogues (IC$_{50}$ Values, μM)

no.	EGFR[a]	c-Src[b]	FGFR[c]	PDGFR[d]	IR[e]
5h	0.0011	>50 (42%)[f]	>50 (41%)	>50 (14%)	>50 (0%)
5k	0.0046	>50 (26%)	>50 (24%)	>50 (12%)	>50 (0%)
5n	0.0007	>50 (14%)	>50 (39%)	>50 (17%)	>50 (12%)

[a] See footnote b, Table 1. [b] For conditions, see ref 36. [c] Fibroblast growth factor receptor; for conditions, see ref 36. [d] Platelet-derived growth factor receptor; for conditions, see ref 36. [e] Insulin receptor; for conditions, see ref 36. [f] Percentage inhibition at 50 μM.

phorylation in cells (Table 2), suggesting they are broad-spectrum inhibitors across the *erbB* family. At the same time, as also shown previously for 5b,[16] these compounds had little or no activity against a series of other receptor tyrosine kinases (Table 3), indicating a high degree of specificity for the *erbB* family.

These compounds were evaluated in four xenograft tumor model systems in nude mice (Table 4), and the 3′-methyl analogue 9b was also studied in the EGFR line. The A431 epidermoid xenograft was selected based on its in vitro mitogenic responsiveness to EGF and inhibition of growth on plastic by anti-EGF receptor monoclonal antibodies. The EGFR cell line was selected due to its expression of the transformed phenotype upon transfection with the human EGF receptor and its EGF requirement for clone formation in soft agar.[26] The MCF-7 breast and SK-OV-3 ovarian tumor models were selected based on their in vivo expression of other EGF receptor family members.

Compound 5b had the best therapeutic effect against the A431 epidermoid carcinoma when administered either intraperitoneally or orally (Table 4) compared to compounds 5h,k,n at equitoxic doses. The latter three compounds produced only marginal responses in this model. All three compounds (5b,h,k) produced measurable, significant effects against a mouse fibroblast transfected with human EGFR. The antitumor effects of these compounds were lost when the dose route was changed from intraperitoneal to peroral. Compounds 5n and 9b were also evaluated against this tumor model but were ineffective.

Neither compound 5b nor 5n was effective against the SK-OV-3 ovarian xenograft. This was unexpected, since this cell line overexpresses *erbB2*. The lack of effectiveness may indicate that although this cell line overexpresses *erbB2* it may not be dependent on this receptor for growth in vivo. Compounds 5b,n produced a significant therapeutic effect against the estrogen-dependent MCF-7 breast carcinoma at equitoxic dose levels, whereas 5k was ineffective against this tumor model. Compound 5b was the most active against the human tumor xenografts A431 and MCF-7 when evaluated at the equitoxic doses reported in the table.

Table 4. In Vivo Activity of Selected Analogues against Tumor Xenografts in Nude Mice

no.	tumor[a]	dose (mg/kg)	schedule[b]	weight change (g)	T/C(%) on last therapy day[c]	T−C (days)[d]	log net cell kill[e]
5b	A431	75	ip. b.i.d. days 7−21	−0.8	41	8.4[g]	−0.3
	A431	100	po, days 7−21	−1.3	38	16.0	+0.1
	EGFR	38	ip. b.i.d. days 1−15	−0.1	38	3.7[g]	−1.0
	EGFR	400[f]	po, days 1−15	+	67	1.2	−1.3
	MCF-7	50	ip. b.i.d. days 1−15	+	27	15.2[g]	+0.1
	MCF-7	25	ip. b.i.d. days 1−15	−0.2	14	11.2[g]	−0.1
	SK-OV-3	30	ip. b.i.d. days 10−14, 17−21, 24−28	−1.6	67	0.8	−0.7
5h	A431	25	ip. b.i.d. days 7−21	−1.4	66	4.7	−0.5
	EGFR	25	ip. b.i.d. days 1−15	−1.1	43	3.3[g]	−1.0
	EGFR	200	po, days 1−15	+	47	1.1	−1.3
5k	A431	25	ip. b.i.d. days 7−21	−0.7	62	5.0	−0.5
	EGFR	25	ip. b.i.d. days 1−15	−0.9	44	5.0[g]	−0.9
	EGFR	200	po, days 1−15	+	94	0	
	MCF-7	25	ip. b.i.d. days 1−15	−0.3	77	3.3	−0.6
5n	A431	12	ip. b.i.d. days 7−21	−0.2	93	1.9	−0.7
	A431	25	ip. b.i.d. days 13−26	−1.1	98	2.1	−0.3
	EGFR	25	ip. b.i.d. days 1−15	−1.3	77	1.2	−1.2
	EGFR	400[f]	po, days 1−15	−2.0	15	2.8	−1.1
	MCF-7	25	ip. b.i.d. days 1−15	+	34	11.7[g]	−0.1
	SKOV-3	25	ip. b.i.d. days 10−14, 17−21, 24−28	−2.1	100	0	
9b	EGFR	38	ip. b.i.d. days 1−15	−0.9	68	2.0	−1.2

[a] The indicated tumor fragments were implanted sc into the right axilla of mice on day 0. [b] Compounds were administered intraperitoneally or orally on the indicated schedules. The maximum tolerated dose (LD_{10}) from a complete dose−response is shown for individual experiments. Reporting the maximum tolerated dose allows comparison of the antitumor effectiveness of test compounds at equitoxic dose levels. [c] Ratio of median treated tumor mass/median control tumor mass × 100%. [d] The difference in days for the treated (T) and control (C) tumors to reach 750 mg. [e] The net reduction in tumor burden, in log, between the first and last treatments. [f] Highest dose tested. [g] Significantly different from control (t-test, $p < 0.05$).

Compound 5n was active only against the MCF-7 tumor model. In the A431 and MCF-7 models the tumors treated with equitoxic doses of these compounds did not increase substantially in size over the course of therapy but resumed growth at the cessation of therapy.

Conclusions

This study was designed to determine the effects of water-soluble groups attached at the 6-NHMe substituent of the extremely potent EGFR inhibitor 5b (PD 158780). A small series of 3′-substituted analogues of 5n confirmed that a 3′-bromo atom provided the most potent derivative, and this was primarily used in the main study. While compounds bearing neutral hydroxylated substituents at the 6-position retained relatively good inhibitory potencies, aqueous solubility was not improved, while anionic substituents resulted in poor cellular uptake (as judged by relatively low potencies in the autophosphorylation assay). The most suitable substituents were weak bases attached through a secondary amine linkage; the corresponding compounds had aqueous solubilities of ≥10 mM and IC_{50}s for inhibition of the isolated enzyme of ca. 1 nM. No clear SAR could be discerned for amine base strength or the distance of the cationic center from the chromophore, suggesting that 6-substituents are in a favorable area of bulk tolerance in the enzyme binding site. More distinct SAR emerged for the ability of the compounds to inhibit EGFR autophosphorylation in A431 cells, where analogues bearing lipophilic weak bases were the best.

Three analogues (5h,k,n), with potent activity against the isolated enzyme and possessing soluble basic side chains where the above important parameters of lipophilicity and base strength were varied, were evaluated for antitumor effectiveness against four in vivo tumor model systems, along with the parent 5b and a 3′-Me analogue (9b). Meaningful in vivo activity against human xenografts was observed only in two model systems: the estrogen-dependent MCF-7 breast and A431 epidermoid tumors. The small but significant in vivo growth delay effects of these compounds against the EGFR tumor model are reflective of the fact that this manufactured cell line doubles in volume each day and hence progresses very rapidly. These results may also indicate that while this cell line requires EGF for clone formation in soft agar, other growth factors may be able to replace EGF in vivo.

No activity was seen for compounds 5b,n against the SK-OV-3 ovarian tumor. While both the MCF-7 and SK-OV-3 tumors are known to express other EGF receptor family members in vivo, these may not be absolutely required for growth in vivo. However, two of the three compounds evaluated against MCF-7 (5b,n) showed significant antitumor effects. These two compounds also had the lowest relative IC_{50} values for the inhibition of heregulin-dependent tyrosine phosphorylation in vitro (Table 2). It is notable that in the human tumor xenografts A431 and MCF-7, where responses were observed, the treated tumors remained approximately the same size throughout therapy, suggesting that these compounds are cytostatic rather than cytotoxic under these test conditions. It remains to be determined if more prolonged therapy would have cytotoxic effects in vivo, resulting in high positive net cell kill values.

Experimental Section

Analyses were performed by the Microchemical Laboratory, University of Otago, Dunedin, New Zealand. Melting points were determined using an Electrothermal model 9200 digital melting point apparatus and are as read. NMR spectra were measured on Bruker AC-200 or DRX-400 spectrometers and referenced to Me₄Si. Mass spectra were recorded on a Varian VG 7070 spectrometer at nominal 5000 resolution. HPLC was

carried out using a Bondclone 10 C18 column, with a Phillips PU4100M gradient elution pump and a Phillips PU 4120 diode array detector, eluting with the appropriate ratios of 80% acetonitrile/20% water (solvent A) and ammonium formate buffer (solvent B; 28 g of ammonium formate + 2.55 mL of formic acid, made up to 1 L in deionized water, pH 4.5).

2-[(2-Aminoethyl)methylamino]ethanol (20), Scheme 3. Condensation of 3-methyloxazolidine (18) and aqueous HCN as reported[22] gave [*N*-(2-hydroxyethyl)methylamino]-acetonitrile (19) (93%) as an oil: bp 70−72 °C/0.03 mmHg (lit.[27] bp 62−63 °C/0.05 mmHg); ^{1}H NMR (CDCl$_3$) δ 3.70−3.64 (br m, with D$_2$O wash collapses to t, J = 5.3 Hz at δ 3.67, 2 H), 3.61 (s, 2 H), 2.69 (t, J = 5.3 Hz, 2 H), 2.43 (s, 3 H), 2.19 (br s, exchanges with D$_2$O); CIMS *m/z* (relative intensity) 115 (MH$^+$, 46), 88 (100).

Reduction of 19 with LiAlH$_4$ gave 20 as an oil: bp 81−82 °C/0.42 mmHg (lit.[28] bp 115−117 °C/16 mmHg, lit.[29] bp 103−104 °C/8 mmHg); ^{1}H NMR (CDCl$_3$) δ 3.61 (t, J = 5.3 Hz, 2 H), 2.81 (t, J = 5.8 Hz, 2 H), 2.55 (t, J = 5.5 Hz, 2 H), 2.50 (t, J = 6.3 Hz, 2 H), 2.35 (br s, 3 H), 2.29 (s, 3 H); CIMS *m/z* (relative intensity) 119 (MH$^+$, 100), 102 (97), 88 (91).

4-[(3-Bromophenyl)amino]-6-fluoropyrido[3,4-*d*]pyrimidine (13), Scheme 1. A stirred suspension of 6-fluoropyrido[3,4-*d*]pyrimidin-4(3*H*)-one[21] (11) (30.0 g, 182 mmol) in 1,2-dichloroethane (182 mL) was treated successively with SOCl$_2$ (182 mL) and then ca. 1 mL of DMF. The mixture was heated at reflux for 2.5 h, then concentrated to a solid, and coevaporated twice with 1,2-dichloroethane. The residue was dissolved in CH$_2$Cl$_2$ and filtered through a short pad of silica gel, eluting with CH$_2$Cl$_2$ to give 4-chloro-6-fluoropyrido[3,4-*d*]-pyrimidine (12) (30.5 g, 91%). A sample was crystallized from *tert*-butyl methyl ether: mp 75−76 °C; ^{1}H NMR (CDCl$_3$) δ 9.29 (s, 1 H, H-2), 9.16 (s, 1 H, H-8), 7.65 (dd, J = 0.7, 2.0 Hz, 1 H, H-5); ^{19}F NMR δ −68.9 (s); ^{13}C NMR δ 162.1 (d, J_{C-F} = 7 Hz), 161.8 (d, J_{C-F} = 242 Hz), 154.1 (d, J_{C-F} = 2 Hz), 153.4 (d, J_{C-F} = 15.3 Hz), 143.7 (d, J_{C-F} = 3 Hz), 130.7 (d, J_{C-F} = 9 Hz), 100.9 (d, J_{C-F} = 39.7 Hz). Anal. (C$_7$H$_3$N$_3$ClF) C, H, N.

A mechanically stirred solution of 12 (30.0 g, 163 mmol) and 3-bromoaniline (33.75 g, 196 mmol) in 2-propanol (400 mL) was heated at reflux for 45 min. The resulting suspension was concentrated to ca. 150 mL, and the resulting precipitate was collected, washed successively with 2% aqueous NaOH to neutral pH, water, and 2-propanol, and dried over P$_2$O$_5$ to give 13 (49.1 g, 94%): mp (2-propanol) 224−226 °C (lit.[15] mp 219.5−221 °C); ^{1}H NMR [(CD$_3$)$_2$SO] δ 10.06 (br s, 1 H, NH), 8.94 (s, 1 H, H-8), 8.73 (s, 1 H, H-2), 8.23 (br s, 2 H, H-5,2′), 7.90 (br d, J = 7.5 Hz, 1 H, H-6′), 7.39 (t, J = 7.8 Hz, 1 H, H-5′), 7.35 (d, J = 8.0 Hz, 1 H, H-4′); ^{19}F NMR δ −74.12 (s); ^{13}C NMR δ 159.8 (d, J_{C-F} = 233 Hz, C-6), 156.6 (d, J_{C-F} = 5 Hz), 154.9 (C-2), 150.7 (d, J_{C-F} = 15 Hz, C-8), 142.8, 140.0, 130.5, 126.7, 124.1, 123.2 (d, J_{C-F} = 9 Hz), 121.2, 120.6, 99.6 (d, J_{C-F} = 40 Hz, C-5); CIMS *m/z* (relative intensity) 321 (MH + 2$^+$, 65), 319 (MH$^+$, 100).

The following compounds were prepared similarly.

4-[(3-Chlorophenyl)amino]-6-fluoropyrido[3,4-*d*]pyrimidine (14): from 12 and 3-chloroaniline (89%); mp (MeOH/H$_2$O) 224−225 °C; ^{1}H NMR [(CD$_3$)$_2$SO] δ 10.11 (s, 1 H, NH), 8.97 (s, 1 H, H-8), 8.76 (s, 1 H, H-5), 8.28 (s, 1 H, H-2), 8.14 (t, J = 2.0 Hz, 1 H, H-2′), 8.26 (dd, J = 8.2, 1.3 Hz, 1 H, H-6′), 7.47 (t, J = 8.1 Hz, 1 H, H-5′), 7.24 (dd, J = 8.0, 1.4 Hz, 1 H, H-4′). Anal. (C$_{14}$H$_{12}$ClN$_5$) C, H, N.

6-Fluoro-4-[[3-(trifluoromethyl)phenyl]amino]pyrido-[3,4-*d*]pyrimidine (15): from 12 and 3-(trifluoromethyl)-aniline (95%); mp (MeOH/H$_2$O) 209−211 °C; ^{1}H NMR [(CD$_3$)$_2$-SO] δ 10.25 (s, 1 H, NH), 8.99 (s, 1 H, H-8), 8.78 (s, 1 H, H-5), 8.35 (s, 1 H, H-2), 8.30 (s, 1 H, H-2′), 8.26 (d, J = 8.3 Hz, 1 H, H-6′), 7.68 (t, J = 8.0 Hz, 1 H, H-5′), 7.53 (d, J = 7.7 Hz, 1 H, H-4′). Anal. (C$_{15}$H$_{12}$F$_3$N$_5$) C, H, N.

6-Fluoro-4-[(3-methylphenyl)amino]pyrido[3,4-*d*]pyrimidine (16): from 12 and *m*-toluidine (92%); mp (MeOH/H$_2$O) 190−192 °C; ^{1}H NMR [(CD$_3$)$_2$SO] δ 9.99 (s, 1 H, NH), 8.93 (s, 1 H, H-8), 8.68 (d, J_{H-F} = 1.8 Hz, 1 H, H-5), 8.29 (s, 1 H, H-2), 7.72−7.68 (m, 2 H, H-2′,6′), 7.32 (t, J = 8.0 Hz, 1 H, H-5′),

7.02 (d, J = 7.4 Hz, 1 H, H-4′), 2.36 (s, 3 H, CH$_3$). Anal. (C$_{14}$H$_{11}$FN$_4$) C, H, N.

4-[(3-Bromophenyl)amino]-6-(methylamino)pyrido[3,4-*d*]pyrimidine (5b), General Method A of Scheme 1. A 2-L stainless steel reactor was flushed with dry N$_2$ and charged with 13 (35.0 g, 108 mmol) and anhydrous MeNH$_2$ (57.5 g, 1.85 mol) in DMSO (1 L). The reactor was sealed and heated at 80 °C for 24 h and then cooled. After venting off the excess MeNH$_2$, the mixture was concentrated to ca. 500 mL and poured slowly into 2.5 L of water with vigorous stirring. The precipitate was collected, washed well with water, and dried over P$_2$O$_5$ to afford 5b: mp (2-propanol) 181−183 °C (lit.[15] mp 172−173 °C from MeOH/H$_2$O). Total yield after chromatography of the mother liquor on silica gel: 32.5 g (91%).

The following compounds were prepared similarly.

4-[(3-Bromophenyl)amino]-6-[(2-hydroxyethyl)amino]-pyrido[3,4-*d*]pyrimidine (5d): from 13 and ethanolamine (35% yield after two recrystallizations from MeOH); mp 209−210 °C; ^{1}H NMR [(CD$_3$)$_2$SO] δ 9.72 (s, 1 H, NH), 8.75 (s, 1 H, H-8), 8.40 (s, 1 H, H-2), 8.20 (br s, 1 H, H-2′), 7.91 (br d, J = 8.0 Hz, 1 H, H-6′), 7.37 (t, J = 8.0 Hz, 1 H, H-5′), 7.31 (br d, J = 8.4 Hz, 1 H, H-4′), 7.15 (s, 1 H, H-5), 6.66 (t, J = 5.7 Hz, 1 H, NH), 4.80 (t, J = 5.3 Hz, 1 H, OH), 3.65 (q, J = 5.8 Hz, 2 H, CH$_2$), 3.38 (q, J = 6.1 Hz, 2 H, CH$_2$). Anal. (C$_{15}$H$_{14}$BrN$_5$) C, H, N.

4-[(3-Bromophenyl)amino]-6-[*N*-(2-hydroxyethyl)-*N*-methylamino]pyrido[3,4-*d*]pyrimidine (5e). A mixture of 13 (0.20 g, 0.63 mmol) and 2-(methylamino)ethanol (2.4 g, 31 mmol, 50 equiv) in EtOH (50 mL) was heated at 95 °C for 18 h in a sealed pressure vessel. The solvent was removed under reduced pressure, and the residue was triturated with water and recrystallized from MeOH to give 5e (0.21 g, 89%): mp 236−237 °C; ^{1}H NMR [(CD$_3$)$_2$SO] δ 9.73 (s, 1 H, NH), 8.82 (s, 1 H, H-8), 8.41 (s, 1 H, H-2), 8.18 (br s, 1 H, H-2′), 7.93 (br d, J = 8.0 Hz, 1 H, H-6′), 7.38 (t, J = 8.0 Hz, 1 H, H-5′), 7.33 (br d, J = 8.4 Hz, 1 H, H-4′), 7.24 (s, 1 H, H-5), 4.73 (t, J = 5.3 Hz, 1 H, OH), 3.76 (t, J = 6.1 Hz, 2 H, CH$_2$), 3.63 (dd, J = 6.1, 5.6 Hz, 2 H, CH$_2$), 3.19 (s, 3 H, CH$_3$). Anal. (C$_{16}$H$_{16}$BrN$_5$O) C, H, N.

4-[(3-Bromophenyl)amino]-6-[(2,3-dihydroxypropyl)-amino]pyrido[3,4-*d*]pyrimidine (5f): from 13 and 2,3-dihydroxypropylamine (42%); mp (MeOH) 186.5−188 °C; ^{1}H NMR [(CD$_3$)$_2$SO] δ 9.74 (s, 1 H, NH), 8.75 (s, 1 H, H-8), 8.41 (s, 1 H, H-2), 8.21 (br s, 1 H, H-2′), 7.91 (br d, J = 7.9 Hz, 1 H, H-6′), 7.37 (t, J = 8.0 Hz, 1 H, H-5′), 7.31 (br d, J = 8.4 Hz, 1 H, H-4′), 7.16 (s, 1 H, H-5), 6.46 (t, J = 5.5 Hz, 1 H, NH), 4.93 (d, J = 4.9 Hz, 1 H, OH), 4.68 (t, J = 5.5 Hz, 1 H, OH), 3.77 (sextet, J = 5.5 Hz, 1 H, CH), 3.47−3.39 (m, 2 H, CH$_2$), 3.27−3.20 (m, 2 H, CH$_2$). Anal. (C$_{16}$H$_{16}$BrN$_5$O$_2$·0.5H$_2$O) C, H; N: found, 18.1; calcd, 18.5.

4-[(3-Bromophenyl)amino]-6-[*N*-(2,3-dihydroxypropyl)-*N*-methylamino]pyrido[3,4-*d*]pyrimidine (5g): from 13 and 2,3-dihydroxypropyl-*N*-methylamine[20] (72%); mp (MeOH) 159−160 °C; ^{1}H NMR [(CD$_3$)$_2$SO] δ 9.71 (s, 1 H, NH), 8.82 (s, 1 H, H-8), 8.41 (s, 1 H, H-2), 8.18 (t, J = 1.9 Hz, 1 H, H-2′), 7.93 (br d, J = 8.2 Hz, 1 H, H-6′), 7.39 (t, J = 8.0 Hz, 1 H, H-5′), 7.33 (br d, J = 8.4 Hz, 1 H, H-4′), 7.22 (s, 1 H, H-5), 4.75 (d, J = 4.9 Hz, 1 H, OH), 4.59 (t, J = 5.7 Hz, 1 H, OH), 3.84−3.79 (m, 2 H, CH$_2$), 3.59 (dd, J = 8.7, 6.7 Hz, 1 H, CH), 3.41−3.35 (m, 2 H, CH$_2$), 3.19 (s, 3 H, CH$_3$). Anal. (C$_{17}$H$_{18}$-BrN$_5$O$_2$) C, H, N.

4-[(3-Bromophenyl)amino]-6-[[2-(dimethylamino)-ethyl]amino]pyrido[3,4-*d*]pyrimidine (5h): from 13 and 2-(dimethylamino)ethylamine (63%); mp (CH$_2$Cl$_2$) 114−118 °C; ^{1}H NMR [(CD$_3$)$_2$SO] δ 9.69 (s, 1 H, NH), 8.76 (s, 1 H, H-8), 8.41 (s, 1 H, H-2), 8.22 (t, J = 1.9 Hz, 1 H, H-2′), 7.91 (br d, J = 8.0 Hz, 1 H, H-6′), 7.37 (t, J = 8.0 Hz, 1 H, H-5′), 7.31 (br d, J = 8.4 Hz, 1 H, H-4′), 7.15 (s, 1 H, H-5), 6.50 (t, J = 5.4 Hz, 1 H, NH), 3.38 (dd, J = 6.6, 5.7 Hz, 2 H, CH$_2$), 2.53 (t, J = 6.6 Hz, 2 H, CH$_2$), 2.23 (s, 6 H, CH$_3$). Dihydrochloride salt (from EtOH): mp 250−252 °C. Anal. (C$_{17}$H$_{19}$BrN$_6$·2HCl) C, H, N, Cl.

4-[(3-Bromophenyl)amino]-6-[[3-(dimethylamino)propyl]amino]pyrido[3,4-*d*]pyrimidine (5i): from 13 and

3-(dimethylamino)propylamine (80%); mp (CH₂Cl₂/hexane) 160–161 °C; ¹H NMR [(CD₃)₂SO] δ 9.72 (s, 1 H, NH), 8.75 (s, 1 H, H-8), 8.40 (s, 1 H, H-2), 8.20 (t, *J* = 1.8 Hz, 1 H, H-2'), 7.91 (br d, *J* = 8.2 Hz, 1 H, H-6'), 7.37 (t, *J* = 8.0 Hz, 1 H, H-5'), 7.31 (br d, *J* = 8.4 Hz, 1 H, H-4'), 7.08 (s, 1 H, H-5), 6.84 (t, *J* = 5.4 Hz, 1 H, NH), 3.29 (q, *J* = 6.2 Hz, 2 H, CH₂), 2.35 (t, *J* = 6.9 Hz, 2 H, CH₂), 2.15 (s, 6 H, CH₃), 1.78 (pentet, *J* = 6.9 Hz, 2 H, CH₂). Anal. (C₁₈H₂₁BrN₆) C, H, N.

4-[(3-Bromophenyl)amino]-6-[[4-(dimethylamino)butyl]-amino]pyrido[3,4-*d*]pyrimidine (5j): from 13 and 4-(dimethylamino)butylamine (98%); mp (CH₂Cl₂/hexane) 176–177 °C; ¹H NMR [(CD₃)₂SO] δ 9.68 (s, 1 H, NH), 8.75 (s, 1 H, H-8), 8.39 (s, 1 H, H-2), 8.21 (t, *J* = 1.8 Hz, 1 H, H-2'), 7.92 (br d, *J* = 8.3 Hz, 1 H, H-6'), 7.37 (t, *J* = 8.0 Hz, 1 H, H-5'), 7.31 (dd, *J* = 8.4, 1.2 Hz, 1 H, H-4'), 7.06 (s, 1 H, H-5), 6.87 (t, *J* = 5.6 Hz, 1 H, NH), 3.27 (q, *J* = 6.4 Hz, 2 H, CH₂), 2.24 (t, *J* = 7.1 Hz, 2 H, CH₂), 2.12 (s, 6 H, CH₃), 1.65 (pentet, *J* = 7.1 Hz, 2 H, CH₂), 1.53 (pentet, *J* = 7.2 Hz, 2 H, CH₂). Anal. (C₁₉H₂₃BrN₆) C, H, N.

4-[(3-Bromophenyl)amino]-6-[[3-(diethylamino)-2-hydroxypropyl]amino]pyrido[3,4-*d*]pyrimidine (5k). A solution of 13 (5.74 g, 18 mmol) and 1-amino-3-(diethylamino)-2-propanol[30] (26.3 g, 180 mmol) in DMSO (27 mL) was heated at 80 °C under N₂ for 23 h. The DMSO was evaporated under reduced pressure (0.1 mm) at 100 °C, and the residue was purified by flash chromatography on silica gel. Elution with a gradient of MeOH in EtOAc containing 2% Et₃N and pooling of appropriate fractions gave **5k** (4.87 g). Rechromatography of the mother liquor gave an additional 0.48 g (total yield 67%): mp (dihydrochloride salt from 'PrOH/CH₂Cl₂/HCl) (EtOAc) 189–192 °C; ¹H NMR [free base, (CD₃)₂SO] δ 9.72 (s, exchanges with D₂O, 1 H), 8.75 (s, 1 H), 8.41 (s, 1 H), 8.21 (t, *J* = 1.9 Hz, 1 H), 7.91 (d, *J* = 7.0 Hz, 1 H), 7.39–7.29 (m, 2 H), 7.14 (s, 1 H), 6.63 (t, *J* = 5.3 Hz, exchanges with D₂O, 1 H), 4.77 (d, *J* = 4.3 Hz, exchanges with D₂O, 1 H), 3.87–3.83 (m, 1 H), 3.39–3.28 (m, 2 H), 2.58–2.41 (m, 6 H), 0.96 (t, *J* = 7.0 Hz, 6 H); CIMS *m/z* (relative intensity) 445 (MH⁺, 13), 447 (13). Anal. (C₂₀H₂₅BrN₆O·2HCl·0.5H₂O) C, H, N.

4-[(3-Bromophenyl)amino]-6-[[2-[*N*-(2-hydroxyethyl)-methylamino]ethyl]amino]pyrido[3,4-*d*]pyrimidine (5l). Reaction of 13 with 2-[(2-aminoethyl)methylamino]ethanol (20), followed by column chromatography, gave 5l (60% as the dihydrochloride salt): mp (CH₂Cl₂/2-propanol) 182–189 °C dec; ¹H NMR [(CD₃)₂SO] δ 11.63 (br s, 1 H, exchanges with D₂O), 10.11 (br s, 1 H, exchanges with D₂O), 8.92 (s, 1 H), 8.72 (s, 1 H), 8.21 (s, 1 H), 7.94 (d overlapping s, 2 H, with D₂O wash collapses to δ 7.85, d, *J* = 8.2 Hz, 1 H, δ 7.68, s, 1 H), 7.60–7.40 (br s overlapping m, 3 H, with D₂O wash collapses to d, 2 H), 3.84–3.75 (m, 4 H), 3.53–3.40 (m, 1 H), 3.40–3.27 (m, 2 H), 3.26–3.16 (m, 1 H), 2.90 (d, *J* = 4.8 Hz, 3 H, with D₂O wash collapses to s); CIMS *m/z* (relative intensity) 417 (MH⁺, 26), 419 (25). Anal. (C₁₈H₂₁BrN₆O·2HCl·0.5 H₂O) C, H, N, Cl.

A higher *R*f component, eluted from the column with EtOAc/MeOH/Et₃N (90:10:1) (29 mg), was identified as **5e**, resulting from nucleophilic addition of the tertiary amine of the side chain followed by extrusion of aziridine.

4-[(3-Bromophenyl)amino]-6-[*N*-[2-(dimethylamino)-ethyl]-*N*-methylamino]pyrido[3,4-*d*]pyrimidine (5m): from 13 and 2-(dimethylamino)-*N*-methylethylamine (72%); ¹H NMR [(CD₃)₂SO] δ 9.72 (s, 1 H, NH), 8.83 (s, 1 H, H-8), 8.41 (s, 1 H, H-2), 8.18 (br s, 1 H, H-2'), 7.92 (br d, *J* = 7.9 Hz, 1 H, H-6'), 7.38 (t, *J* = 8.0 Hz, 1 H, H-5'), 7.33 (br d, *J* = 8.0 Hz, 1 H, H-4'), 7.21 (s, 1 H, H-5), 3.80 (t, *J* = 6.8 Hz, 2 H, CH₂), 3.14 (s, 3 H, CH₃), 2.45 (t, *J* = 6.8 Hz, 2 H, CH₂), 2.19 (s, 6 H, CH₃). Dihydrochloride salt (from EtOH): mp 260–262 °C. Anal. (C₁₈H₂₁BrN₆·2HCl) C, H, N, Cl.

4-[(3-Bromophenyl)amino]-6-[[2-(4-morpholino)ethyl]-amino]pyrido[3,4-*d*]pyrimidine (5n). A mixture of 13 (0.20 g, 0.63 mmol) and 4-(2-aminoethyl)morpholine (4.1 g, 31 mmol, 50 equiv) in DMSO (40 mL) was heated at 95 °C for 18 h. Most of the DMSO was removed under reduced pressure at 80 °C, and the residue was diluted with water and extracted into EtOAc. After being washed twice with water, the organic layer

was dried (Na₂SO₄), and the solvent was removed under reduced pressure. Chromatography of the residue on silica gel, eluting with EtOAc/MeOH (99:1), gave **5n** (0.19 g, 71% yield): mp (MeOH) 185–187 °C; ¹H NMR [(CD₃)₂SO] δ 9.69 (s, 1 H, exchangeable with D₂O, NH), 8.76 (s, 1 H, H-8), 8.41 (s, 1 H, H-2), 8.21 (t, *J* = 1.9 Hz, 1 H, H-2'), 7.91 (br d, *J* = 8.1 Hz, 1 H, H-6'), 7.37 (t, *J* = 8.0 Hz, 1 H, H-5'), 7.31 (br d, *J* = 7.9 Hz, 1 H, H-4'), 7.15 (s, 1 H, H-5), 6.55 (t, *J* = 5.5 Hz, 1 H, exchangeable with D₂O, NH), 3.60 (t, *J* = 4.6 Hz, 4 H, CH₂O), 3.41 (dd, *J* = 6.5, 5.9 Hz, 2 H, CH₂N), 2.60 (t, *J* = 6.7 Hz, 2 H, CH₂N), 2.46 (m, 4 H, CH₂N). Anal. (C₁₉H₂₁BrN₆O) C, H, N. Dihydrochloride salt: mp (MeOH/EtOH) 267 °C dec. Anal. (C₁₉H₂₁BrN₆O·2HCl) C, H, N, Cl.

4-[(3-Bromophenyl)amino]-6-[[3-(4-morpholino)propyl]amino]pyrido[3,4-*d*]pyrimidine (5o): from 13 and 4-(3-aminopropyl)morpholine (87%); mp (MeOH/H₂O) 177–178 °C; ¹H NMR [(CD₃)₂SO] δ 9.70 (s, 1 H, NH), 8.75 (s, 1 H, H-8), 8.40 (s, 1 H, H-2), 8.20 (t, *J* = 1.9 Hz, 1 H, H-2'), 7.91 (ddd, *J* = 8.0, 1.8, 1.2 Hz, 1 H, H-6'), 7.37 (t, *J* = 8.0 Hz, 1 H, H-5'), 7.31 (dd, *J* = 8.0, 1.2 Hz, 1 H, H-4'), 7.08 (s, 1 H, H-5), 6.86 (t, *J* = 5.5 Hz, 1 H, NH), 3.58 (t, *J* = 4.6 Hz, 4 H, CH₂O), 3.31 (q, *J* = 6.4 Hz, 2 H, CH₂), 2.41 (t, *J* = 7.0 Hz, 2 H, CH₂), 2.36 (br m, 4 H, CH₂), 1.81 (pentet, *J* = 6.9 Hz, 2 H, CH₂). Anal. (C₂₀H₂₃BrN₆O) C, H, N.

4-[(3-Bromophenyl)amino]-6-[[3-(4-methyl-1-piperazinyl)propyl]amino]pyrido[3,4-*d*]pyrimidine (5p): from 13 and 3-(4-methylpiperazyl)propylamine (83%); mp (CH₂Cl₂/hexane) 182–183 °C; ¹H NMR [(CD₃)₂SO] δ 9.70 (s, 1 H, NH), 8.75 (s, 1 H, H-8), 8.40 (s, 1 H, H-2), 8.20 (t, *J* = 1.9 Hz, 1 H, H-2'), 7.92 (br d, *J* = 8.2 Hz, 1 H, H-6'), 7.37 (t, *J* = 8.0 Hz, 1 H, H-5'), 7.31 (dd, *J* = 8.3, 1.2 Hz, 1 H, H-4'), 7.07 (s, 1 H, H-5), 6.85 (t, *J* = 5.5 Hz, 1 H, NH), 3.30 (q, *J* = 6.3 Hz, 2 H, CH₂), 2.40 (t, *J* = 7.0 Hz, 2 H, CH₂), 2.33 (br m, 4 H, CH₂), 2.13 (s, 3 H, CH₃), 1.79 (pentet, *J* = 7.2 Hz, 2 H, CH₂). Anal. (C₂₁H₂₆BrN₇) C, H, N.

4-[(3-Bromophenyl)amino]-6-[[2-[*N*,*N*-bis(2-hydroxyethyl)amino]ethyl]amino]pyrido[3,4-*d*]pyrimidine (5q): from 13 and *N*,*N*-bis(2-hydroxyethyl)ethylamine (41%); mp (MeOH) 210–211 °C; ¹H NMR [(CD₃)₂SO] δ 9.70 (s, 1 H, NH), 8.76 (s, 1 H, H-8), 8.41 (s, 1 H, H-2), 8.22 (br s, 1 H, H-2'), 7.92 (br d, *J* = 8.1 Hz, 1 H, H-6'), 7.37 (t, *J* = 8.0 Hz, 1 H, H-5'), 7.31 (br d, *J* = 8.0 Hz, 1 H, H-4'), 7.14 (s, 1 H, H-5), 6.59 (t, *J* = 5.4 Hz, 1 H, NH), 4.44 (t, *J* = 5.4 Hz, 2 H, OH), 3.46 (dd, *J* = 5.9, 5.7 Hz, 4 H, CH₂), 3.34 (q, *J* = 6.2 Hz, 2 H, CH₂), 2.78 (t, *J* = 6.3 Hz, 2 H, CH₂), 2.62 (t, *J* = 6.1 Hz, 4 H, CH₂). Anal. (C₁₉H₂₃BrN₆O₂) C, H, N.

4-[(3-Bromophenyl)amino]-6-[[3-[*N*,*N*-bis(2-hydroxyethyl)amino]propyl]amino]pyrido[3,4-*d*]pyrimidine (5r): from 13 and *N*,*N*-bis(2-hydroxyethyl)propylamine (48%); ¹H NMR [(CD₃)₂SO] δ 9.68 (s, 1 H, NH), 8.75 (s, 1 H, H-8), 8.40 (s, 1 H, H-2), 8.21 (t, *J* = 1.8 Hz, 1 H, H-2'), 7.91 (br d, *J* = 8.4 Hz, 1 H, H-6'), 7.37 (t, *J* = 8.0 Hz, 1 H, H-5'), 7.31 (br d, *J* = 8.3 Hz, 1 H, H-4'), 7.07 (s, 1 H, H-5), 6.87 (t, *J* = 5.5 Hz, 1 H, NH), 4.40 (t, *J* = 4.9 Hz, 2 H, OH), 3.45 (dd, *J* = 5.9, 5.3 Hz, 4 H, CH₂), 3.31 (dd, *J* = 6.2, 5.9 Hz, 2 H, CH₂), 2.61 (t, *J* = 6.9 Hz, 2 H, CH₂), 2.55 (t, *J* = 6.3 Hz, 4 H, CH₂), 1.76 (pentet, *J* = 6.7 Hz, 2 H, CH₂). Dihydrochloride salt (from EtOH): mp 205–207 °C. Anal. (C₂₀H₂₅BrN₆O₂·2HCl) C, H, N, Cl.

4-[(3-Bromophenyl)amino]-6-[(3-pyridyl)methylamino]-pyrido[3,4-*d*]pyrimidine (5s): from 13 and 3-(aminomethyl)pyridine (37%); ¹H NMR [(CD₃)₂SO] δ 9.72 (s, 1 H, NH), 8.78 (s, 1 H, H-8), 8.64 (d, *J* = 1.7 Hz, 1 H, H-2''), 8.44 (dd, *J* = 4.7, 1.4 Hz, 1 H, H-4''), 8.41 (s, 1 H, H-2), 8.21 (t, *J* = 1.9 Hz, 1 H, H-2'), 7.89 (br d, *J* = 7.9 Hz, 1 H, H-6'), 7.79 (br d, *J* = 6.2 Hz, 1 H, H-6''), 7.47 (t, *J* = 6.3 Hz, 1 H, NH), 7.37 (t, *J* = 8.0 Hz, 1 H, H-5'), 7.35–7.30 (m, 2 H, H-4',5''), 7.25 (s, 1 H, H-5), 4.60 (d, *J* = 4.4 Hz, 2 H, CH₂). Dihydrochloride salt (from EtOH): mp 260–262 °C. Anal. (C₁₉H₁₆BrN₆·2HCl) C, H, N.

4-[(3-Bromophenyl)amino]-6-[[2-(2-pyridyl)ethyl]amino]pyrido[3,4-*d*]pyrimidine (5t): from 13 and 3-(2-aminoethyl)pyridine (87%); mp (MeOH/H₂O) 170–171.5 °C; ¹H NMR [(CD₃)₂SO] δ 9.72 (s, 1 H, NH), 8.76 (s, 1 H, H-8), 8.53 (dd, *J* = 4.2, 0.9 Hz, 1 H, H-6''), 8.41 (s, 1 H, H-2), 8.20 (t, *J* = 1.9 Hz, 1 H, H-2'), 7.90 (br d, *J* = 7.7 Hz, 1 H, H-6'), 7.73 (td, *J* =

7.6, 1.7 Hz, 1 H, H-4″), 7.38–7.34 (m, 2 H, H-5′,3″), 7.31 (br d, J = 8.1 Hz, 1 H, H-4′), 7.24 (ddd, J = 8.2, 4.9, 0.8 Hz, 1 H, H-5″), 7.12 (s, 1 H, H-5), 6.88 (t, J = 5.4 Hz, 1 H, NH), 3.65 (dd, J = 7.0, 5.5 Hz, 2 H, CH₂), 3.12 (t, J = 7.2 Hz, 2 H, CH₂). Anal. (C₂₀H₁₇BrN₆) C, H, N.

4-[(3-Bromophenyl)amino]-6-[[2-(4-imidazolyl)ethyl]-amino]pyrido[3,4-*d*]pyrimidine (5u): from 13 and 2-(imidazol-4-yl)ethylamine (66%); mp (MeOH) 200–201 °C; ¹H NMR [(CD₃)₂SO] δ 11.87 (br, 1 H, NH), 9.71 (s, 1 H, NH), 8.76 (s, 1 H, H-8), 8.41 (s, 1 H, H-2), 8.20 (t, J = 1.8 Hz, 1 H, H-2′), 7.91 (br d, J = 8.0 Hz, 1 H, H-6′), 7.57 (d, J = 0.8 Hz, 1 H, H-2″), 7.37 (t, J = 8.0 Hz, 1 H, H-5′), 7.31 (br d, J = 8.2 Hz, 1 H, H-4′), 7.13 (s, 1 H, H-5), 6.89 (br s, 1 H, H-5″), 6.85 (t, J = 5.4 Hz, 1 H, NH), 3.51 (dd, J = 7.2, 5.7 Hz, 2 H, CH₂), 2.88 (t, J = 7.3 Hz, 2 H, CH₂). Anal. (C₁₉H₁₈BrN₇) C, H, N.

4-[(3-Bromophenyl)amino]-6-[[3-(1-imidazolyl)propyl]-amino]pyrido[3,4-*d*]pyrimidine (5v): from 13 and 3-(imidazol-1-yl)propylamine (64%); mp (MeOH/H₂O) 195.5–197 °C; ¹H NMR [(CD₃)₂SO] δ 9.71 (s, 1 H, NH), 8.77 (s, 1 H, H-8), 8.41 (s, 1 H, H-2), 8.20 (t, J = 1.9 Hz, 1 H, H-2′), 7.90 (br d, J = 8.1 Hz, 1 H, H-6′), 7.66 (s, 1 H, H-2″), 7.37 (t, J = 8.0 Hz, 1 H, H-5′), 7.32 (br d, J = 8.2 Hz, 1 H, H-4′), 7.22 (s, 1 H, H-5″), 7.08 (s, 1 H, H-5), 6.98 (t, J = 5.4 Hz, 1 H, NH), 6.91 (s, 1 H, H-4″), 4.11 (t, J = 7.0 Hz, 2 H, CH₂), 3.25 (q, J = 6.1 Hz, 2 H, CH₂), 2.09 (pentet, J = 6.8 Hz, 2 H, CH₂). Anal. (C₁₈H₁₆BrN₇) C, H, N.

4-[(3-Bromophenyl)amino]-6-(4-methyl-1-piperazinyl)-pyrido[3,4-*d*]pyrimidine (5w): from 13 and 1-methylpiperazine (25%); mp (CH₂Cl₂) 219.5–222 °C; ¹H NMR [(CD₃)₂SO] δ 9.75 (s, 1 H, NH), 8.86 (s, 1 H, H-8), 8.48 (s, 1 H, H-2), 8.19 (t, J = 1.7 Hz, 1 H, H-2′), 7.92 (br d, J = 8.1 Hz, 1 H, H-6′), 7.50 (s, 1 H, H-5), 7.39 (t, J = 8.0 Hz, 1 H, H-5′), 7.33 (br d, J = 8.3 Hz, 1 H, H-4′), 3.63 (t, J = 4.8 Hz, 4 H, CH₂), 2.49 (t, J = 4.8 Hz, 4 H, CH₂), 2.26 (s, 3 H, CH₃). Anal. (C₁₈H₁₉BrN₆) C, H, N.

4-[(3-Chlorophenyl)amino]-6-(methylamino)pyrido-[3,4-*d*]pyrimidine (7b): from 14 and MeNH₂ (82%); mp (MeOH/H₂O) 185.5–187 °C; ¹H NMR [(CD₃)₂SO] δ 9.72 (s, 1 H, NH), 8.76 (s, 1 H, H-8), 8.42 (s, 1 H, H-2), 8.11 (t, J = 2.0 Hz, 1 H, H-2′), 7.87 (ddd, J = 7.9, 2.0 Hz, 1 H, H-6′), 7.43 (t, J = 8.1 Hz, 1 H, H-5′), 7.18 (ddd, J = 7.8, 1.8 Hz, 1 H, H-4′), 7.07 (s, 1 H, H-5), 6.83 (q, J = 4.9 Hz, 1 H, NH), 2.89 (d, J = 4.8 Hz, 3 H, CH₃). Anal. (C₁₄H₁₂ClN₅) C, H, N.

6-(Methylamino)-4-[[3-(trifluoromethyl)phenyl]amino]-pyrido[3,4-*d*]pyrimidine (8b): from 15 and MeNH₂ (72%); mp (MeOH/H₂O) 172–173 °C; ¹H NMR [(CD₃)₂SO] δ 9.85 (s, 1 H, NH), 8.77 (s, 1 H, H-8), 8.42 (s, 1 H, H-2), 8.31 (br s, 1 H, H-2′), 8.27 (br d, J = 8.2 Hz, 1 H, H-6′), 7.64 (t, J = 8.0 Hz, 1 H, H-5′), 7.47 (br d, J = 7.7 Hz, 1 H, H-4′), 7.08 (s, 1 H, H-5), 6.85 (q, J = 4.9 Hz, 1 H, NH), 2.90 (d, J = 5.0 Hz, 3 H, CH₃). Anal. (C₁₅H₁₂F₃N₅) C, H, N.

6-(Methylamino)-4-[(3-methylphenyl)amino]pyrido-[3,4-*d*]pyrimidine (9b): from 16 and MeNH₂ (74%); mp (MeOH/H₂O) 189–190 °C; ¹H NMR [(CD₃)₂SO] δ 9.57 (s, 1 H, NH), 8.72 (s, 1 H, H-8), 8.34 (s, 1 H, H-2), 7.69 (br d, J = 7.9 Hz, 1 H, H-6′), 7.65 (br s, 1 H, H-2′), 7.29 (t, J = 7.8 Hz, 1 H, H-5′), 7.08 (s, 1 H, H-5), 6.96 (br d, J = 7.6 Hz, 1 H, H-4′), 6.76 (q, J = 4.9 Hz, 1 H, NH), 2.88 (d, J = 4.9 Hz, 3 H, CH₃), 2.35 (s, 3 H, CH₃). Anal. (C₁₅H₁₅N₅) C, H, N.

6-(Dimethylamino)-4-[(3-methylphenyl)amino]pyrido-[3,4-*d*]pyrimidine (9c): from 16 and dimethylamine (68%); mp 239–241 °C; ¹H NMR [(CD₃)₂SO] δ 9.61 (s, 1 H, NH), 8.81 (s, 1 H, H-8), 8.36 (s, 1 H, H-2), 7.69 (br d, J = 7.9 Hz, 1 H, H-6′), 7.64 (br s, 1 H, H-2′), 7.30 (m, 1 H, H-5′), 7.30 (s, 1 H, H-5), 6.98 (br d, J = 7.7 Hz, 1 H, H-4′), 3.17 (s, 6 H, CH₃), 2.35 (s, 3 H, CH₃). Anal. (C₁₆H₁₇N₅) C, H, N.

4-[(3-Methylphenyl)amino]-6-[[2-(4-morpholino)ethyl]-amino]pyrido[3,4-*d*]pyrimidine (9n): from 16 and 1-(2-aminoethyl)morpholine (78%); mp 168–170 °C; ¹H NMR [(CD₃)₂SO] δ 9.56 (s, 1 H, NH), 8.72 (s, 1 H, H-8), 8.34 (s, 1 H, H-2), 7.67 (br d, J = 8.0 Hz, 1 H, H-6′), 7.64 (br s, 1 H, H-2′), 7.29 (t, J = 7.8 Hz, 1 H, H-5′), 7.17 (s, 1 H, H-5), 6.97 (br d, J = 7.5 Hz, 1 H, H-4′), 6.48 (q, J = 5.5 Hz, 1 H, NH), 3.60 (t, J = 4.6 Hz, 4 H, CH₂), 3.31 (m, 2 H, CH₂), 2.60 (t, J = 6.7 Hz, 2

H, CH₂), 2.47 (br m, 4 H, CH₂), 2.35 (s, 3 H, CH₃). Anal. (C₂₀H₂₄N₆O·0.5 H₂O) C, H, N.

4-[(3-Methylphenyl)amino]-6-[[3-(4-morpholino)pro-pyl]amino]pyrido[3,4-*d*]pyrimidine (9o): from 16 and 1-(3-aminopropyl)morpholine (81%); mp 200–203 °C; ¹H NMR [(CD₃)₂SO] δ 9.57 (s, 1 H, NH), 8.71 (s, 1 H, H-8), 8.33 (s, 1 H, H-2), 7.67 (br d, J = 8.1 Hz, 1 H, H-6′), 7.63 (br s, 1 H, H-2′), 7.28 (t, J = 7.8 Hz, 1 H, H-5′), 7.10 (s, 1 H, H-5), 6.96 (br d, J = 7.4 Hz, 1 H, H-4′), 6.79 (q, J = 5.6 Hz, 1 H, NH), 3.58 (t, J = 4.6 Hz, 4 H, CH₂), 3.30 (q, J = 6.4 Hz, 2 H, CH₂), 2.42 (t, J = 7.1 Hz, 2 H, CH₂), 2.37 (br m, 4 H, CH₂), 2.35 (s, 3 H, CH₃), 1.80 (pentet, J = 6.9 Hz, 2 H, CH₂). Anal. (C₂₁H₂₆N₆O·0.5H₂O) C, H, N.

6-[[2-(4-Imidazolyl)ethyl]amino]-4-[(3-methylphenyl)-amino]pyrido[3,4-*d*]pyrimidine (9u): from 16 and 2-(imidazol-4-yl)ethylamine (70%); mp 207–209 °C; ¹H NMR [(CD₃)₂-SO] δ 11.85 (br, 1 H, NH), 9.58 (s, 1 H, NH), 8.72 (s, 1 H, H-8), 8.34 (s, 1 H, H-2), 7.67 (br d, J = 8.1 Hz, 1 H, H-6′), 7.63 (br s, 1 H, H-2′), 7.56 (br s, 1 H, H-2″), 7.28 (t, J = 7.8 Hz, 1 H, H-5′), 7.15 (s, 1 H, H-5), 6.96 (br d, J = 7.2 Hz, 1 H, H-4′), 6.90 (m, 1 H, NH), 6.78 (t, J = 5.0 Hz, 1 H, H-5″), 3.50 (dd, J = 7.2, 5.7 Hz, 2 H, CH₂), 2.88 (t, J = 6.8 Hz, 2 H, CH₂), 2.34 (s, 3 H, CH₃). Anal. (C₁₉H₁₉N₇·0.25H₂O) C, H, N.

4-[(3-Bromophenyl)amino]-6-[(2-carboxyethyl)amino]-pyrido[3,4-*d*]pyrimidine (5z), General Example of Method B of Scheme 1. A mixture of 13 (0.20 g, 0.63 mmol) and sodium 2-aminopropanoate (3.4 g, 31 mmol, 50 equiv) (prepared from β-alanine and Na in EtOH) in EtOH (50 mL) was heated at 95 °C for 48 h in a sealed pressure vessel. The solvent was removed under reduced pressure, the residue was dissolved in water and filtered to remove insolubles, and the filtrate was acidified (AcOH) to give 5z (0.11 g, 45%): mp (MeOH) 276–280 °C; ¹H NMR [(CD₃)₂SO] δ 12.25 (br, 1 H, CO₂H), 9.74 (s, 1 H, NH), 8.76 (s, 1 H, H-8), 8.41 (s, 1 H, H-2), 8.20 (t, J = 1.9 Hz, 1 H, H-2′), 7.90 (br d, J = 8.0 Hz, 1 H, H-6′), 7.37 (t, J = 8.0 Hz, 1 H, H-5′), 7.31 (br d, J = 8.0 Hz, 1 H, H-4′), 7.14 (s, 1 H, H-5), 6.80 (t, J = 5.5 Hz, 1 H, NH), 3.51 (dd, J = 6.8, 5.7 Hz, 2 H, CH₂), 2.63 (t, J = 7.0 Hz, 2 H, CH₂). Anal. (C₁₆H₁₄BrN₅O₂) C, H, N.

The following compounds were prepared similarly.

4-[(3-Bromophenyl)amino]-6-[(carboxymethyl)amino]-pyrido[3,4-*d*]pyrimidine (5x): from 13 and the sodium salt of glycine (34%); mp (MeOH) 234–239 °C; ¹H NMR [(CD₃)₂-SO] δ 12.54 (br, 1 H, CO₂H), 9.76 (s, 1 H, NH), 8.77 (s, 1 H, H-8), 8.42 (s, 1 H, H-2), 8.20 (t, J = 1.9 Hz, 1 H, H-2′), 7.90 (br d, J = 8.0 Hz, 1 H, H-6′), 7.37 (t, J = 8.0 Hz, 1 H, H-5′), 7.32 (br d, J = 8.2 Hz, 1 H, H-4′), 7.31 (s, 1 H, H-5), 7.01 (t, J = 6.0 Hz, 1 H, NH), 4.05 (d, J = 5.9 Hz, 2 H, CH₂). Anal. (C₁₅H₁₂-BrN₅O₂·0.5H₂O) C, H, N.

4-[(3-Bromophenyl)amino]-6-[*N*-(carboxymethyl)me-thylamino]pyrido[3,4-*d*]pyrimidine (5y): from 13 and the sodium salt of *N*-methylglycine (79%); mp (MeOH) 225–227 °C; ¹H NMR [(CD₃)₂SO] δ 12.59 (br, 1 H, CO₂H), 9.77 (s, 1 H, NH), 8.82 (s, 1 H, H-8), 8.45 (s, 1 H, H-2), 8.19 (t, J = 1.9 Hz, 1 H, H-2′), 7.92 (br d, J = 8.3 Hz, 1 H, H-6′), 7.39 (t, J = 8.0 Hz, 1 H, H-5′), 7.35–7.32 (m, 2 H, H-5,4′), 4.43 (s, 2 H, CH₂), 3.20 (s, 3 H, CH₃). Anal. (C₁₆H₁₄BrN₅O₂) C, H, N.

6-Amino-4-[(3-methylphenyl)amino]pyrido[3,4-*d*]pyri-midine (9a). Reaction of 16 (0.254 g, 1 mmol) with 4-meth-oxybenzylamine (4.1 g, 30 mmol) in DMSO at 100 °C for 2 days gave crude 6-[(4-methoxyphenyl)amino]-4-[(3-methylphenyl)-amino]pyrido[3,4-*d*]pyrimidine (0.67 g): ¹H NMR [(CD₃)₂SO] δ 9.54 (s, 1 H, NH), 8.72 (s, 1 H, H-8), 8.33 (s, 1 H, H-2), 7.66 (br d, J = 8.1 Hz, 1 H, H-6′), 7.62 (br s, 1 H, H-2′), 7.34 (d, J = 8.6 Hz, 2 H, H-2″,6″), 7.29 (t, J = 7.7 Hz, 1 H, H-5′), 7.25 (t, J = 6.4 Hz, 1 H, NH), 7.21 (s, 1 H, H-5), 6.96 (br d, J = 7.6 Hz, 1 H, H-4′), 6.88 (br d, J = 8.6 Hz, 2 H, H-3″,5″), 4.49 (d, J = 6.2 Hz, 2 H, CH₂), 3.71 (s, 3 H, OCH₃), 2.34 (s, 3 H, CH₃).

Hydrolysis of the crude material with refluxing TFA for 1 h and chromatography on alumina, eluting with CH₂Cl₂/MeOH (97:3), gave 9a (0.14 g, 56%): mp 235.5–237 °C; ¹H NMR [(CD₃)₂SO] δ 9.59 (s, 1 H, NH), 8.68 (s, 1 H, H-8), 8.33 (s, 1 H, H-2), 7.67 (br s, 1 H, H-2′), 7.23 (m, 1 H, H-6′), 7.26 (t, J = 8.0

Hz, 1 H, H-5'), 7.18 (s, 1 H, H-5), 6.94 (br d, $J = 7.5$ Hz, 1 H, H-4'), 6.24 (br s, 1 H, NH), 2.34 (s, 3 H, CH_3). Anal. ($C_{14}H_{13}N_5$) C, H, N.

4-[(3-Bromophenyl)amino]-2-methyl-6-[[2-(4-morpholino)ethyl]amino]pyrido[3,4-d]pyrimidine (10n), Scheme 3). A solution of 13 (320 mg, 1 mmol) and nitromethane (0.28 mL, 5 mmol) in DMSO (2 mL) was treated at 25 °C with DBU (0.45 mL, 3 mmol). The mixture was stirred at 25 °C under nitrogen for 24 h and then diluted with 15 mL of 5% aqueous HCl. The resulting suspension was stirred for 20 min, sonicated briefly to break up solids, filtered, and washed well with water and then a small amount of 2-propanol to give 4-[(3-bromophenyl)amino]-6-fluoro-2-methylpyrido[3,4-d]pyrimidine hydrochloride (17) (307 mg, 84%): mp 230−240 °C dec; ^{1}H NMR [CD_3)$_2$SO] δ 10.30 (br s, exchanges with D_2O, 1 H, NH), 8.78 (s, 1 H, H-8), 8.26 (d, $J = 1.7$ Hz, 1 H, H-2'), 8.20 (s, 1 H, H-5), 7.91 (dt, $J = 2.1$, 1.9 Hz, 1 H, H-6'), 7.43−7.36 (m, 2 H, H-4',5'), 5.14 (br s, exchanges with D_2O, 1 H), 2.85 (s, 3 H, CH_3); ^{19}F NMR δ −74.0; CIMS *m/z* (relative intensity) 333 (MH$^+$, 100), 335 (78). Anal. ($C_{14}H_{10}N_4BrF\cdot HCl$) C, H, N.

A solution of 17 (207 mg, 0.56 mmol) and 4-(2-aminoethyl)-morpholine (1.1 mL, 8.4 mmol) in DMSO (1.2 mL) was heated at 80 °C for 22 h. The DMSO was removed under reduced pressure, and the residue was dissolved in EtOAc and purified by flash chromatography on silica gel, eluting with EtOAc followed by a gradient (5%, 7.5%, and 10%) of MeOH in EtOAc. The residue from appropriate pooled fractions was dissolved in a minimal volume of hot EtOAc and treated with excess dry HCl in 2-propanol to give 10n as the dihydrochloride salt (177 mg, 60%): mp >260 °C dec; ^{1}H NMR [(CD$_3$)$_2$SO] δ 11.08 (br s, exchanges D_2O, 1 H), 10.98 (br s, exchanges D_2O, 1 H), 8.61 (s, 1 H, H-8), 8.25 (s, 1 H, H-2'), 7.96 (d, $J = 7.7$ Hz, 1 H, H-6'), 7.71 (s, 1 H, shifts to 7.49 with D_2O wash, H-5), 7.46−7.22 (m, overlapping with br exchangeable s, 3 H), 4.5 (br s, exchanges D_2O, ca. 1.5 H), 3.99 (d, $J = 11$ Hz, 2 H), 3.85−3.78 (m, 4 H), 3.55 (d, $J = 11.8$ Hz, 2 H), 3.36 (d, $J = 4.8$ Hz, 2 H), 3.18 (q, $J = 11$ Hz, 2 H), 2.76 (s, 3 H, CH_3); CIMS *m/z* (relative intensity) 443 (MH$^+$, 58), 445 (53). Anal. ($C_{20}H_{23}N_6OBr\cdot 2HCl$) N, H, C: found, 45.9; calcd 46.5.

Measurement of Aqueous Solubility. Stock solutions of drugs were made up in MeOH or DMSO and used to calibrate the HPLC (peak area in nanomoles, assuming a linear response). Accurately weighed amounts (to give approximately a 50 mM solution) were then sonicated for 30 min in 0.05 M sodium lactate buffer (neutral compounds, hydrochloride salts of amines) or in water (sodium salts of acids). After standing for an additional 30 min, the samples were centrifuged at 13 000 rpm for 3 min, and the concentration of drug in the supernatant was determined by HPLC, using the calibration determined previously.

Enzyme Assay. Epidermal growth factor receptor was prepared from human A431 carcinoma cell shed membrane vesicles by immunoaffinity chromatography as previously described,[31] and the assays were carried out as reported previously.[8] The substrate used was based on a portion of phospholipase C1, having the sequence Lys-His-Lys-Lys-Leu-Ala-Glu-Gly-Ser-Ala-Tyr472-Glu-Glu-Val. The reaction was allowed to proceed for 10 min at room temperature and then was stopped by the addition of 2 mL of 75 mM phosphoric acid. The solution was then passed through a 2.5-cm phosphocellulose disk which bound the peptide. This filter was washed with 75 mM phosphoric acid (5×), and incorporated label was assessed by scintillation counting in an aqueous fluor. Control activity (no drug) gave a count of approximately 100 000 cpm. At least two independent dose−response curves were done and the IC_{50} values computed. The reported values are averages; variation was generally ±15%.

EGFR Autophosphorylation in A431 Human Epidermoid Carcinoma Cells. Cells were grown to confluence in 6-well plates (35-mm diameter) and exposed to serum-free medium for 18 h. The cells were treated with compound for 2 h and then with 100 ng/mL EGF for 5 min. The monolayers were lysed in 0.2 mL of boiling Laemmli buffer (2% sodium dodecyl sulfate, 5% β-mercaptoethanol, 10% glycerol, and 50

mM Tris, pH 6.8), and the lysates were heated to 100 °C for 5 min. Proteins in the lysate were separated by polyacrylamide gel electrophoresis and electrophoretically transferred to nitrocellulose. The membrane was washed once in a mixture of 10 mM Tris, pH 7.2, 150 mM NaCl, and 0.01% azide (TNA) and blocked overnight in TNA containing 5% bovine serum albumin and 1% ovalbumin. The membrane was blotted for 2 h with anti-phosphotyrosine antibody (UBI, 1 μg/mL in blocking buffer) and then washed twice in TNA, once in TNA containing 0.05% Tween-20 and 0.05% nonidet P-40, and twice in TNA. The membranes were then incubated for 2 h in blocking buffer containing 0.1 Ci/mL [^{125}I]protein A and then washed again as above. After the blots were dry they were loaded into a film cassette and exposed to X-AR X-ray film for 1−7 days. Band intensities were determined with a Molecular Dynamics laser densitometer.

In Vivo Chemotherapy. Immune-deficient mice were housed in microisolator cages within a barrier facility on a 12-h light/dark cycle and received food and water ad libitum. Animal housing was in accord with AAALAC guidelines. All experimental protocols involving animals were approved by the Institutional Animal Care and Use Committee. The A431 epidermoid carcinoma, NIH 3T3 fibroblast transfected with the human EGF receptor (EGFR), estrogen-dependent MCF-7 breast, and SK-OV-3 ovarian were maintained by serial passage in nude mice (NCr nu/nu). Nude mice were also used as tumor hosts for anticancer agent evaluations against these tumor models.

In each experiment for anticancer activity evaluation, test mice weighing 18−22 g were randomized and implanted with tumor fragments in the region of the right axilla on day 0. Animals were treated with test compounds on the basis of average cage weight (6 mice/dose group) on the days indicated in the tables. In every experiment, each test compound was evaluated over a range of dose levels ranging from toxic to ineffective. The doses reported in Table 4 are the maximum doses that could be administered without exceeding 10% compound-induced mortality. This dose level, the maximum tolerated dose, allows comparisons to be made among the tested compounds at an equitoxic dose level. The vehicle for 5b was 6% dimethylacetamide and 94% 50 mM sodium lactate buffer, pH 4.0 (suspension). Compounds 5h,k,n and 9b were administered as isethionate salts in water. Compound dosing solutions were prepared for 5 days at a time. Host body weight change data are reported as the maximum treatment-related weight loss in these studies. Calculation of tumor growth inhibition (% T/C), tumor growth delay (T−C), and net logs of tumor cell kill was performed as described previously.[32−35] A positive net cell kill indicates that the tumor burden at the end of therapy was less than at the beginning of therapy. A negative net log cell kill indicates that the tumor grew during treatment. Net cell kills near 0 indicate no tumor growth during therapy.

References

(1) Bridges, A. J. The epidermal growth factor receptor family of tyrosine kinases and cancer: can an atypical exemplar be a sound therapeutic target? *Curr. Med. Chem.* **1996**, *3*, 167−194.

(2) Fry, D. W. Recent advances in tyrosine kinase inhibitors. *Annu. Rep. Med. Chem.* **1996**, *31*, 151−160.

(3) Rusch, V.; Mendelsohn, J.; Dmitrovsky, E. The epidermal growth factor receptor and its ligands as therapeutic targets in human tumors. *Cytokine Growth Factor Rev.* **1996**, *7*, 133−141.

(4) Yamada, M.; Ikeuchi, T.; Hatanaka, H. The neurotrophic action and signaling of epidermal growth factor. *Prog. Neurobiol.* **1997**, *51*, 19−37.

(5) Lupu, R.; Lippmann, M. E. The role of erbB2 signal transduction pathways in human breast cancer. *Breast Cancer Res. Treat.* **1993**, *27*, 83−93.

(6) Hickey, K.; Grehan, D.; Reid, I. M.; O'Briain, S.; Walsh, T. N.; Hennessy, T. P. J. Expression of epidermal growth factor receptor and proliferating cell nuclear antigen predicts response of esophageal squamous cell carcinoma to chemoradiotherapy. *Cancer* **1994**, *74*, 1693−1698.

Synthesis and application of functionally diverse 2,6,9-trisubstituted purine libraries as CDK inhibitors

Young-Tae Chang[1], Nathanael S Gray[1], Gustavo R Rosania[1], Daniel P Sutherlin[1], Soojin Kwon[1], Thea C Norman[1], Radhika Sarohia[1], Maryse Leost[2], Laurent Meijer[2] and Peter G Schultz[1]

Background: Purines constitute a structural class of protein ligands involved in mediating an astonishing array of metabolic processes and signal pathways in all living organisms. Synthesis of purine derivatives targeting specific purine-binding proteins *in vivo* could lead to versatile lead compounds for use as biological probes or drug candidates.

Results: We synthesized several libraries of 2,6,9-trisubstituted purines using both solution- and solid-phase chemistry, and screened the compounds for inhibition of cyclin-dependent kinase (CDK) activity and human leukemic cell growth. Lead compounds were optimized by iterative synthesis based on structure–activity relationships (SARs), as well as analysis of several CDK–inhibitor cocrystal structures, to afford several interesting compounds including one of the most potent CDK inhibitors known to date. Unexpectedly, some compounds with similar CDK inhibitory activity arrested cellular proliferation at distinctly different phases of the cell cycle, and another inhibitor directly induced apoptosis, bypassing cell-cycle arrest. Some of these compounds selectively inhibited growth of cells derived from specific tumors.

Conclusions: 2,6,9-Trisubstituted purines have various and potent biological activities, despite high concentrations of competing endogenous purine ligands in living cells. Purine libraries constitute a versatile source of small molecules that affect distinct biochemical pathways mediating different cellular functions.

Introduction

Purines are ubiquitous molecules that exist at relatively high (millimolar) concentrations in living organisms. Guanine and adenine, two of the most common purines, are essential components of nucleic acids, cofactors and signaling molecules that modulate protein function. Indeed, more than 10% of the proteins encoded by the yeast genome evidently depend on a purine-containing ligand for their function (see the database search at http://www.quest7.proteome.com) [1]. These include kinases, DNA (or RNA) polymerases, ATPases, GTPases, purine receptors, and purine biosynthetic and metabolic enzymes. For this reason, diverse purine libraries might be expected to have a high probability of yielding bioactive compounds when screened in a variety of enzyme- and cell-based assays. It seemed likely that structural variation at the 2, 6, 8 and 9 positions might impart specificity towards a variety of target proteins. This possibility prompted us to explore purine libraries as a source of both drug leads and probes for analyzing complex cellular processes.

We chose first to screen our purine libraries for inhibitors of the cyclin-dependent kinases (CDKs) because CDKs have recently attracted considerable interest in light of their essential role in regulating the cell cycle. The CDKs are in turn regulated by a variety of intracellular signals including the binding of inhibitory factors, phosphorylation and cellular localization. Previously, a number of purines, as well as nonpurine compounds, such as olomoucine and staurosporine have been developed as CDK inhibitors, but they suffer from potency or selectivity problems, respectively (Figure 1). For example, purine analogs such as olomoucine and roscovitine have been shown to selectively inhibit a subset of the CDKs (olomoucine has an IC_{50} value of 7 µM against both CDK1 and CDK2 [2], and roscovitine has IC_{50} values of 0.65 and 0.7 µM against CDK1 and CDK2 [3]). A 2.4 Å resolution X-ray crystal structure of olomoucine bound to CDK2 revealed that the purine ring occupies the conserved ATP-binding pocket [4]. Unexpectedly, however, the purine ring of olomoucine is rotated nearly 180° with respect to that of ATP. Although the interactions between the amino-acid residues in the binding site are different for olomoucine and ATP, the amount of solvent-accessible surface that becomes buried is similar for the two ligands.

Figure 1

Olomoucine: R_1=H, R_2=Me
(R)-Roscovitine: R_1=Et, R_2=iPr

Flavopiridol

Staurosporine

Chemistry & Biology

Structures of olomoucine, roscovitine, flavopiridol and staurosporine.

Although CDK1 and CDK2 serve different functions in controlling cell-cycle progression [5], the binding affinities of synthetic inhibitors [3] and the structures of their ATP-binding pockets are nearly identical, on the basis of amino-acid sequence [5]. Starting with the CDK2–olomoucine model, our goal is to use combinatorial chemistry to generate selective high-affinity inhibitors for CDK1 and CDK2, as well as other key cellular kinases, by introducing substituents at the 2, 6 and 9 positions of the purine ring. We and others previously reported several strategies for the solution- or solid-phase synthesis of purine derivatives [6–11], and have assayed these compounds against CDKs to determine structure–activity relationships (SARs). Our previous solid-phase synthesis scheme required that one position of the purine ring be held invariant to allow attachment to the solid support (Figure 2). Two positions were then varied combinatorially in order to identify optimal substituents in a pairwise fashion. In general, the effects of substituents at the 2, 6 and 9 positions on binding affinity appear to be additive, allowing one to rapidly identify potent purines by combining optimal substituents identified from simple binary libraries.

We describe new solid- and solution-phase syntheses of 2,6,9-trisubstituted purine libraries that can be used to combine rapidly and efficiently those substituents identified in the primary screens to afford second-generation libraries. Several specific and highly potent CDK2/CDK1

inhibitors have been identified from these libraries. In addition we characterized the cell-cycle inhibitory activities of a number of highly potent CDK inhibitors and found that some compounds arrested cellular proliferation at distinctly different phases of the cell cycle.

Results and discussion
Solid-phase synthesis
We used the crystal structures of various CDK2–ligand complexes to design the initial binary libraries with respect to the steric and electronic properties of the substituents to be introduced at the 2, 6 and 9 positions. A comparative analysis of the binding mode of olomoucine, flavopiridol [12] and staurosporine [13] in the ATP-binding pocket of CDK2 provided important information about functional groups that could be accommodated. For example, comparison of the bound purines and flavopiridol/staurosporine revealed that substituents at the 2 or 9 position of the purine ring might be able to occupy the same region of the active site as does the N-methyl piperidyl ring of flavopiridol (Figure 3c).

Synthesis and assays of the binary libraries against CDK2 indicated that aniline and 3- and 4-substituted benzylamine substituents led to significant improvements when introduced at the 6 position of the purine ring. Although a variety of hydroxyalkylamino, dihydroxyalkylamino and cycloalkylamino substituents at the 2 position resulted in moderate improvements, greater improvements were achieved with amino alcohols derived from valine and isoleucine. In contrast to many other protein kinases that can accommodate larger substituents at the 9 position of the purine ring, CDK2 binding was strongest for those purines bearing isopropyl functionality, followed by ethyl or hydroxyethyl [6].

Our previous synthetic routes involved tethering the purine core to the solid support through either a glycinamido, a 4-aminobenzyl amino or a 2-hydroxyethyl group at the 2, 6 and 9 positions, respectively. The drawback of these approaches is that one potential combinatorial site is lost. To circumvent this limitation a new solid-phase strategy and a versatile solution-phase route were developed. The solid-phase synthesis allows the introduction of substituents

Figure 2

1. Amination

1. Amination

2. Amination

2. Amination

1. Mitsunobu alkylation
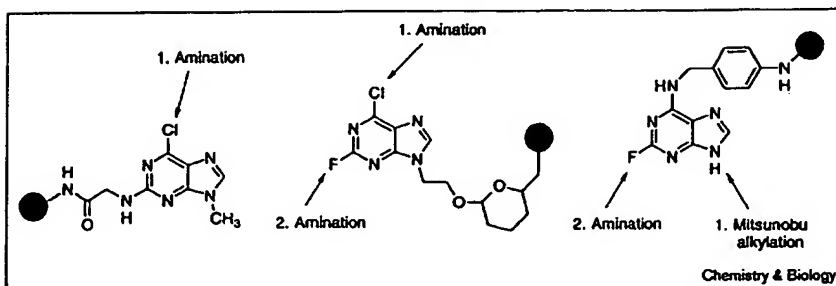
Precursors for binary library solid-phase synthesis.

Chemistry & Biology

Figure 3

Purvalanol B bound to CDK2 (black sticks, principal conformation only) is compared with (a) bound olomoucine (white sticks) and bound roscovitine (orange sticks), (b) bound ATP (yellow sticks), (c) bound flavopiridol (green sticks) and (d) bound staurosporine (purple sticks). The comparisons are based on superposition of the C_α atoms of CDK2. The ligands are shown in ball-and-stick representation with carbon atoms in white, nitrogen atoms in blue, oxygen atoms in red, phosphorous atoms in violet and the chlorine atoms of purvalanol B in green.
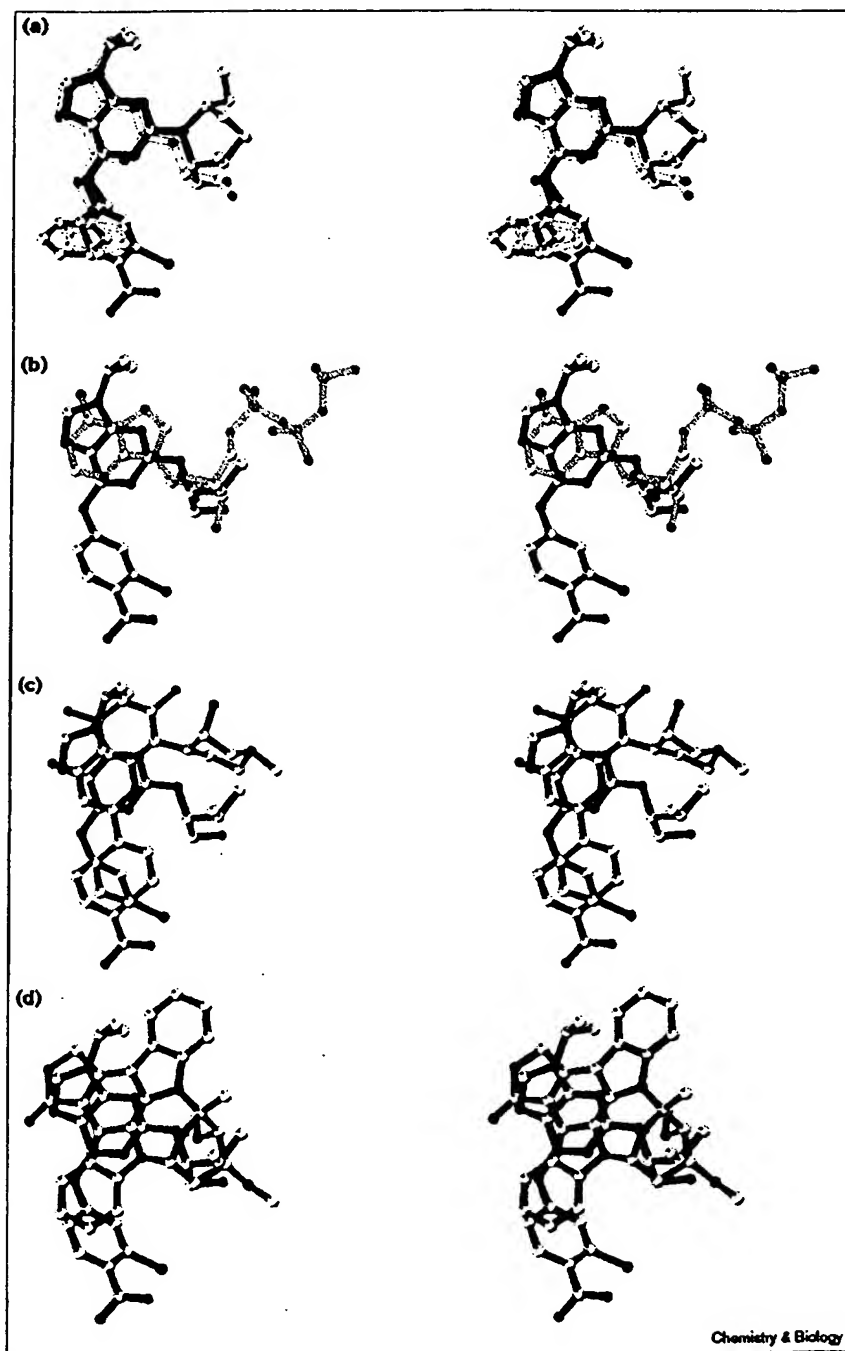
Chemistry & Biology

at the 2, 6 and 9 positions by immobilizing the purine through the N6 amino group. This is accomplished by starting with a library of resin-bound amines obtained from the reductive amination of a 5-(4-formyl-3,5-dimethoxyphenyloxy)valeric acid (BAL)-derivatized solid support with a collection of primary amines. By treating the resin-bound amines with a purine activated for substitution at

the 6 position, combinatorial modification at the 6 position is achieved. Modification of the N9 and C2 positions is then accomplished using Mitsunobu and amination chemistry as described previously (Figure 4) [7].

The synthetic scheme outlined above required that the electrophilicity of the purine ring be increased so that the

Figure 4
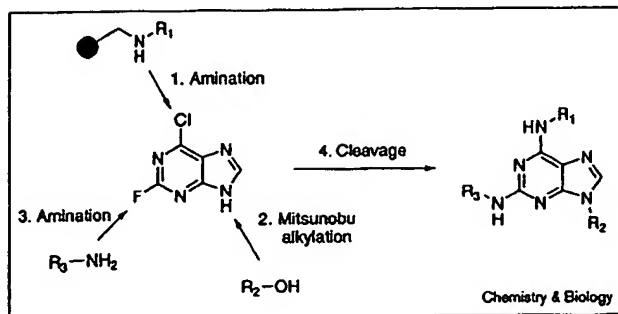
General scheme for solid-phase synthesis.

first amination reaction at the 6 position of the purine could be performed with weakly nucleophilic and α-branched amines. In order to facilitate the ability of a secondary amine to displace the 6-chloro group, we acylated the N9 position, which is expected to increase the overall electrophilicity of the purine ring. Unfortunately, the resulting activated amido group is more susceptible to nucleophilic attack than the 6-chloro group in the subsequent amination reaction. Another group that activates the 6 position of the purine ring without itself being susceptible to nucleophilic displacement is a N9-substituted tetrahydropyranyl (THP) aminal. Unfortunately, the acid lability of most commercially available solid supports made it difficult to cleave the THP group selectively without the concomitant release of the purine core. We therefore turned our attention to an N9-trimethylsilylethoxymethyl (SEM) activating group

that is stable to amino nucleophiles and can be cleaved using fluoride under nonacidic conditions. The N9-SEM-2-fluoro-6-chloro purine 1 (Figure 5) was prepared (in 50% yield) by alkylation of 2-fluoro-6-chloropurine [7], with SEM-Cl in the presence of Hunig's base. This substitution significantly increased the reactivity of the ring system to amination, allowing an amination reaction with benzylamine to proceed at room temperature (which had previously required extended heating at 50°C).

The optimized scheme starts with the reductive amination of BAL-derivatized 4-methylbenzhydrylamine (MBHA) resin to give resin bound amine, R2 [7]. A variety of amines including alkylamines, benzylamines and anilines were used in this first step. The purine core is then loaded onto solid support by reacting 2 equivalents of 1 with the amine-derivatized solid support R2 at 50°C to give R3. The removal of the SEM protecting group was performed using 0.25 M tetrabutylammonium fluoride in THF at 60°C. The deprotected purine was then reacted with various alcohols and amines at the 9 and 2 positions using Mitsunobu and nucleophilic-substitution chemistry respectively, as is shown for 2-(3-hydroxypropylamino)-6-(4-methoxybenzyl-amino)-9-isopropylpurine (209; Figure 5).

Although we have used this solid-phase chemistry to prepare a variety of 2,6,9-trisubstituted purines, there are two limitations to this approach. First, secondary amines cannot be introduced at the 6 position because one nitrogen substituent is required to attach the amine to solid support. More significantly, amination at the 2 position with bulky groups proceeded in low yield, perhaps due to

Figure 5
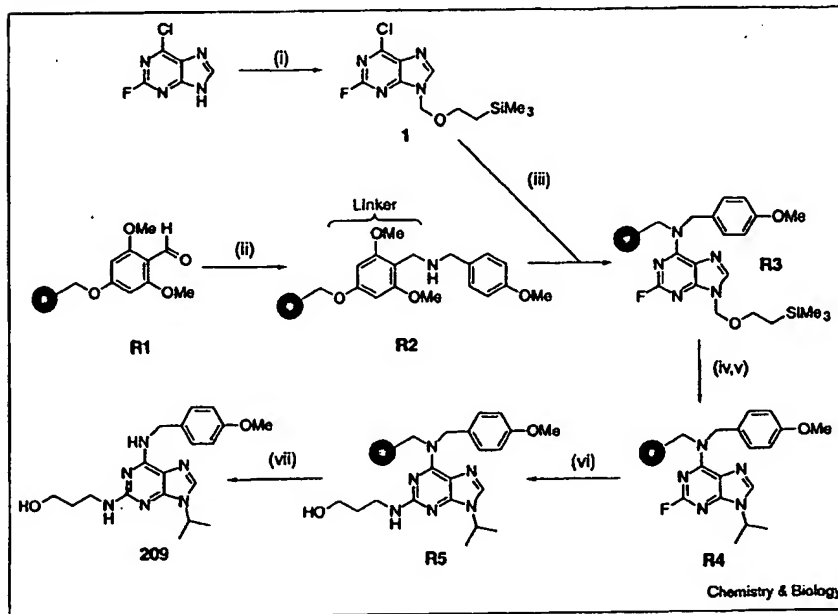
Representative scheme for solid-phase chemistry. (i) SEM-Cl (1.2 eq), DIEA, DMF, 0°C → rt. (ii) p-methoxybenzylamine, NaBH(OAc)$_3$, AcOH (2%), DMF, rt. (iii) DIEA, nBuOH-DMSO (1:1) 50°C. (iv) TBAF (0.25 M), THF, 60°C. (v) iPrOH (0.5 M), DIAD (0.5 M), PPh$_3$ (1.0 M), THF-CH$_2$Cl$_2$ (1:1). (vi) 3-amino-1-propanol, DIEA, N-methyl-pyrrolidinone, 110°C. (vii) TFA-water (95:5), rt.

Figure 6
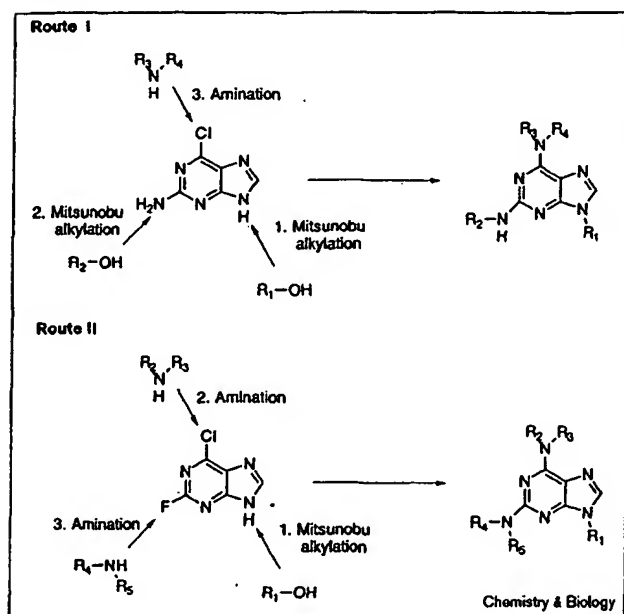
General schemes for solution-phase synthesis.

the decreased reactivity of purines attached to solid support. To overcome these limitations, we developed two versatile solution-phase synthetic routes to diverse trisubstituted purines.

Solution-phase synthesis

In route I (Figure 6), 2-amino-6-chloropurine was functionalized sequentially at the 9, 2 and 6 positions. Substituents at N9 were introduced by regioselective alkylation with a primary or secondary alcohol under Mitsunobu conditions [14]. In order to render the 2 position sufficiently acidic to undergo Mitsunobu alkylation, it was first acylated with trifluoroacetic anhydride. The trifluoroacetyl group is conveniently removed by hydrolysis with aqueous potassium carbonate prior to purification of the alkylated product by chromatography. Finally, a variety of primary and secondary benzylamines or anilines are introduced at the 6 position by reacting 3 with 1–2 equivalents of amine in n-butanol at elevated temperatures (Figure 7) (primary amines require 60°C whereas secondary amines and anilines require 110–120°C).
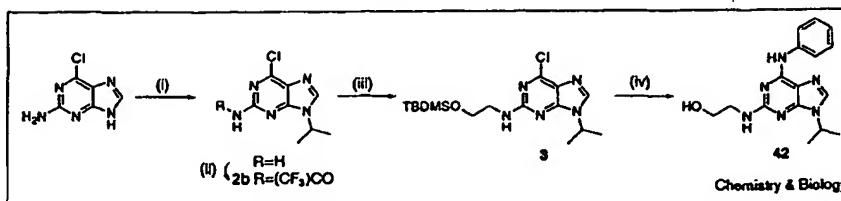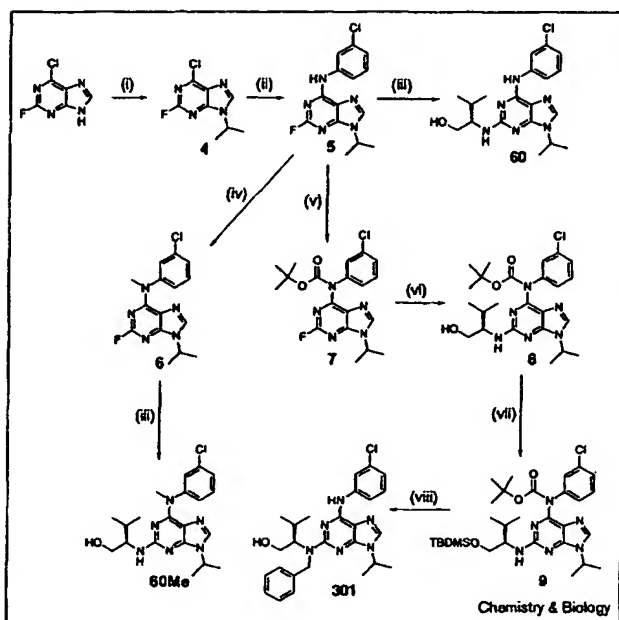
In route II (Figure 6), 2-fluoro-6-chloropurine was functionalized sequentially at the 9, 6 and 2 positions. As before, substituents at N9 position were introduced by Mitsunobu alkylation with either primary or secondary alcohols. This alkylation reaction tolerates virtually any alcohol without additional acidic hydrogens (pKa < 10–12). The more electrophilic 6-chloro substituent was selectively substituted with one equivalent of a benzylamine or aniline in analogy to route I. The resulting 2-fluoro-6,9-disubstituted purines were purified either by chromatography on silica or if solubility permitted, by trituration with dichloromethane and 0.1 N aqueous hydrochloric acid. Finally, the 2-fluoro position was aminated using an excess of primary or secondary amines in a small volume of n-butanol typically in a sealed tube (Figure 8). Representative procedures for two members of a purine library, 42 (synthesized by route I) and 60 (synthesized by route II), are shown in Figure 7 and 8.

CDK1/Cyclin B inhibition assay

Due to the limited information available concerning the N9 position SARs, we prepared a library to focus on this site. Libraries of 2-fluoro-6-(4-aminobenzylamino)-9-alkylpurines were synthesized using a 4-aminobenzyl-amino linkage strategy on resin-derivatized pins (Figure 2) [7]. In order to allow direct comparison of the efficacy of a range of substituents at the N9 position, a portion of the library was cleaved prior to amination at the 2 position. As can be seen from the assay results, optimal CDK2 inhibitory activity is observed for small alkyl groups with isopropyl exhibiting enhanced activity relative to ethyl, methyl and cyclopentyl (Figure 9). A similar result was obtained with another series of purines substituted with (2R)-pyrrolidin-2-yl-methanol at the C2 position [15].

To further enhance the CDK affinity of purine derivatives identified in previous screens of first-generation purine libraries, the synthetic methods described above were iteratively applied to the 2, 6 and 9 positions, and compounds were tested for activity against starfish oocyte CDK1/cyclin B [3]. Based on the improved activities of a 9 position isopropyl over methyl, and aniline over the benzyl group of olomoucine, we first derivatized the 9 position with an isopropyl substituent and tested various aniline substituents at the 6 position (Figure 10). Among the 2,3,4-substituted anilines, the 3-chloroaniline derivative 52 is the best CDK

Figure 7

Representative scheme I for solution chemistry.
(i) iPrOH (2.0 eq), DEAD (1.1 eq), PPh₃
(2.0 eq),THF, −10 → 25°C. (ii) (CF₃CO)₂O,
CH₂Cl₂, 0 → 25°C. (iii) TBDMSOCH₂CH₂OH
(2.0 eq), DEAD (1.0 eq), PPh₃ (2.0 eq), THF,
0 → 25°C. Then K₂CO₃, MeOH. (iv) aniline
(4.0 eq), DIEA, nBuOH, 110°C. Then AcOH-
H₂O-THF (3:1:1).

Figure 8

Representative scheme for solution chemistry II. (i) iPrOH (1.2 eq), DEAD (1.3 eq). PPh$_3$ (1.3 eq), THF −10 → 25°C. (ii) 3-chloroaniline (1.0 eq), DIEA, nBuOH, 140°C. (iii) (R)-(−)-2-amino-3-methyl-1-butanol (1.5 eq), DIEA, nBuOH, 150−170°C in sealed tube. (iv) MeI (2 eq), NaH, DMF, rt. (v) Boc$_2$O, DIEA, DMAP, THF, rt. (vi) (R)-(−)-2-amino-3-methyl-1-butanol (1.2 eq), DIEA, DMSO, 70−80°C. (vii) TBDMS-Cl, imidazole, DMAP, THF, rt. (viii) BnBr, Bu$_4$NI, NaH, DMF. Then pTSA, MeOH-CH$_2$Cl$_2$, rt.

inhibitor, showing a 30-fold improvement over olomoucine (with an IC$_{50}$ value of 220 nM). The 3-bromo, fluoro and trifluoromethyl groups exhibited comparable

activities, whereas the same 2-substituted purines are tenfold less active.

Next, we explored variations at the 2 position with the 6 position derivatized with either 4-methoxybenzylamine, the best among the benzyl substituents or 3-chloroaniline, chosen from the first-round solution-phase synthesis (Figure 11). Many compounds that have moderate activity (100–1000 nM) were found in this series. In general, we observed a preference for hydroxyalkyl or dihydroxyalkyl groups at the 2 position. An eightfold improvement in the IC$_{50}$ value, however, was obtained by replacing the 2 position hydroxyethylamino (52) with R-valinol attached via the α-amino group (60, named purvalanol A). In agreement with other reports [3], compounds with the R-stereochemistry were 2–16-fold more potent than those with the S-stereochemistry (75 versus 76, 60 versus 58, 66 versus 59 and 68 versus 69). Although most of the cyclic secondary amines were in general not preferred at 2 position, 2-hydroxyethylpiperidyl (10) improved the inhibitory activity threefold over hydroxyethyl (118).

In the third round, we fixed the 2 position with the R-valinol substituent, and refocused attention to the 6 position with a variety of benzylamine and aniline groups (Figure 12). This resulted in a set of the most active small-molecule CDK inhibitors known to date. The halogens on the 3 and 4 positions significantly improved the activity, and both the activity and solubility were enhanced with an additional carboxylate or amino group.

In parallel with the third round, we also fixed the 2 position with 2-(2-hydroxyethyl)piperidyl substituent and derivatized the 6 position with various benzylamine and aniline substituents (Figure 13). Simple aniline (220) or
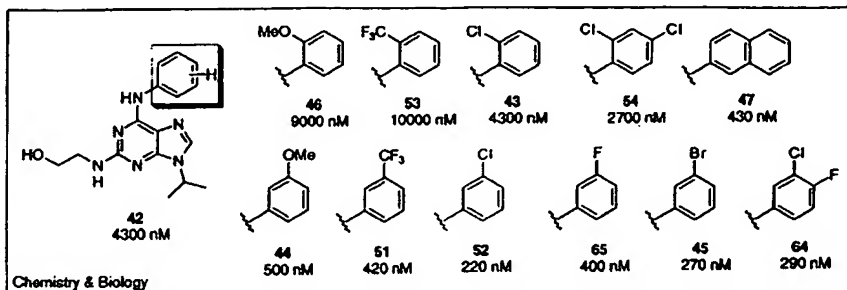
Figure 9
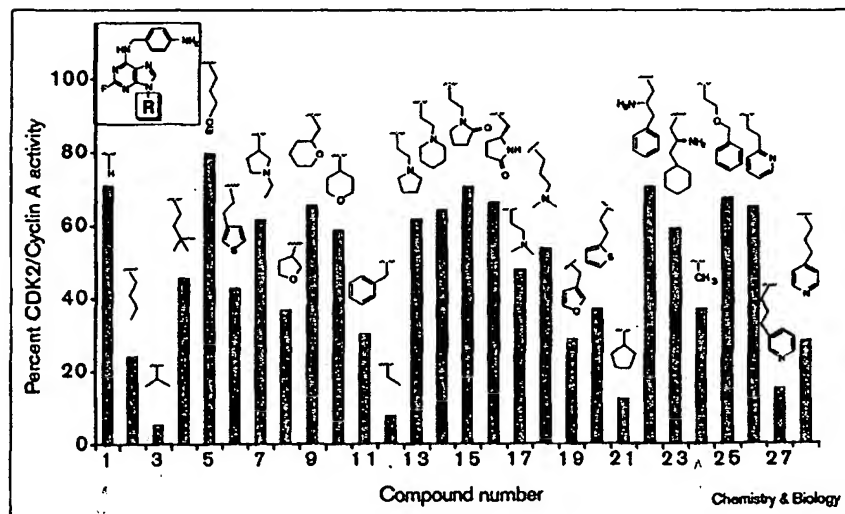
CDK2/cyclin A activity for representative compounds from an N9-directed library.

Figure 10

SAR class 1. Various C6-substituents on a
2-(2-hydroxyethylamino)-9-isopropylpurine core.

Chemistry & Biology

benzylamine (212) substituents proved to be slightly better than 4-methoxybenzylamine (10). Although 4-substituted benzylamine was tolerated (216), 3-substituted benzylamine (113, 222) decreased the activity significantly. Linear alkyl substituents (219), bulky substituents (225, 226, 227) and substituted anilines (359, 306) also decreased the activity.

During these rounds of optimization, we relied on the approximate additivity of substituents. The observed additivity allowed us to more efficiently assess greater numbers of substituents at a single site, thereby enhancing our ability to explore each of the binding sites without having to make all combinatorial possibilities. In this format, evaluation of 10 substituents at each site requires three sets of 10 compounds rather than one set of 1000. The simplest explanation for the observed additivity is that the rigid purine scaffold prevents substituents at the 2, 6 and 9 positions from binding in overlapping regions of the active site.

One of our most potent inhibitors, purvalanol B (95; Figure 12), was cocrystalized with CDK2 (Figure 14) [16], and the structure was compared with the structures of CDK2–flavopiridol, CDK2–staurosporine and CDK2–ATP (Figure 3). Purvalanol B occupied 86% of the available space in the binding pocket of CDK2, whereas flavopiridol occupied 74%, ATP occupied 78% and olomoucine occupied 76%.

Another of the most potent inhibitors, aminopurvalanol (97; Figure 12) was tested for its activity against a variety of kinases (Table 1). As expected, aminopurvalanol had almost the same activity against CDK1 as CDK2, with IC_{50} values ranging from 28–33 nM. Among the enzymes tested, only CDK5/p35 was inhibited to the same extent as CDK1/ CDK2, whereas other kinases exhibited much weaker inhibition by 97. The high degree of specificity observed for 97 is similar to that observed for purvalanol A and B [16].

The crystal structures of CDK2 with purvalanol B, ATP, flavopiridol or staurosporine suggested that additional contacts could be introduced by appending an extra group at

the N2 position of purvalanol B (Figure 14). We therefore attempted to synthesize N2-disubstituted derivatives of 60 by amination of 2-fluoro-6-(3-chloroanilino)-9-isopropylpurine (5) with N-alkyl valinol derivatives. Several N-alkyl valinol derivatives were synthesized by reductive alkylation of valinol with a variety of alkyl, aromatic and heteroaromatic aldehydes using sodium triacetoxyborohydride in 1,2-dichloroethane. Unfortunately, these branched secondary amines could not be installed at the 2 position, presumably due to their steric bulkiness. Attempts to activate the 2-fluoro group by introducing an electron withdrawing *tert*-butoxycarbonyl (Boc) group at the 6-position also failed to promote nucleophilic substitution. Finally, the O-silyl and 6-N-Boc protected derivative, 9, was successfully alkylated using sodium hydride, alkyl halide and tetrabutylammonium iodide in dimethylformamide (Figure 8). The desired compounds were obtained by removing the protecting groups and tested against CDK1/cyclin B. Unexpectedly, this class of compounds showed substantially reduced activity (with an IC_{50} value between 5 and 10 μM; Figure 15). This is not simply a consequence of disubstitution at the 2 position because 2-bishydroxyethyl derivatives such as 16, 26, 211, 303, 304 and 305 (IC_{50} 220–350 nM) show comparable activity to their parent hydroxyethyl derivatives 118 (IC_{50} 700 nM), and 52 (IC_{50} 220 nM; Figure 11). Potentially the combination of the sterically hindered R-valinol with additional substitution at the 2 position may prevent the inhibitors from accessing a productive binding conformation. Alternatively, the hydrophobic N-alkyl valinol derivatives that we introduced at the 2 position might have been poorly suited to the binding site.

For many of the biological applications described in the next section, we wanted access to a collection of negative control compounds that were structurally very similar to our potent inhibitors but lacked CDK inhibitory activity. We could then use these inactive derivatives to test if an observed *in vivo* effect is correlated with *in vitro* CDK activity. From the cocrystal structure of purvalanol B with CDK2 it was apparent that addition of a methyl group to N6 should lead to significantly reduced CDK inhibitory activity due to steric hindrance and the loss of a hydrogen

Figure 11
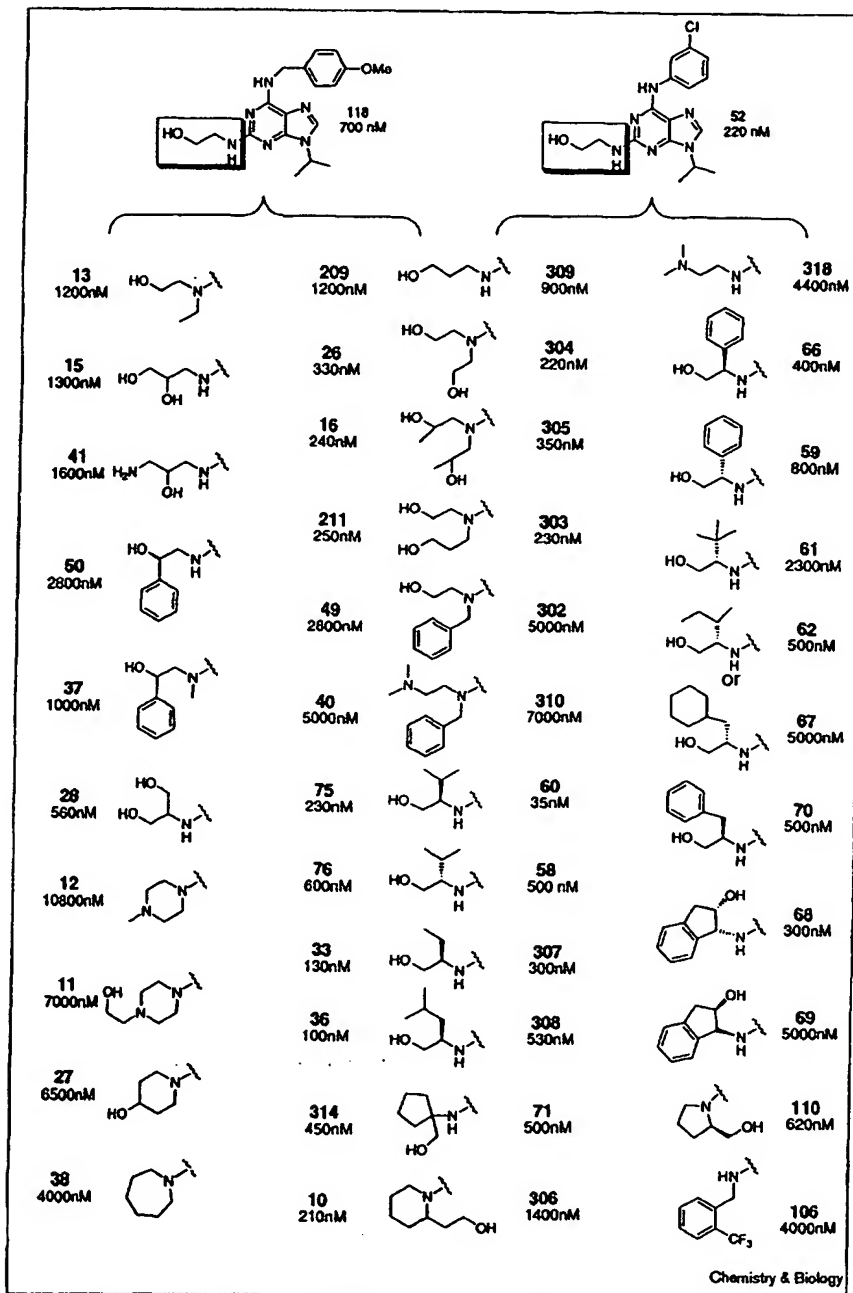
SAR class 2. Various C2-substituents on a 6-(4-methoxybenzylamino)- or a 6-(3-chloroanilino)-9-isopropylpurine core.

bond to Leu83 (Figure 14). We synthesized N6-methylated derivatives of four of our most potent CDK inhibitors (52, 60, 97 and 212; Figure 8). As expected, these compounds (52Me, 60Me, 97Me and 212Me) are completely inactive as CDK1/cyclin B inhibitors *in vitro*.

Cellular effects and cell cycle studies

We investigated the biological activity of the most potent CDK inhibitors from each SAR class by testing their ability to inhibit growth of U937 human leukemic cells. Cell populations were treated with the various compounds, and then assayed for the percentage decrease in the number of viable cells, using the 3-(4,5-dimethylthiazole-2-yl)-2,5-diphenyl-2H-tetrazolium bromide (MTT) assay [17]. The most potent CDK inhibitors in SAR classes 2 and 3 (Figures 11 and 12), compounds 60 and 97, were also found to be active inhibitors of cell growth (with IC_{50} values of 7.5 and 5 µM, respectively). The significant increase in the

Figure 12

SAR class 3. Various C6-substituents on a
2-(1R-isopropyl-2-hydroxyethylamino)-
9-isopropylpurine core.

Chemistry & Biology
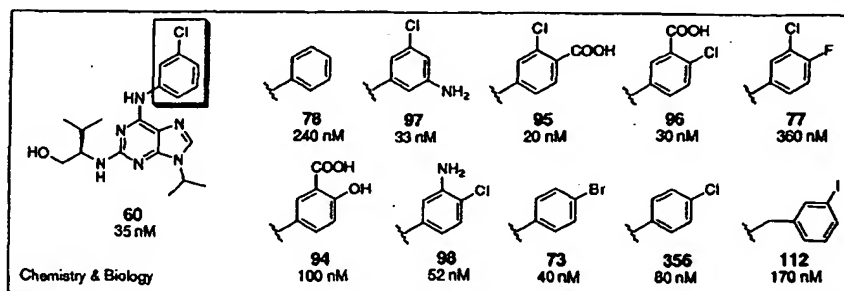
cell-based IC_{50} values relative to the *in vitro* IC_{50} values is presumably a result of competition with high concentrations of intracellular ATP (estimated to be in the millimolar range). Indeed when the kinase assay concentration of ATP was increased from 15 μM to 1.5 mM, the IC_{50} value for compound 60 increased (as expected) from 4 nM to 500 nM [16]. Compounds 94 and 95 were equally active in the kinase assay but inactive *in vivo*, probably due to the decreased cell permeability resulting from the negatively charged carboxylate group. From SAR class 4 (Figure 13), 212 is both a potent inhibitor of CDK activity and of cell growth (IC_{50} = 2.5 μM).

To study the specific effects of different purine derivatives on cell-cycle progression, unsynchronized proliferating U937 cells were treated with compounds 60, 97, 212 and 52. Treated cells were then subjected to cell-cycle analysis using flow cytometry and to morphological analysis using fluorescence microscopy. For flow cytometry, unsynchronized cell populations were labeled with propidium iodide (PI), a fluorescent DNA intercalator, and for the TUNEL assay, with a marker of DNA fragmentation that is characteristic of apoptosis. For morphological analysis, cells were labeled with Hoescht 33258, a DNA-specific dye, and with an antitubulin antibody that could be visualized using a FITC-conjugated secondary antibody. Using dose-response and time-course assays, differences in the effects of the compounds due to variations in compound permeability or the kinetics of the cellular response were investigated.

Initially, U937 cell populations were examined after treatment with 97 or 60, the most potent and bioactive CDK inhibitors. By flow cytometry, treatment of cells with 97 or 60 at doses lower than 10 μM specifically arrested cells in the G2–M phase of the cell cycle, based on the accumulation of cells with a 4 N DNA content, and the absence of DNA fragmentation (Figure 16). At higher concentrations (≥ 20 μM), however, both 97 and 60 triggered apoptosis after 8 h treatments, as detected with the TUNEL assay and confirmed by the appearance of nucleosome-sized DNA ladders as assessed by electophoresis (data not shown). The only apparent difference between the effects conferred by 60 or 97 to proliferating U937 cells related to their specific activity: 97 was four times more active than 60 in inducing a G2–M cell-cycle arrest (with IC_{50} values of 1.25 μM and 5 μM, respectively). The effect of 97 and 60 on microtubule architecture and on chromatin condensation were consistent with G2 cell-cycle arrest, based on the low percentage of mitotic cells (< 5%) seen in the treated populations. Because entry into mitosis depends on CDK1/CDK2 activity [18], inhibition of the G2–M phase transition was the expected result, based on the high activity of the compounds against CDK *in vitro*. Indeed, cells treated with either compound displayed fibrous microtubule organization, decondensed chromatin and intact nuclear architecture characteristic of interphase cells. Nevertheless, consistent with centrosome duplication occurring independently of CDK1 activity [19], a significant fraction of cells possessed two distinct

Figure 13

SAR class 4. Various C6-substituents on a
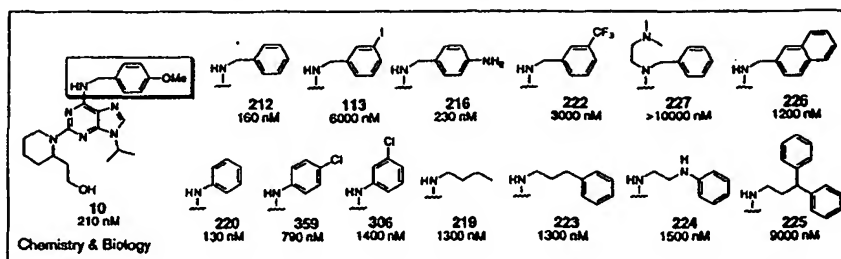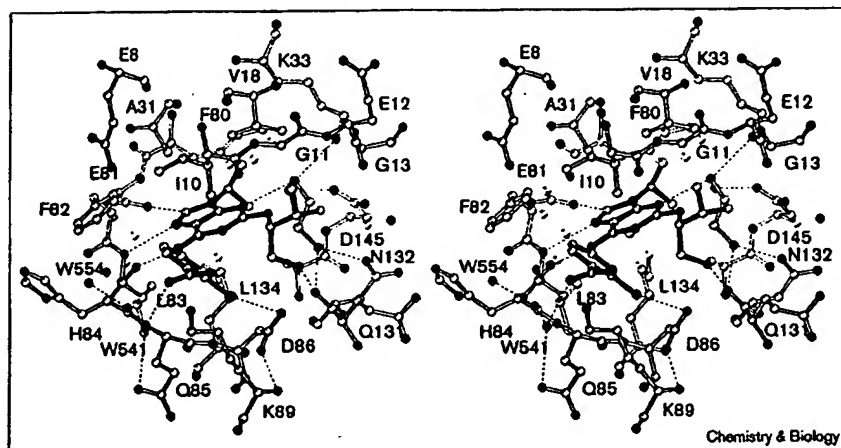2-(2-hydroxyethylpiperidyl)-9-isopropylpurine
core.

Chemistry & Biology

Figure 14

Binding site structure of CDK2–95 (purvalanol B).

Chemistry & Biology

microtubule arrays nucleated by discernible microtubule-organizing centers (Figure 17). In the presence of 97, these duplicated microtubule-organizing centers nucleated long microtubules characteristic of interphase cells. In the presence of 60, some of the microtubule arrays appeared shorter and more polarized, reminiscent of half spindles without attached chromosomes. Based on these results, the effects of compounds 60 and 97 on proliferating U937 cells appeared consistent with their specific CDK1/CDK2 inhibitory activity.

The CDK inhibitory activity of compounds 60 and 97 was significantly different from that of 52, the most

Table 1

Inhibition of purified kinases by aminopurvalanol (97).

Kinase	IC_{50} (µM)
CDK1/cyclin B	0.033
CDK2/cyclin A	0.033
CDK2/cyclin E	0.028
CDK5/p35	0.020
Erk1	12.0
Erk2	3.1
c-Raf	>100
MAPKK	>100
PKC-α	>100
PKC-β1	>100
PKC-β2	>100
PKC-γ	>100
PKC-δ	36.0
PKC-ε	>100
PKC-η	>100
PKC-ζ	>100
PKA	18.0
PKG	>100
Casein kinase 1	3.0
Casein kinase 2	>100
Insulin receptor Tyr-K	4.4

potent CDK1 inhibitor from SAR class 1 (Figure 10). By flow cytometry, 52 affected cell-cycle progression at concentrations of 25 µM or greater. Unlike cells treated with 60 or 97, however, cells treated with a comparable concentration of 52 did not become apoptotic (Figure 16b) and did not exhibit the characteristic accumulation of cells with a 4 N DNA content indicative of a G2 arrest. Instead, 52-treated cell populations displayed a reproducible depletion of the late-S/early-G2 cell population (Figure 16a). Morphologically, more than 20% of the cell population treated with 52 had bipolar microtubule spindles and condensed chromosomes, compared with less than 5% in control cell populations. This indicates that treatment of U937 cells with 52 causes arrest at mitosis. Interestingly, all of the 52-arrested, mitotic cells were in metaphase, as judged by the presence of two centrosomes, which nucleated polarized microtubules that were oriented towards each other, and fully condensed chromosomes aligned at the equator. Given the structural
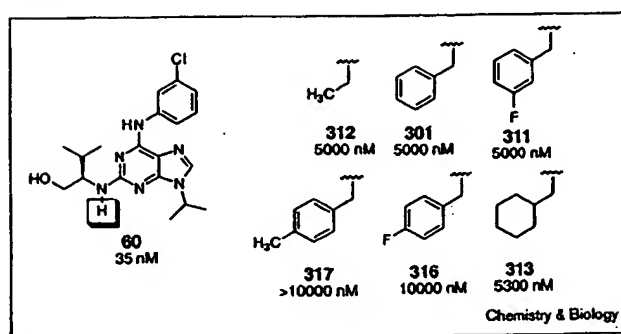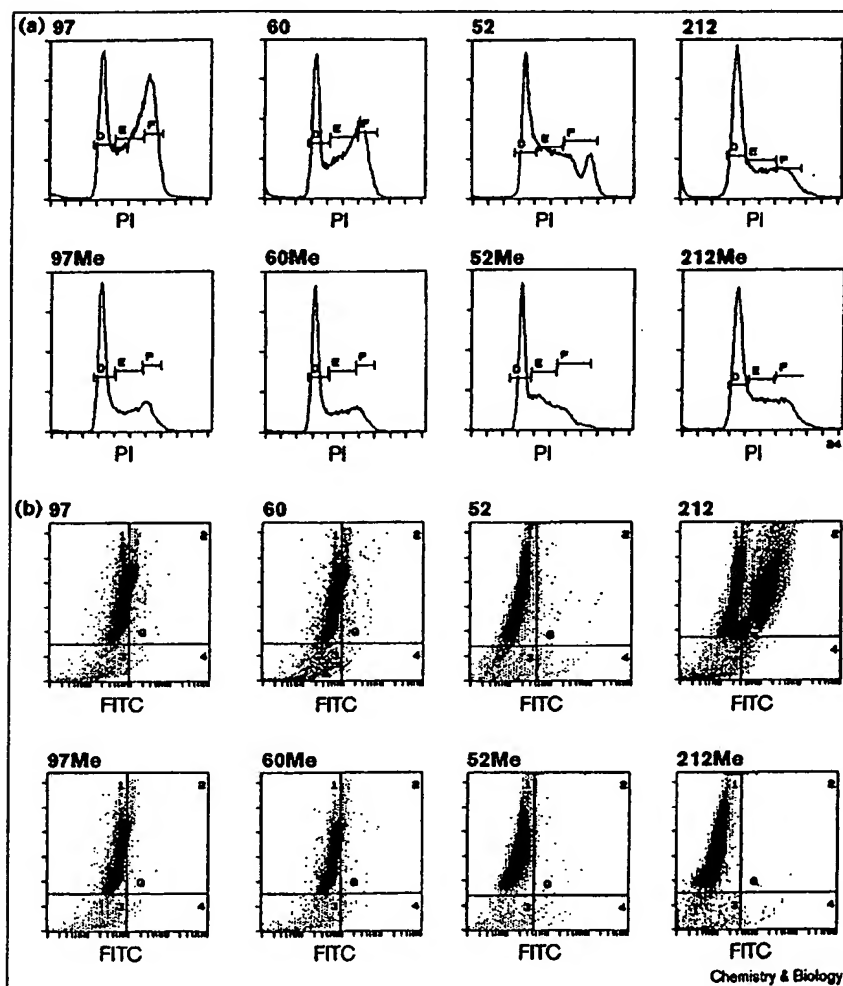
Figure 15

SAR class 5. Various C2-substituents on a 2-((1 R-isopropyl)-2-hydroxyethylamino)-6-(3-chloroanilino)-9-isopropylpurine core.

Figure 16

Flow cytometric analysis of (a) cell-cycle distribution and (b) apoptosis in U937 cell populations treated with different CDK inhibitors and their inactive, N6-methylated analogs. For each experiment, cells were treated for 0, 2, 4, 6 or 8 h, with increasing concentrations of compounds. Plots represent the most specific effect of each compound, as determined with the dose-response and time-course assays. For all the experiments, cells were co-labeled with PI, to stain the DNA, and with the TUNEL assay, to incorporate FITC-labeled nucleotides onto the ends of DNA fragments resulting from the apoptotic process. (a) Plots showing the distribution of cells with different DNA contents, after 8 h treatment with 5 µM 97 or 97Me, 10 µM 60 or 60Me, 50 µM 52 or 52Me or 5 µM 212 or 212Me. Bars indicate approximate DNA contents of cells with a 2N (D), intermediate (E) and 4N (F) DNA content, characteristic of cells in G1, S or G2-M phases of the cell cycle, respectively. DNA distribution of untreated cell populations are similar to those treated with the inactive, N6-methylated derivatives. (b) Bivariate plots of FITC versus PI staining of the same cell populations as in (a). Note that 212 is the only compound that nonspecifically induces apoptosis throughout the cell cycle without changing the cell-cycle distribution of the treated cell population.


Chemistry & Biology

similarity between compounds 52 and 60, we were surprised by their different effects on cells.

The effect of 212, one of the most potent CDK inhibitors from SAR class 4 (Figure 13), on proliferating U937 cell populations was also different from that of 52, 60 or 97. Flow cytometric analysis revealed that compound 212 was a nonspecific inducer of apoptosis at concentrations as low as 5 µM: it triggered DNA fragmentation at all phases of the cell cycle, without affecting cell-cycle progression (Figure 16). With the TUNEL assay, the effects of 212 could be observed at concentrations as low as 2.5 µM, making this compound one of the most potent inducers of apoptosis in the library. The induction of apoptosis was confirmed by the electrophoretic demonstration of nucleosome-sized DNA from the 212-treated cells (data not shown). Morphologically, cells treated with 212 exhibited characteristic apoptotic features, such as condensed DNA, fragmented nuclei and little microtubule staining

(Figure 17). By phase-contrast microscopy, cellular fragmentation was also apparent (data not shown).

As controls, the N6-methylated derivatives of 52, 60, 97 and 212 were tested side-by-side with the respective active non-methylated compounds. At the same concentrations as the active analogs, none of the control compounds induced the cell-cycle effects, apoptosis, nor the abnormal microtubule features (Figures 16,17). It appears, therefore, that although closely related purine derivatives had different effects when tested on cultured cells, the effects of the compounds on cell-cycle progression were specifically related to their chemical structure and their CDK-inhibitory activity. Previously, treatment of cells with olomoucine or roscovitine had been reported to lead to a G1/S and G2/M cell cycle arrest by a single mechanism [12,20,21]. In contrast, the different effects of these more potent and specific CDK inhibitors indicates a broader spectrum of activity. It remains to be determined whether the selectivity of different purines is

Figure 17
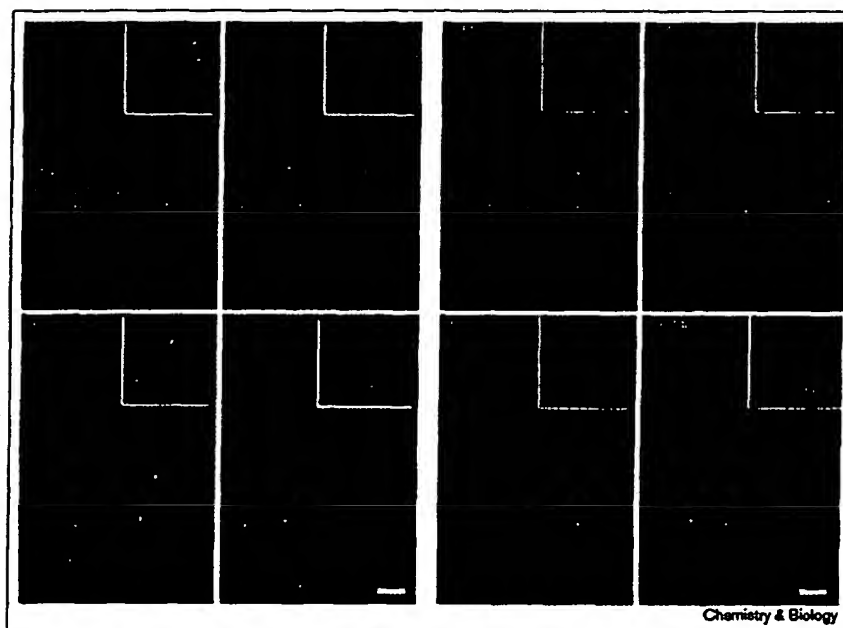
Morphological analysis of U937 cells treated with different CDK inhibitors and their inactive, N6-methylated analogs. For these experiments, cells were treated with the selected compounds for 6 h. Cells were then stained with fluorescein antitubulin immunocytochemistry to label the microtubules (green) and with the DNA-specific dye Hoescht 33258 to label the chromatin (blue). Samples were analyzed under the fluorescence microscope. Insets show the representative morphology of cells possessing duplicated microtubule organizing centers. In 60 and 97, arrows indicate the abnormal, interphase-like microtubule arrays nucleated from these duplicated microtubule organizing centers. Note that the chromatin remains decondensed in these cells. Unlabeled cells are those with interphasic microtubule arrays and decondensed chromatin. M, cells with mitiotic bipolar spindles and condensed chromosomes. A, cells with apoptotic features such as condensed or fragmented nuclei accompanied by little microtubule staining.

related to the specific molecular mechanism of cell-cycle deregulation accompanying cellular transformation.

Cell-type selectivity study

Because different tumors are characterized by genetic defects affecting different cell-cycle regulatory pathways, it has been hypothesized that compounds that act upon a specific pathway might be able to selectively inhibit growth of a particular tumor. Given the multiplicity of cell-cycle inhibitory activities exhibited by the purine inhibitors described, it seemed plausible that different purines would show selective growth-inhibitory activity against different tumor cell lines. Several active purines (60, 75, 95, 97 and

Table 2

GI_{50} values for selected cancer cell lines (μM).

	52	60	75	97	212
IGROV1 (ovarian cancer)	6.9	0.98	5.0	0.47	0.79
SR (leukemia)	7.6	1.9	2.3	0.42	4.7
NCI-H522 (lung cancer)	2.6	0.35	1.9	1.0	1.4
KM12 (colon cancer)	7.4	0.076	1.4	0.030	1.2
Average GI_{50}*	14	2.0	3.7	1.8	2.1
Average TGI†	53	10	17	8.1	9.8
Average LC_{50}‡	91	66	65	35	35

*GI_{50}, growth inhibitory effect. †TGI, cytostatic effect. ‡LC_{50}, cytotoxic effect.

212) were therefore selected for testing against the National Cancer Institute (NCI) panel of 60 cancer cell lines derived from different tumors. Cell growth inhibitory and cytotoxic activities of the compounds were found in the micromolar to nanomolar range. Although 75 and 212 were less selective to different cell types, 60 and 97 showed significant selectivity to KM12 colon cancer cells (Table 2). Compound 95 did not show significant cytotoxicity in these cell lines, presumably due to its decreased cell permeability.

Significance

Purine ligands are bound by a tremendous variety of enzymes in living organisms. Synthetic purine derivatives with diverse substituents may have the ability to bind selectively to one class of purine-recognizing enzymes. We synthesized several hundred 2,6,9-trisubstituted purine derivatives using solid- and solution-phase chemistry and screened them for inhibition of cyclin-dependent kinase (CDK1)/cyclin B. In addition to finding several highly specific and potent CDK inhibitors, we identified several compounds that elicited significantly different effects when tested in living cells. Compounds 60 (purvalanol A) and 97 (aminopurvalanol) arrest the cell cycle specifically in the G2 phase and induced morphological features consistent with their observed CDK1/CDK2 inhibitory activity. In contrast, compound 52, a moderate CDK inhibitor, induced M-phase arrest, and compound 212, also an active CDK inhibitor, induced apoptosis independent of cell-cycle phase. This broad spectrum of biological activities suggests that different purines might selectively act on different biochemical pathways affecting cell-cycle progression.

The degree of specificity exhibited by some of these purines, in terms of their ability to inhibit the cell-division cycle at different stages, is quite remarkable. Indeed, both structure–activity relationship (SAR) studies and the complete inactivity of the N-methylated analogs indicate that the effects of the different compounds are closely related to their chemical structures and to their CDK inhibitory activity. One possible interpretation of how similar CDK inhibitors display different cell-cycle inhibitory activities is that they are inhibiting different kinases in vivo. Alternatively, they might be inhibiting different activities of the same CDK, complexed with specific cyclins conferring different substrate specificities.

Materials and methods
Representative solution phase synthesis
2-Amino-6-chloro-9-isopropylpurine (2a). Anhydrous THF (120 ml) was added to a flame-dried flask under nitrogen containing 2-amino-6-chloropurine (2.0 g, 11.8 mmol) and triphenylphosphine (6.2 g, 23.6 mmol). To this was added 2-propanol (1.4 ml, 23.6 mmol), after which the solution was stirred and cooled to -10°C using an ethyleneglycol/dry-ice bath. Following the dropwise addition of diethyl azodicarboxylate (2.0 ml, 13.0 mmol), the mixture was gradually warmed to rt. After 24 h, the reaction was quenched with 2-propanol (1.5 ml) and the solvent was removed in vacuo. The resulting yellow/white gum was purified by column chromatography (1000 ml SiO_2, eluted sequentially with 99:1 and then 98:2 CH_2Cl_2:MeOH) to afford 2.9 g of 2a as a colorless foam (this product was contaminated with triphenylphosphine oxide and the diethyl hydrazine-N,N'-dicarboxylate ester byproducts). The crude product was trifluoroacetylated without further purification. An analytical sample was prepared using preparative thin-layer chromatography (TLC; 1.0 mm thickness, developed with 95:5 CH_2Cl_2:MeOH). Rf 0.35 (CH_2Cl_2:MeOH 95:5); ^{1}H NMR (400 MHz, $CDCl_3$) δ 1.58 (d, 6H, 6.8 Hz), 4.70 (sept., 1H, 6.8 Hz), 5.29 (br s, 2H), 7.85 (s, 1H); ^{13}C NMR (101 MHz, $CDCl_3$) δ 22.3, 47.1, 125.6, 140.0, 151.1, 153.4, 158.8; mass spectrum (FAB$^+$) m/e 212 (MH$^+$); HRMS calc'd for ($C_8H_{10}N_5Cl$)H$^+$: 212.0703, found: 212.0703.

2-Trifluoroacetamino-6-chloro-9-isopropylpurine (2b). 2-Amino-6-chloro-9-isopropylpurine (3.11 g, 14.7 mmol) was dissolved in distilled CH_2Cl_2 (29 ml) and the resulting solution cooled to 0°C. Trifluoroacetic anhydride (6.2 ml, 44 mmol) was added dropwise. The reaction mixture was warmed to rt over 3 h, concentrated in vacuo and dried further under high vacuum. The crude product was purified by chromatography (600 ml SiO_2, eluted with 20:80 EtOAc:CH_2Cl_2) to yield 4.0 g of 2b (88%). Rf 0.41 (CH_2Cl_2:MeOH 95:5); ^{1}H NMR (400 MHz, $CDCl_3$) δ 1.68 (d, 6H, 6.8 Hz), 4.92 (sept., 1H, 6.8 Hz), 8.59 (s, 1H), 10.20 (s, 1H).

2-(2-tert-Butyldimethylsilyloxyethylamino)-6-chloro-9-isopropylpurine (3). Trifluoroacetamide 2b (4.52 g, 14.7 mmol), 2-tert-butyldimethylsilyloxyethanol (5.18 g, 29.4 mmol) and triphenylphosphine (7.71 g, 29.4 mmol) were dissolved in freshly distilled THF (500 ml). The reaction mixture was stirred and cooled to 0°C and diethyl azodicarboxylate (2.31 ml, 14.7 mmol) was added dropwise over 5 min. The reaction mixture was warmed to rt, stirred for 12 h, and concentrated in vacuo to yield a yellow oil. This crude reaction mixture was redissolved in methanol (50 ml) and combined with an aqueous solution of potassium carbonate (16 ml, 1.0 M). The hydrolysis was complete within 1 h as judged by the disappearance of the trifluoroacetamide (Rf 0.74 EtOAc:hexane 75:25) by TLC. The resulting white slurry was partitioned between ethyl acetate and water (300 ml of each) and the organic layer collected, dried over sodium sulfate and concentrated in vacuo. The resulting oil was purified by column chromatography (1000 ml SiO_2, eluted with EtOAc:CH_2Cl_2 5:95) to yield 3.0 g of 3 (55%). Rf 0.26 (EtOAc:hexane 1:1); ^{1}H NMR (500 MHz, $CDCl_3$) δ 0.06 (s, 6H), 0.90 (s, 9H), 1.57 (d, 6H, 6.8 Hz),

3.57 (q, 2H, 5.6 Hz), 3.80 (t, 2H, 5.6 Hz), 4.69 (sept., 1H, 6.8 Hz), 5.49 (bs, 1H), 7.76 (s, 1H); ^{13}C NMR (126 MHz, $CDCl_3$) δ -4.8, 21.1, 24.8, 25.0, 43.5, 47.2, 60.2, 123.1, 139.7, 149.8, 152.7, 158.5; mass spectrum for $C_{16}H_{28}N_5ClOSi$ (FAB$^+$) m/e 371 (MH$^+$).

2-(2-Hydroxyethylamino)-6-anilino-9-isopropylpurine (42). Compound 3 (24 mg, 0.06 mmol), aniline (24 μl, 0.26 mmol) and diisopropylethylamine (45 μl, 0.26 mmol) were dissolved in nBuOH (1.5 ml). The reaction mixture was stirred at 90°C for 12 h and then concentrated in vacuo. The crude product was dissolved in a mixture of THF (200 μl), water (200 μl) and acetic acid (600 μl). The reaction mixture was stirred at rt for 12 h, concentrated in vacuo and azeotroped 3 × with methanol (3 ml × 3). The crude product was purified by preparative TLC (2 plates 1.0 mm thickness, developed twice with 60:40 EtOAc:hexane) to yield 16.4 mg (81%) of 42 as an oil. ^{1}H NMR (400 MHz, $CDCl_3$): δ 1.52 (d, 6H, 6.8 Hz), 3.59–3.63 (m, 2H), 3.84–3.87 (m, 2H), 4.57–4.65 (m, 1H), 5.51–5.53 (m, 1H), 7.03–7.07 (m, 1H), 7.27–7.33 (m, 2H), 7.59 (s, 1H), 7.75–7.77 (m, 2H), 8.16 (s, 1H); ^{13}C NMR (126 MHz, $CDCl_3$) δ 22.4, 45.1, 46.6, 63.8, 114.8, 120.2, 123.0, 128.7, 135.0, 139.1, 150.5, 152.4, 160.6; mass spectrum (FAB$^+$) m/e 313 (MH$^+$); HRMS calc'd for ($C_{16}H_{20}N_6Cl$)H$^+$: 313.1777, found: 313.1778.

2-Fluoro-6-chloro-9-isopropylpurine (4). Anhydrous THF (60 ml) was added under nitrogen to a flame-dried flask containing 2-fluoro-6-chloropurine (0.90 g, 5.2 mmol) and triphenylphosphine (3.0 g, 10.4 mmol). To this was added 2-propanol (800 μl, 10.4 mmol), after which the solution was cooled to -10°C. Following the dropwise addition of diethyl azodicarboxylate (850 μl, 10.4 mmol), the mixture was warmed gradually to rt. After 12 h, the reaction was quenched with water (500 μl) and the solvent removed in vacuo. The resulting yellow oil was purified by column chromatography (600 ml SiO_2, eluted with 100% CH_2Cl_2). The resulting solid was triturated with methanol (to remove the diethyl hydrazine-N,N'-dicarboxylate ester byproducts) to yield 630 mg (57 %) of 4 as a white crystalline solid. Rf 0.54 (MeOH:CH_2Cl_2 10:90); ^{1}H NMR (500 MHz, $CDCl_3$): δ 1.65 (d, 6H, J = 6.8 Hz), 4.85 (sept, 1H, 6.8 Hz), 8.15 (s, 1H); ^{13}C NMR (126 MHz, $CDCl_3$): δ 22.3, 48.4, 130.5, 143.7, 152.3, 153.1, 156.9 (J_{C-F} = 870 Hz); mass spectrum (EI$^+$) m/e 214 (M$^+$); anal. calc'd for $C_8H_8N_4FCl$: C, 44.77; H, 3.76; N, 26.10; Cl, 16.52. Found: C, 44.97; H, 3.76; N, 26.09; Cl 16.37.

2-Fluoro-6-(3-chloroanilino)-9-isopropylpurine (5). A mixture of 4 (3.75 g, 17.5 mmol), 3-chloroaniline (1.85 ml, 17.5 mmol) and diisopropylethylamine (3.05 ml, 17.5 mmol) were dissolved in n-butanol in a sealed tube. After 12 h at 140°C, the solvent was evaporated in vacuo, the crude product triturated with water, filtered and rinsed with CH_2Cl_2 and ether to yield 3.11 g (58%) of 5 as a white solid. Rf 0.66 (MeOH:CH_2Cl_2 5:95); ^{1}H NMR (400 MHz, $CDCl_3$) δ 1.61 (d, 6H, J = 6.8 Hz), 4.78 (sept., 1H, 6.8 Hz), 7.08 (d, 1H, J = 6.2 Hz), 7.26–7.30 (m, 1H), 7.64 (d, 1H, 8.2 Hz), 7.84 (s, 2H), 8.72 (s, 1H); ^{13}C NMR (101 MHz, $CDCl_3$) δ 22.4, 47.5, 118.9, 120.4, 123.8, 129.9, 134.4, 138.9, 139.3,150.7, 153.2(J_{C-F} = 20 Hz), 157.4(J_{C-F} = 19 Hz), 159.5; mass spectrum (EI$^+$) m/e 305 (M$^+$); HRMS calc'd for ($C_{14}H_{13}N_5ClF$)H$^+$: 305.0844, found: 305.0839; anal. calc'd for $C_{14}H_{13}N_5ClF$: C, 55.00; H 4.29; N, 22.91. Found: C, 55.35, H, 4.37, N, 23.10.

2-(1R-Isopropyl-2-hydroxyethylamino)-6-(3-chloroanilino)-9 isopropylpurine (60). Compound 6 (1.55 g, 5.1 mmol), R(-)2-amino-3-methyl-1-butanol (559 μl, 5.1 mmol) and diisopropylethylamine (892 μl, 5.1 mmol) were dissolved in n-butanol (1 ml) in a sealed tube. After heating the reaction mixture for 12 h at 140°C, the n-butanol was removed in vacuo and the crude product purified by column chromatography (400 ml SiO_2, eluted with 99:1 CH_2Cl_2:MeOH) to yield 1.2 g (57%) of 60 as a white solid. Rf 0.2 (MeOH:CH_2Cl_2 5:95); ^{1}H NMR (500 MHz, $CDCl_3$) δ 1.04 (d, 6H, 2.0, 6.8 Hz), 1.51 (d, 6H, 2.0, 6.8 Hz), 1.97–2.05 (m, 1H), 3.72–3.77 (m, 1H), 3.91–4.00 (m, 2H), 4.53 (sept., 1H, 6.8 Hz), 5.06 (d, 1H, 7.8 Hz), 6.97–7.00 (m, 1H), 7.20 (t, 3H, 8.1 Hz), 7.42 (d, 1H, 7.9 Hz), 7.55 (s, 1H), 8.00 (s, 1H), 8.03 (s, 1H); ^{13}C NMR (126 MHz, $CDCl_3$) δ 18.9, 19.4, 22.4, 30.0, 46.5, 59.6, 65.1, 114.9, 117.5, 119.6, 122.4, 129.6, 134.2, 135.1, 140.5, 150.8,

151.8, 159.7; mass spectrum (FAB⁺) m/e 389 (MH⁺); HRMS calc'd for $(C_{19}H_{25}N_6OCl)H^+$: 389.1857, found, 389.1859; anal. calc'd for $C_{19}H_{25}N_6OCl$: C, 58.68; H, 6.48; N, 21.61; Cl, 9.12; O, 4.11. Found: C, 58.54; H, 6.61; N, 21.58; Cl, 9.10; O, 3.96.

2-Fluoro-6-(N,N'-(methyl),(3-chloroanilino)-9-isopropylpurine (6). A solution of 5 (110 mg, 0.36 mmol) in dry DMF (1.5 ml) was added dropwise to a suspension of NaH (18 mg, 0.43 mmol) in dry DMF (1 ml). This mixture was stirred for 20 min at rt, after which a solution of methyl iodide (35 µl, 0.36 mmol) in DMF (0.5 ml) was added slowly. After stirring 12 h, the DMF was removed *in vacuo* and the crude product purified by chromatography (200 ml SiO₂, eluted with 98:2 CH₂Cl₂:MeOH) to yield 115 mg of 6 (100%) as a white solid. Rf 0.61 (MeOH:CH₂Cl₂ 5:95); ¹H NMR (CDCl₃, 400 MHz) δ 1.47 (d, 6H, 6.8 Hz), 3.73 (s, 3H), 4.68 (sept., 1H, 6.8 Hz), 7.15–7.38 (m, 5H), 7.63 (s, 1H); mass spectrum (FAB⁺) m/e 320 (MH⁺); HRMS calc'd for $(C_{15}H_{15}N_5ClF)H^+$: 320.1080, found, 320.1080.

2-(1R-isopropyl-2-hydroxyethylamino)-6-(N,N'-(methyl),(3-chloroanilino)-9-isopropylpurine (60Me). Procedure same as that used to prepare compound 60. Rf 0.25 (MeOH:CH₂Cl₂ 5:95); ¹H NMR (300 MHz, CDCl₃) δ 0.99 (d, 6H, 6.8 Hz), 1.51 (d, 6H, 6.8 Hz), 1.65 (br s, 2H), 1.94 (sept., 1H, 6.8 Hz), 3.61–3.73 (m, 2H), 3.79 (s, 3H), 4.62 (sept, 1H, 6.8 Hz), 4.83–4.85 (m, 1H), 7.19–7.36 (m, 4H), 7.49 (s, 1H); ¹³C NMR (75 MHz, CDCl₃) δ 19.0, 19.4, 22.4, 22.5, 30.0, 39.8, 46.1, 59.8, 66.2, 115.6, 124.7, 126.1, 127.1, 129.7, 134.1, 134.5, 146.9, 152.5, 154.4, 159.3; mass spectrum (FAB⁺) m/e 403 (MH⁺); HRMS calc'd for $(C_{20}H_{27}N_6OCl)H^+$: 403.2013, found, 403.2013.

2-Fluoro-6-(N-tert-butoxycarbonyl-3-chloroanilino)-9-isopropylpurine (7). Compound 5 (169 mg, 0.55 mmol), di-tert-butyldicarbonate (219 mg, 1.0 mmol), diisopropylethylamine (0.8 ml, 4.6 mmol) and dimethylaminopyridine (36 mg) were dissolved in THF (10 ml). After the reaction mixture was stirred at rt for 5 h, the solvent was removed *in vacuo* and the crude product was purified by column chromatography (80 ml SiO₂, eluted with ethyl acetate-hexane gradient) to yield 176 mg (79%) of 7 as a white solid. Rf 0.4 (EtOAc:hexane 1:2); ¹H NMR (500 MHz, CDCl₃) δ 1.47 (s, 9H), 1.63 (d, 6H, 7.0 Hz), 4.84 (m, 1H), 7.19–7.33 (m, 4H), 8.06 (S, 1H); mass spectrum (FAB⁺) m/e 406.1 (MH⁺); HRMS calc'd for $(C_{19}H_{21}N_5O_2FCl)H^+$: 406.1446, Found 406.1437; anal. calc'd for $C_{19}H_{21}N_5O_2FCl$: C 56.23; H, 5.22; N, 17.26. Found: C, 56.48; H, 5.47; N, 16.99.

2-(1R-Isopropyl-2-hydroxyethylamino)-6-(N-tert-butoxycarbonyl-3-chloroanilino)-9-isopropylpurine (8). To a stirring solution of 7 (108 mg, 0.27 mmol) in DMSO (10 ml) was added R(-)2-amino-3-methyl-1-butanol (202 mg, 1.96 mmol) and diisopropylethylamine (1 ml, 5.7 mmol). After heating for 12 h at 80°C, the DMSO was removed *in vacuo* with heating to 70°C, and the crude product purified by chromatography (400 ml SiO₂, eluted with ethyl acetate-hexane gradient) to yield 88 mg (67%) of 8 as an oil. Rf 0.4 (EtOAc:hexane 2:1); ¹H NMR (500 MHz, CDCl₃) δ 0.95 (d, 3H, 7.0 Hz), 0.96 (d, 3H, 7.0 Hz), 1.47 (S, 9H), 1.57 (d, 3H, 7.0 Hz), 1.58 (d, 3H, 7.0 Hz), 1.94 (m, 1H), 3.44 (bs, 1H), 3.65 (m, 1H), 3.75–3.77 (m, 2H), 4.68 (m, 1H), 5.18 (d, 1H, 8.0 Hz), 7.21–7.31 (m, 4H), 7.77 (S, 1H); mass spectrum (FAB⁺) m/e 489.2 (MH⁺); HRMS calc'd for $(C_{24}H_{33}N_6O_3Cl)H^+$: 489.2381, found 489.2377.

2-(1R-isopropyl-2-dimethyl-tert-butylsilyloxyethylamino)-6-(N-tert-butoxycarbonyl-3-chloroanilino)-9-isopropylpurine (9). Compound 8 (40 mg, 0.081 mmol), tert-butyldimethylsilyl chloride (200 mg, 1.33 mmol) and imidazole (380 mg, 5.58 mmol) were dissolved in THF (10 ml) and stirred at rt. After 24 h, a precipitate had developed which was removed by filtration. The solid byproduct was washed with THF, concentrated *in vacuo* and purified by preparative thin layer chromatography (20 × 20 cm, 0.5 mm, ethyl acetate-hexane 1:1) to give 33 mg (68%) of 9 as an oil. Rf 0.7 (EtOAc:hexane 1:1); ¹H NMR (500 MHz, CDCl₃) δ −0.04 (s, 3H), −0.02 (s, 3H), 0.84 (s, 9H), 0.88–0.92 (m, 6H), 1.44 (s, 9H), 1.55 (d, 3H, 7.0 Hz), 1.56 (d, 3H, 7.0 Hz), 1.97 (br, 1H), 3.59 (m, 1H), 3.70 (m, 1H), 3.82 (m, 1H), 4.69 (m, 1H), 5.06 (d, 1H, 9.5 Hz),

7.16–7.30 (m, 4H), 7.73 (s, 1H); mass spectrum (FAB⁺) m/e 603.3 (MH⁺); HRMS calc'd for $(C_{30}H_{47}N_6O_3ClSi)H^+$: 603.3246, found 603.3247; anal. calc'd for $C_{30}H_{47}N_6O_3ClSi$: C 59.73; H, 7.85; N, 13.93. Found: C, 59.83; H, 8.04; N, 13.87.

2-(N-Benzyl-1R-isopropyl-2-hydroxyethylamino)-6-(3-chloroanilino)-9-isopropylpurine (301). To a solution of 9 (33 mg, 0.055 mmol) in DMF (7 ml) was added sequentially sodium hydride (60% dispersed in mineral oil, 94 mg, 2.4 mmol), benzyl bromide (100 µl, 0.84 mmol) and tetrabutylammonium iodide (68 mg, 0.18 mmol) at rt under nitrogen. The reaction mixture was stirred for 17 h and then diluted with CH₂Cl₂ (50 ml) and filtered through SiO₂ (100 ml). The filtrate was concentrated *in vacuo*, and hydrolysed with p-toluenesulfonic acid (30 mg) in a mixture of MeOH-CH₂Cl₂ (1:1, 20 ml) at rt for 24 h. After removal of the solvent, the product was purified using preparative thin layer chromatography (20 × 20 cm, 0.5 mm, ethyl acetate-hexane 2:1) to give 5 mg (19%) of 301 as an oil. Rf 0.2 (EtOAc:hexane 2:1); ¹H NMR (500 MHz, CDCl₃) δ 0.87 (d, 3H, 6.5 Hz), 1.08 (d, 3H, 6.5 Hz), 1.25 (s, 6H), 2.40 (m, 1H), 3.79 (m, 1H), 3.88 (m, 2H), 4.67 (m, 1H), 4.85 (br s, 2H), 6.99 (br, 1H), 7.12–7.96 (m, 10H); mass spectrum (FAB⁺) m/e 479.2 (MH⁺); HRMS calc'd for $(C_{26}H_{31}N_6OCl)H^+$: 479.2326, found 479.2321.

Supplementary material

General synthetic methods and spectroscopic data for all compounds included in the main text, as well as details of solid-phase synthesis of representative library members and all biological assays (kinase assays, cell culture, cell viability assays, cell-cycle and apoptosis assays, flow cytometry and cell-cycle analysis and immunocytochemistry) are published with the online version of this paper.

References

1. Hodges, P.E. (Ed).*Yeast Proteome Handbook* (1998, 5th ed.), Proteome, Inc., Beverly, USA.
2. Vesely, J., et al., & Meijer, L. (1994). Inhibition of cyclin-dependent kinases by purine analogues. *Eur. J. Biochem.* **224**, 771-786.
3. Meijer, L. et al., & Moulinoux, J.-P. (1997). Biochemical and cellular effects of roscovitine, a potent and selective inhibitor of the cyclin-dependent kinases cdc2, cdk2 and cdk5. *Eur. J. Biochem.* **243**, 527-536.
4. Schulze-Gahmen, U. et al., & Kim, S.-H. (1995). Multiple modes of ligand recognition – crystal structure of cyclin dependent protein kinase 2 in complexes with ATP and two inhibitors, olomoucine and isopentenyladenine. *Proteins* **22**, 378-391.
5. Nigg, E.A. (1995). Cyclin-dependent protein kinases – key regulators of the eukaryotic cell cycle. *BioEssays* **17**, 471-480.
6. Norman, T.C., Gray, N.S., Koh, J.T. & Schultz, P.G. (1996). A structure-based library approach to kinase inhibitors. *J. Am. Chem. Soc.* **118**, 7430-7431.
7. Gray, N.S., Kwon, S. & Schultz, P.G. (1997). Combinatorial synthesis of 2,9-substituted purines. *Tetrahedron Lett.* **38**, 1161-1164.
8. Nugiel, D.A., Cornelius, L.A.M. & Corbett, J.W. (1997). Facile preparation of 2,6-disubstituted purines using solid-phase chemistry. *J. Org. Chem.* **62**, 201-203.
9. Legraverend, M., Ludwig, O., Bisagni, E., Leclerc, S. & Meijer, L. (1998). Synthesis of C2 alkynylated purines, a new family of potent inhibitors of cyclin-dependent kinases. *Bioorg. Med. Chem. Lett.* **8**, 793-798.
10. Schow, S.R., et al., & Lum, R.T. (1997). Synthesis and activity of 2,6,9-trisubstituted purines. *Bioorg. Med. Chem. Lett.* **7**, 2697-2702.
11. Fiorini, M.T. & Abell, C. (1998). Solution-phase synthesis of 2,6,9-trisubstituted purines. *Tetrahedron Lett.* **39**, 1827-1830.
12. de Azevedo, Jr., W.F., Mueller-Diechmann, H.-J., Schulze-Gahmen, U., Worland, P.J., Sausville, E. & Kim, S.-H. (1996). Structural basis for specificity and potency of a flavonoid inhibitor of human CDK2, a cell cycle kinase. *Proc. Natl Acad. Sci. USA* **93**, 2735-2740.

13. Lawrie, A.M., Noble, M.E.M., Tunnah, P., Brown, N.R., Johnson, L.N. & Endicott, J.A. (1997). Protein kinase inhibition by staurosporine revealed in details of the molecular interaction with CDK2. *Nat. Struct. Biol.* **4**, 796-801.

14. Toyota, A., Katagiri, N. & Kaneko, C. (1993). The alkylation of 2-amino-6-chloropurine with alcohols by Mitsunobu reaction for a synthesis of carbocyclic guanosine analogs. *Heterocycle* **36**, 1625-1630.

15. Legraverend, M., *et al.*, & Fovaudon, V. (1999). *Bioorg. Med. Chem.*, in press.

16. Gray, N.S., *et al.*, & Schultz, P.G. (1998). Exploiting chemical libraries, structure and genomics in the search for kinase inhibitors. *Science* **281**, 533-538.

17. Hansen, M.B., Nielsen, S.E. & Berg, K.J. (1989). Re-examination and further development of a precise and rapid dye method for measuring cell growth/cell kill. *Immunol. Methods* **119**, 203-210.

18. Guadagno, T.M. & Newport, J.W. (1996). CDK2 kinase is required for entry into mitosis as a positive regulator of cdc2-cyclin B kinase activity. *Cell* **84**, 73-82.

19. Hinchliffe, E.H., Cassels, G.O., Rieder, C.L. & Sluder, G. (1998). The coordination of centrosome reproduction with nuclear events of the cell cycle in the sea urchin zygote. *J. Cell Biol.* **140**, 1417-1426.

20. Schutte, B., Nieland, L., van Engeland, M., Henfling, M.E.R., Meijer, L. & Ramaekers, F.C.S. (1997). The effect of the cyclin-dependent kinase inhibitor olomoucine on cell cycle kinetics. *Exp. Cell Res.* **236**, 4-15.

21. Planchais, S. *et al.*, & Bergounioux, C. (1997). Roscovitine, a novel cyclin-dependent kinase inhibitor, characterizes restriction point and G2/M transition in tobacco BY-2 cell suspension. *Plant J.* **12**, 191-202.

This Page is Inserted by IFW Indexing and Scanning Operations and is not part of the Official Record

BEST AVAILABLE IMAGES

Defective images within this document are accurate representations of the original documents submitted by the applicant.

Defects in the images include but are not limited to the items checked:

❑ BLACK BORDERS

☑ IMAGE CUT OFF AT TOP, BOTTOM OR SIDES

❑ FADED TEXT OR DRAWING

❑ BLURRED OR ILLEGIBLE TEXT OR DRAWING

❑ SKEWED/SLANTED IMAGES

❑ COLOR OR BLACK AND WHITE PHOTOGRAPHS

❑ GRAY SCALE DOCUMENTS

☑ LINES OR MARKS ON ORIGINAL DOCUMENT

❑ REFERENCE(S) OR EXHIBIT(S) SUBMITTED ARE POOR QUALITY

❑ OTHER: _____

IMAGES ARE BEST AVAILABLE COPY.
As rescanning these documents will not correct the image problems checked, please do not report these problems to the IFW Image Problem Mailbox.